UMI University Microfilms International

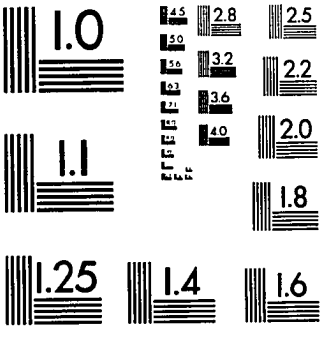

MICROCOPY RESOLUTION TEST CHART
NATIONAL BUREAU OF STANDARDS
STANDARD REFERENCE MATERIAL 1010a
(ANSI and ISO TEST CHART No. 2)

University Microfilms Inc.
300 N. Zeeb Road, Ann Arbor, MI 48106

Downloaded from SHAREOK. Persistent Handle URL: https://hdl.handle.net/11244/5362

INFORMATION TO USERS

This reproduction was made from a copy of a manuscript sent to us for publication and microfilming. While the most advanced technology has been used to photograph and reproduce this manuscript, the quality of the reproduction is heavily dependent upon the quality of the material submitted. Pages in any manuscript may have indistinct print. In all cases the best available copy has been filmed.

The following explanation of techniques is provided to help clarify notations which may appear on this reproduction.

1. Manuscripts may not always be complete. When it is not possible to obtain missing pages, a note appears to indicate this.

2. When copyrighted materials are removed from the manuscript, a note appears to indicate this.

3. Oversize materials (maps, drawings, and charts) are photographed by sectioning the original, beginning at the upper left hand corner and continuing from left to right in equal sections with small overlaps. Each oversize page is also filmed as one exposure and is available, for an additional charge, as a standard 35mm slide or in black and white paper format.*

4. Most photographs reproduce acceptably on positive microfilm or microfiche but lack clarity on xerographic copies made from the microfilm. For an additional charge, all photographs are available in black and white standard 35mm slide format.*

***For more information about black and white slides or enlarged paper reproductions, please contact the Dissertations Customer Services Department.**

UMI University Microfilms International

8601143

Hailey, Christine Elizabeth Meersman

RAY TRACING OF SHEAR FLOW INSTABILITY WAVES THROUGH A SLIGHTLY INHOMOGENEOUS BACKGROUND FLOW

The University of Oklahoma PH.D. 1985

University
Microfilms
International 300 N. Zeeb Road, Ann Arbor, MI 48106

Copyright 1985

by

Hailey, Christine Elizabeth Meersman

All Rights Reserved

THE UNIVERSITY OF OKLAHOMA

GRADUATE COLLEGE

RAY TRACING OF SHEAR FLOW INSTABILITY WAVES THROUGH A SLIGHTLY INHOMOGENEOUS BACKGROUND FLOW

A DISSERTATION

SUBMITTED TO THE GRADUATE FACULTY

in partial fulfillment of the requirements for the

degree of

DOCTOR OF PHILOSOPHY

By

CHRISTINE ELIZABETH MEERSMAN HAILEY

Norman, Oklahoma

1985

RAY TRACING OF SHEAR FLOW INSTABILITY WAVES

THROUGH A SLIGHTLY INHOMOGENEOUS BACKGROUND FLOW

A DISSERTATION

APPROVED FOR THE SCHOOL OF AEROSPACE, MECHANICAL,

AND NUCLEAR ENGINEERING

By

John M. Russell

Martin C. Jischke

Omer Savaz

M Rasmussen

Luther White

[illegible]

© Copyright by Christine Elizabeth Hailey 1985
All Rights Reserved

To
Jennifer Michelle and Gavain Andrew

ACKNOWLEDGEMENTS

Let me begin by stating that there are too many people to thank in this short space. I have been blessed to have had the support of friends, family, and faculty throughout my entire graduate program. There are certain key people however, that must be acknowledged. First my major professor, John M. Russell who has known when to offer guidance and support and has known when to leave me be. I am also indebted to the other members of my committee who have taken the time to read this work: Doctors Martin Jischke, Tom Love, Maurice Rasmussen, Omer Savas, and Luther White. I am especially indebted to Professor Jischke for initially urging me to pursue a graduate degree and then "watching over" my progress throughout the years.

I have also had the privilege of working with Professor Joakim Laguros for the last three years who has shown me by example the sort of faculty member I hope to be one day. His counsel and friendship have helped immeasurably in the completion of this work.

Finally, I am very indebted to my husband, David, who rescued me during a very difficult time and urged me to move forward and complete this degree. Without him this work would never have been completed.

ABSTRACT

An extension of Whitham's kinematic wave theory, which holds for modal waves in a non-conservative system, has been applied in order to find the trajectories of shear flow instability waves. Two cases of flat-plate boundary-layer transition flow are considered. In the first case, the slowly varying background flow is given by velocity profiles fitted to the experimental work of Klebanoff et al. (1962); the second case uses the recent work of Williams et al. (1984). A family of cubic-tanh profiles is fitted to the experimental instantaneous profiles thus providing the local dispersion relation which is given by a small wavenumber approximation to the Rayleigh equation. In both cases the secondary wave packets experience focussing in the location of breakdown. The results also indicate the importance of wave trapping in the breakdown process. This work is further verification of Landahl's theory of breakdown originally proposed in 1972.

In addition to ray tracing, this work explores the mixed spatial and temporal instability problem for a Falkner-Skan-like family of velocity profiles. An analog in the mixed spatial-temporal instability problem of a well-known result due to Tollmien (1935) in the temporal instability problem is derived. The results also suggest there is a counterpart to the Rayleigh inflection point theorem for the mixed temporal and spatial instability problem.

TABLE OF CONTENTS

ACKNOWLEDGMENTS iv

ABSTRACT vi

TABLE OF CONTENTS viii

LIST OF ILLUSTRATIONS x

NOMENCLATURE xvi

Chapter

I INTRODUCTION 1

II LANDAHL'S THEORY CONCERNING THE WAVE MECHANICS OF BREAKDOWN AND SUBSEQUENT MODIFICATIONS TO ACCOUNT FOR NON-CONSERVATIVE SYSTEMS 18

2.1 Whitham's Kinematic Wave Theory 19

2.1.1 Several Interpretations of Group Velocity. 20

2.2 Whitham's Variational Principle and Wave Action Density. 25

2.3 Landahl's Formulation of the Wave Action Density Equation and His Breakdown Theory. 29

2.4 Criticisms of Landahl's Work and Subsequent Modifications 42

2.5 Russell's Derivation of the Wave Action Density Equation 45

III DERIVATION OF CLASSICAL TEMPORAL STABILITY RESULTS AND INTRODUCTION TO THE MIXED STABILITY PROBLEM

3.1 Derivation of Several Results from Classical Stability Theory 56

3.1.1 Derivation of the Rayleigh Stability Equation 56

3.1.2 Derivation of the Rayleigh Inflection Point Theorem 61

3.1.3 Derivation of the Small-Wavenumber Approximation to the Rayleigh Equation . . 62

3.1.4 Derivation of Tollmien's Vanishingly Small Wavenumber Expression. 65

3.1.5 Derivation of Tollmien's Neutral Mode Solution 68

Chapter Page

3.2 Russell's Small-Wavenumber Approximation Solution of the Rayleigh Equation 71
3.3 Comparison of Stability Results for Cubic-Tanh Family of Profiles with Known Results. 75
3.4 The Mixed Stability Problem for the Falkner-Skan-like Family of Profiles . . . 85
3.4.1 Derivation of Vanishingly Small-Wavenumber Expression for the Mixed Stability Problem 96

IV ONE DIMENSIONAL SHEAR WAVE TRAJECTORIES 103
4.1 Equations of One-Dimensional Shear Flow . . 104
4.1.1 Landahl's Breakdown Condition for One-Dimensional Waves 113
4.2 Comparing Landahl's Theory of Breakdown with the Experimental Results of Klebanoff et al. 117
4.3 Comparison with the Experimental Results of Williams et al 141

V SUMMARY AND CONCLUSIONS 157
5.1 Summary . . . . . .
5.2 Conclusions 160

APPENDIX
Equations Governing the Motion of Secondary Instability Waves in a Three Dimensional Shear Flow 165

REFERENCES 174

LIST OF ILLUSTRATIONS

Figure		Page
1.1	Typical sketch of a boundary layer on a flat plate from an undergraduate engineering textbook (from Fox & McDonald (1978))	2
1.2	Spanwise distribution of intensity of u-fluctuations at different distances downstream of vibrating ribbon. 145 c/s wave y=0.042 in. $U_\infty/\nu = 3.1 \times 10^5$ ft^{-1} $x_1 = 3$ in. $x_1 = 6$ in. $x_1 = 7.5$ in. (from Klebanoff et al. (1962))	5
1.3	Growth in intensity of u-fluctuation, 145 c/s wave y = 0.12 in. z = -0.2 in. $U_\infty/\nu = 3.1 \times 10^5$ ft^{-1} (from Klebanoff et al. (1962))	7
1.4	Variation in u'_{rms} maxima in the streamwise direction measured at the fixed spanwise location, Z = 0.5 cm. The point Z=0 corresponds to the center of the flat plate The point Z=0.5 cm seems to correspond to the location of the "head" of the vortex loop observed at X=60 cm. Note the rapid growth in u'_{rms} between X=50 and X=60 cm (data taken from Figure 8 of Williams et al. (1984)) . .	13
2.1	The linear combination of two sine-waves	22
2.2	A geometrical interpretation of the Jacobian J	37
2.3	Fitted velocity profiles to the instantaneous velocity profiles at station C and station D (from Landahl (1972), figures 6 and 8)	41
2.4	(a) Dispersion diagram for instantaneous profile at station C (b) Dispersion diagram for instantaneous profile at station D. (from Landahl (1972), figures 7 and 9) .	41
3.1	Schematic diagram illustrating the four profiles admitting four classes of modes from Russell's solution to the small wavenumber approximation of the Rayleigh equation	73

3.2 The left graph shows a member of the Falkner-Skan-like family of velocity profiles, the corresponding graph on the right indicates d^2U/dy^2 as a function of y. The second derivatives are extremely small for y=0, but not exactly zero. y_o/δ=-0.01 with (a) n=0.1; (b) n=0.2; (c) n=0.35; (d) n=0.5; (e) n=0.7. Profile (f) represents the Blasius profile with n=0.74985 and y_o/δ= 0.02 78

3.3 Comparison between profile (f) of the Falkner-Skan-like family of profiles and the Blasius profile. The Blasius results are shown as □ with the solid line indicating the result of setting n=0.74985 and $y_o/$ =0.02 in the cubic-tanh profile 79

3.4 A member of the Falkner-Skan-like family of velocity profiles is shown to the left, with the corresponding temporal dispersion relation to the right. In all cases, stricly real $k\delta$ was the input parameter, giving complex value of c. y_o/δ = -0.01 with variable values of n to model the effect of the adverse pressure gradient. (a) n=0.1; (b) n=0.2; (c) n=0.35; (d) n=0.5; (e) n=0.7. Profile (f) corresponds to the Blasius profile with n=0.74985, y_o/δ = 0.02 83

3.5 A member of the Falkner-Skan-like family of velocity profiles is shown to the left with the corresponding "mixed" dispersion relation to the right. In all cases, strictly real group velocity, c_g, was the input parameter, giving complex values $k\delta$ and c. y_o/δ =-0.01 with variable values of n. (a) n=0.01; (b) n=0.2; (c) n=0.35; (d) n=0.5; (e) n=0.7. Profile (f) corresponds to the Blasius profile with n=0.74985, y_o/δ=0.02 95

3.6 A member of the Falkner-Skan-like family of velocity profiles is shown to the left with the corresponding "mixed" dispersion to the right. $-Im(d\theta/dt)$ represents the total rate of growth of a disturbance, both in space and time. In all cases, strictly real group velocity, c_g, was the input parameter, giving complex values for $d\theta/dt$. $y_o/\delta = -0.01$ with variable values of n. (a) n=0.1; (b) n=0.2; (c) n=0.35; (d) n=0.5; (e) n=0.7. Profile (f) corresponds to the Blasius profile with n=0.74985, $y_o/\delta = 0.02$. 99

4.1 Schematic diagram showing the "filtering scheme" proposed to approximate the solution of the characteristic equations (4.11 a,b,) 110

4.2 The instantaneous velocity profiles and dispersion relations for station C of the Klebanoff et al. data (1962)
(a) Klebanoff et al. data is shown as•. The solid line is the velocity profile that Landahl fitted to the data. The corresponding dispersion relations are shown to the right, found from a numerical solution of the Orr-Sommerfeld equation.
(b) Curve fitted using n= 0.15, y_o = 0.65. Klebanoff et al. data is shown as □. The dispersion relations for the temporal instability problem found using the small $k\delta$ approximation to the Rayleigh equation. 118

4.3 (a) Landahl's curve fit to the data of Klebanoff et al. for the instantaneous velocity profile at station D. The corresponding dispersion relations are shown to the right, found from a numerical solution of the Orr-Sommerfeld equation.
(b) Curve fitted to the instantaneous velocity data, shown as □ , at station D using y_o=0.8, n=0.15. The dispersion relations for the temporal stability problem found using the small $k\delta$ approximation are shown to the right.
(c) Curve fitted to the average velocity data, shown as □ , at station D using y_o=1.0, n=0.3. The dispersion relations for the temporal stability problem found by using the small $k\delta$ approximation are shown to the right. 120

4.4 (a) Dispersion relations for the velocity profile fit to the average velocity data at station D. The group velocity is the input parameter, giving the results shown. On the graphs for Im(c) versus Re(c) and Im(kδ) versus Re(kδ) the input values for group velocity, c_g are indicated by the following symbols: □ c_g/U =0.6; △ c_g/U =0.7; ○ c_g/U =0.8; ○ c_g/U =0.9
(b) Dispersion relations for the velocity profile fit to the instantaneous velocity data at station D. The group velocity is the input parameter, giving the results shown. The same symbols were used to indicate increments in c_g.
(c) Dispersion relations for the velocity profile fit to the instantaneous velocity data at station C. The group velocity is the input parameter, giving the results shown. The same symbols were used to indicate increments in c_g. 127

4.5 Velocity profiles of the cubic-tanh family of profiles that model the slowly varying background flow "felt" by the secondary wave packet.
$y_o = 1 - 0.2 \cos(\varepsilon\xi)$; $n = 0.5 - 0.15 \cos(\varepsilon\xi)$. 130

4.6 Secondary wave packet trajectories in the vicinity of the primary wave crest where $\xi = 0$ corresponds to the primary wave crest where $\xi = x - c_o t$. $c_o/U_\infty = 0.575$, the phase velocity of the primary wave. Focussing occurs when $c_g/U_\infty = c_o/U_\infty = 0.575$. 131

4.7 A family of trajectories with initial position, $\xi = -1.0$. The phase velocity of the prime wave is $c_o = 0.575$. 132

4.8 Two sets of trajectories plotted in order to compare the "manipulated" solution ($Im(c_g) = 0$) with the "unmanipulated" solution ($Im(c_g) \neq 0$, $\xi = x + i\sigma$). All have the same initial position, $\xi_o = -1.0$. The phase velocity of the primary wave is $c_o/U_\infty = 0.575$. . 136

4.9 (a) The value of $Im(\Omega)$ as a function of distance, , is shown in the top graph. The value of $Re(\Omega)$ as a function of distance, , along a trajectory is shown in the bottom of the graph. Note that $\Omega_i \ll \Omega_r$
(b) The value of $Im(c_g)$ along a trajectory is plotted versus the value of $Re(c_g)$. The focus point is indicated in the figure, along with the initial value of c_g. Note that $Im(c_g) \ll Re(c_g)$ 137

4.10 Trajectories for a secondary wave packer whose initial position is farther from the primary wave crest, $\xi = -\pi/6$. The phase velocity of the primary wave $c_o = 0.575$. 140

4.11 Trajectories of a secondary wave packet whose initial position is $\xi = -\pi/3$. The bottom two trajectories focus at $c_g/U = 0.575$ 141

4.12 (a) The top figure is reproduced from Williams et al. (1984) for the instantaneous velocity profiles in the (y,t) - plane superposed with the instantaneous projections of the velocity vectors as X=60cm. The circle shows the approximate location of the tip of the vortex loop observed by Williams et al.
(b) Members of the cubic-tanh family of velocity profiles fit to the Williams data at phase = 0°, and 120°. For phase equal to 0°, yo = 1.2 and n = 0.1. For phase equal to 120°, yo = 1.4, and n=0.65. The squares represent data points taken from Williams et al.'s data 146

4.13 Velocity profiles of the cubic-tanh family of profiles that model that slowly varying background flow "felt" by the secondary wave packet for the Williams et al. data. 147

4.14 Copy of a figure from Williams et al. (1984). The results presented in this figure were used to calculate the phase velocity of the primary wave, c_o 148

4.15 (a) Dispersion relations for the velocity profile fit to the data of Williams et al. at 0°. The group velocity is the input parameter, giving the results shown. On the graphs for Im(c) versus Re(c) and Im($k\delta$) versus Re($k\delta$) the imput values for group velocity, c, are indicated by the following symbols:
⌓ $c_g/U_\infty = 0.5$; □ $c_g/U_\infty = 0.6$;
△ $c_g/U_\infty = 0.7$; ○ $c_g/U_\infty = 0.8$;
○ $c_g/U_\infty = 0.9$. 151
(b) Dispersion relations for the velocity profile fit to the data of Williams et al. at 120°. The group velocity is the input parameter, giving the results shown. On the graphs for Im(c) versus Re(c) and

Im($k\delta$) versus Re($k\delta$) the input values for group velocity, c_g are indicated by the following symbols:
⊠ c_g/U_∞ = 0.2; ⊖ c_g/U_∞ = 0.3;
+ c_g/U_∞ = 0.4; ⌓ c_g/U_∞ = 0.5;
□ c_g/U_∞ = 0.6; △ c_g/U_∞ = 0.7;
○ c_g/U_∞ = 0.8; ○ c_g/U_∞ = 0.9 151

4.16 Secondary wave packet trajectories in the vicinity of the primary wave crest. $c_o/U = 0.64$, the phase velocity of the primary wave. $\xi = 0$ is the primary wave crest. Trajectory 1 will be referred to in the text 152

4.17 Secondary wave packet trajectories far from the primary wave crest. $c_o/U = 0.64$, the phase velocity of the primary wave. These trajectories have the same initial position, $\xi_o = \pi/2$. Trajectory 1' will be referred to in the text 153

NOMENCLATURE

This list includes the most frequently used symbols. Other special symbols used only in a derivation will be defined within the text of the derivation.

a^2	square-amplitude for dispersive wave
A^2	observed square-amplitude for shear flow waves
A_0	dimensionless constant in cubic-tanh velocity profile
A_1	dimensionless constant in cubic-tanh velocity profile
A_2	dimensionless constant in cubic-tanh velocity profile
c	phase velocity
c_o	phase velocity of primary wave
c_g	group velocity
Im	imaginary part of a complex quantity
J	Jacobian
k	wavenumber
L	Lagrangian
$\mathcal{L}$	phase averaged Lagrangian
$\mathcal{L}_\omega$	wave action density

n	dimensionless constant in cubic-tanh velocity profile
r	dimensionless coordinate normal to surface
Re	real part of a complex quantity
U	streamwise velocity component of mean flow
W	spanwise velocity component of mean flow
x	streamwise coordinate
y	coordinate normal to surface
y_o	constant in cubic-tanh velocity profile
$y_{o.e.}$	y-value at edge of boundary layer
z	spanwise coordinate
α	wavenumber component in x-direction
β	wavenumber component in z-direction
δ	reference length in y-direction
ϵ	small parameter
ϵ_{rf}	small parameter associated with smallness of reference flow
ϵ_δ	small parameter associated with smallness of disturbance amplitude
ϵ_w	small parameter associated with smallness of changes of the wave packet
ξ	dimensionless streamwise coordinate
ν	kinematic viscosity
θ	phase function
ω	frequency
Ω	the dispersion relation $\omega = \Omega(k,x,t)$

subscripts

α	derivative with respect to α keeping x,z,t,β constant
β	derivative with respect to β keeping x,z,t,α constant
c	critical layer
e	extremum
i	imaginary part of a complex quantity
o	initial value
q	disturbance amplitude measure
r	real part of a complex quantity
rf	reference flow measure
w	wall
∞	free stream
x	derivative with respect to x keeping z,t, α, β constant
z	derivative with respect to z keeping x,t, α, β constant

CHAPTER ONE

INTRODUCTION

Typical engineering undergraduates may initially hear the word "transition", in the context of flat-plate boundary layers, in their first fluid mechanics course. The instructor may sketch a figure similar to the one in Figure 1.1, reproduced from an undergraduate text in fluid mechanics by Fox and McDonald (1978). The transition region is left blank and several sentences involving the word "instability" may be mentioned. The instructor will spend most of the transition lecture time on the notion of a critical Reynolds number or a range of Reynolds numbers which indicate whether a laminar-flow analysis is needed or whether the student can assume turbulent flow.

For most undergraduate engineering students little more need be said about transition, in practice they will be asked to give a skin-friction coefficient estimate, and not explain the details of the transition process. Furthermore, there is such a large volume of

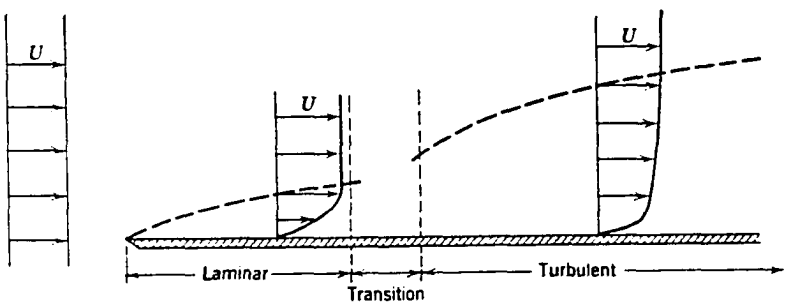

Figure 1.1: Typical sketch of a boundary layer on a flat plate from an undergraduate engineering textbook (from Fox & McDonald (1978))

material covered in the first fluid mechanics course that there is little time to cover the known details of transition.

The "blank" region shown in Figure 1.1 doesn't provide a clue to the complex physical mechanisms involved in the transition process, neither does the "blank" do justice to the research efforts spent in understanding transition. Historically, some of the most brilliant fluid mechanics researchers have worked on the transition problem, trying to fill in the "blank" region, either with theoretical or experimental analysis. To date, no theory exists to describe the entire transition process, in part because there is no general agreement on the physical processes involved. However, many experimental studies have contributed to the current understanding of the details of the transition process. The list of classic experiments in transition would include, among many research efforts, the following: the work of Osborne Reynolds (1883) describing the circumstances of transition in pipe flow; the detailed experiments of Schubauer and Skramstad (1948) verifying the existence of Tollmien-Schlicting waves; Emmons' (1951) investigation of the turbulent spot; and the work of Schubauer and Klebanoff (1956) and I. Tani (1962, 1967) investigating the three-dimensional flow structure seen after the appearance of the Tollmien-Schlichting waves.

The following work by no means fills in the "blank". It offers a theoretical explanation for one small part of the transition process documented by the experimentalists, namely the conditions

necessary for the flow to "breakdown" into higher frequency oscillations. But before describing the breakdown theory, originally proposed by Landahl (1972), two experimental studies will be discussed in order to define the term "breakdown".

We begin with a list prepared by Williams et al. (1984) summarizing the current understanding of the stages of transition.

I. appearance of two-dimensional small amplitude linear oscillations (Tollmien-Schlicting waves)
II. amplification (or damping) of TS waves
III. large-amplitude nonlinear oscillations
IV. emergence of transversely periodic three-dimensionality
V. formation of longitudinal vortices and their intensification
VI. formation of inflectional high shear layer
VII. appearance of multiple hairpin eddies (spikes)
VIII. initial appearance of random motions
IX. formation of a turbulent spot
X. coagulation of turbulent spots (turbulent flows)

The experimental investigations of Williams et al. were concerned with stages V and VI of the transition process, in particular mapping the three-dimensional vorticity field at stage VI. Their experiment was conducted in a low turbulence water channel. A tightly stretched 0.25 mm diameter, oscillating wire introduced a two-dimensional disturbance into the boundary layer. Sixty cm downstream of the oscillating wire, a primary vortex loop, or

Λ-vortex, formed of the type visualized by Hama, Long, and Hegarty (1957). According to Williams et al., the fluid in the outer part of the boundary layer travels over the Λ -loop to form the inflexional high shear layer, which breaks down into the hairpin vortices.

The process of breakdown to the observed hairpin vortices was also investigated in detail by Klebanoff et al. (1962). Three dimensional controlled disturbances produced by a vibrating ribbon technique were introduced into a two-dimensional boundary layer and their growth and evolution were studied. Spanwise variation in waveamplitude was controlled by placing cellophane tape spacers on the surface beneath the vibrating ribbon. Figure 1.2 shows the spanwise distribution of intensity -- where it is observed the peaks and valleys maintain fixed spanwise position.

Klebanoff et al. observed an abrupt change in the character of the wave motion at a peak. Growth in intensity of u-fluctuations at a fixed y-position (about 0.6 boundary layer thicknesses) measured at a peak is shown in figure 1.3. The distance measured downstream from the vibrating ribbon is x_1 (in inches). The term breakdown was employed by Klebanoff et al. to describe the rapid, almost instantaneous rise in u-fluctuations at a distance of $x_1 = 9$ inches. An oscilloscope trace shows a primary wave relatively free of distortion for $x_1 < 9$ inches. At $x_1 = 9$ inches, the primary wave becomes distorted by a series of high-frequency fluctuations which

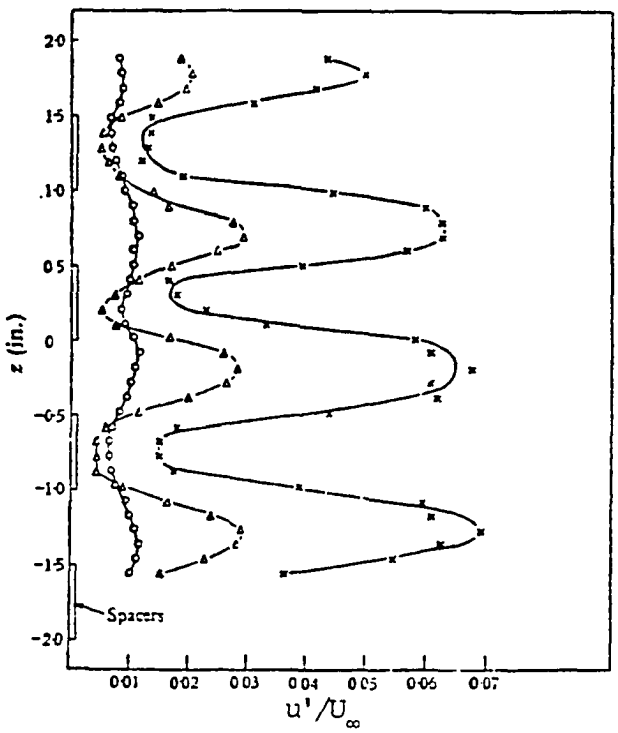

Figure 1.2: Spanwise distribution of intensity of u-fluctuations at different distances downstream of vibrating ribbon. 145c/s wave y=0.042 in.
U_∞/ν = 3.1 x10^5 ft^{-1} o x_1 = 3 in.
Δ x_1 = 6 in. × x_1 = 7.5 in.
(from Klebanoff et al. (1962))

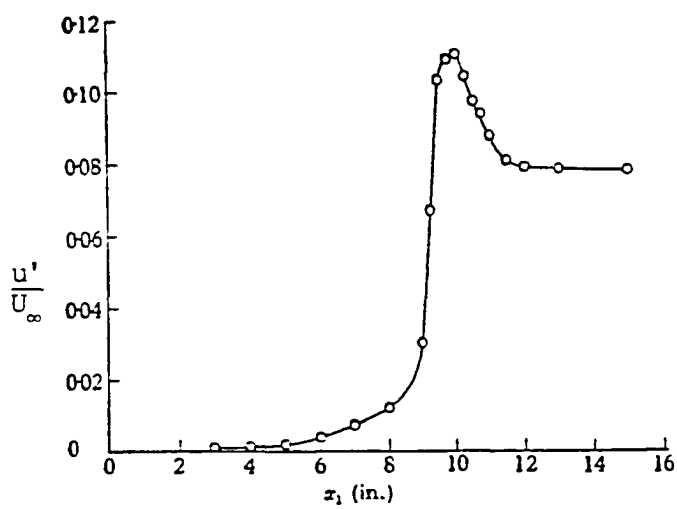

Figure 1.3: Growth in intensity of u-fluctuation
145 c/s wave y = 0.12 in. z = -0.2 in.
$U_\infty/\nu = 3.1 \times 10^5$ ft^{-1}
(from Klebanoff et al. (1962))

form packets. Packet upon packet follow in succession and after about one cycle of the primary wave they have caught up with one another. After breakdown, a new secondary disturbance evolves by about x_1 = 10 inches, which is of higher frequency, shorter wave length than the primary wave. Hairpin vortices are then observed to form in this region. Fully developed turbulent flow is present at around x_1 = 16 inches.

Additional experiments by Kovasznay, Komoda, and Vasudeva (1962), Hama and Nutant (1963), and Obremski and Fejer (1967) confirm the abruptness and localized initial appearance of the high frequency oscillations.

Roughly ten years after Klebanoff et al. published their experimental results, Landahl's article "Wave Mechanics of Breakdown" (1972) appeared. Based on the experimental findings of Klebanoff et al., Landahl proposed a flow condition necessary for breakdown. He had oberved that the growth in intensity of u'-fluctuations in the region from 8 to 10 inches was very rapid. He ruled out the cause of the rapid growth as the lifting up of a small-scale, intense disturbance. Once the higher frequency oscillations appeared, they were felt all across the boundary layer. Landahl also argued that secondary instability resulting from the local, highly inflexional, instantaneous velocity profiles could not be the cause. Exponential amplification of some normal mode could not account for the rapidity

of the streamwise growth of the disturbance. Landahl argued such a rapid increase in u'-fluctuation had to be caused by a highly non-linear mechanism.

For a moment, we will digress from discussing Landahl's specific theory and mention that nonlinear stability theories abound in the literature. A good review of nonlinear stability can be found in Chapter 7 of Drazin and Reid's book (1981). They contend the foundations of nonlinear hydrodynamic stability theory were laid by Landau in 1944, where in a "prophetic essay", he outlined the development of linear instability leading to the onset of turbulence. Almost twenty years later, Stuart (1960) and Watson (1960) applied Landau's equation to plane parallel flow. Other well-known nonlinear stability analyses have been carried out by Stewartson and Stuart (1971) for plane Poiseuille flow. The works mentioned above are weak nonlinear stability theories. For Reynolds number, R, close to the critical Reynolds number, R_c, the amplitude is expressed in terms of an expansion in power of $(R-R_c)$, and some perturbation technique is applied. A recent work by Herbert (1983) surveys the various expansion methods used in weakly nonlinear analysis of a modal disturbance.

Landahl argued the mechanism causing breakdown is strongly nonlinear such as in a shock wave or a hydraulic jump. The "primary wave" which originated at the oscillating wire, distorts as it moves

downstream. This primary wave acts as a wave guide for a series of secondary wave packets that collect at a crest of the primary wave until there is such a build up of energy that the primary wave cannot maintain its present configuration and "breakdown" into a new wave form of higher frequency and shorter wavelength takes place.

In order to trace the trajectories of the secondary wave packets, Landahl assumed the main effect of the primary wave is to produce a slowly inhomogeneous background flow. There is a disparity of length scales between the primary wave and the secondary wave packet so that the packet "feels" a slowly varying background flow. Then the so-called "kinematic wave theory", associated with the name of Whitham (cf. Whitham (1974)) can be applied. Landahl's most important contribution was to propose that kinematic wave theory could be applied to shear waves despite their non-conservative, modal, dispersive nature in the case of small amplification rates. He proposed a modification of the amplitude propagation equation to account for slighlty non-conservative effects. He used work done by Hayes (1970) to account for the modal nature of shear flow instability waves, i.e. waves which propagate in x-z space while their behavior in the cross-space is given as a solution of the Orr-Sommerfeld or Rayleigh equation. Subsequent work by Itoh (1980), Nayfeh (1980), and Landahl (1982), to name a few, has placed kinematic wave theory for shear flow instability waves on a firm mathematical foundation.

Since the secondary wave packets are dispersive waves, a dispersion relation is needed. Landahl used the solution of the Orr-Sommerfeld equation to define the local dispersion relation. He showed the condition for breakdown to be when the secondary wave packet's group velocity, c_g, is equal to the phase velocity of the primary wave, c_o. When c_g equal c_o, the wave packets exhibit space-time focussing on the primary wave crest. He applied the theory to the experimental results of Klebanoff et al. by looking at dispersion relations for instantaneous velocity profiles at various stations and noting that only at the downstream station associated with breakdown did c_g equal c_o.

Landahl's work has left certain unanswered questions, some of which will be addressed in this dissertation. First, Landahl's theory was motivated primarily by the results of Klebanoff et al. We propose to look at the recent results of Williams et al. to see if Landahl's theory can be applied to their experimental findings. This is a risky venture because the focus of Klebanoff et al. research efforts was different than that of Williams et al. Klebanoff et al. were primarily interested in the three dimensionality associated with boundary-layer instability. They introduced well-controlled, spanwise-periodic, three-dimensional disturbances into a two-dimensional

laminary boundary layer. They were seeking a general understanding of the evolution of these well-controlled, three-dimensional disturbances during transition. Williams et al. were interested in a greater understanding of the three-dimensional vorticity field in a special region of the transition process. Specifically, they were interested in the formation of the longitudinal vortices and the formation of the inflectional high-shear layers.

We feel it is possible to use the experimental results of Williams et al. because the focus of their research is in the region of breakdown. The breakdown data presented in Figure 1.3 of Klebanoff et al. were taken at a clearly defined "peak" of the spanwise-periodic disturbance. In the results of Williams et al., a vibrating wire was used to introduce a spanwise disturbance into a laminar boundary layer, but cellophane tape spacers were not used to produce a strong peak-valley structure in the initial disturbance. By looking at the variations in u'_{rms} maxima across the span, for several measuring stations (cf. Figure 8 of Williams et al.), we assume a "peak" occurs at Z = 0.5 cm. A pair of counterrotating mean longitudinal vortices were observed centered about Z = 0.5 cm, X = 60 cm, which suggests Z = 0.5 cm is a local point of symmetry with respect to Z of the flow. It is possible to aruge that a point of symmetry with respect to Z must be either a peak or valley, and the u'_{rms} values suggest a peak. The data shown in Figure 1.4 were taken from the spanwise location, Z = 0.5 cm.

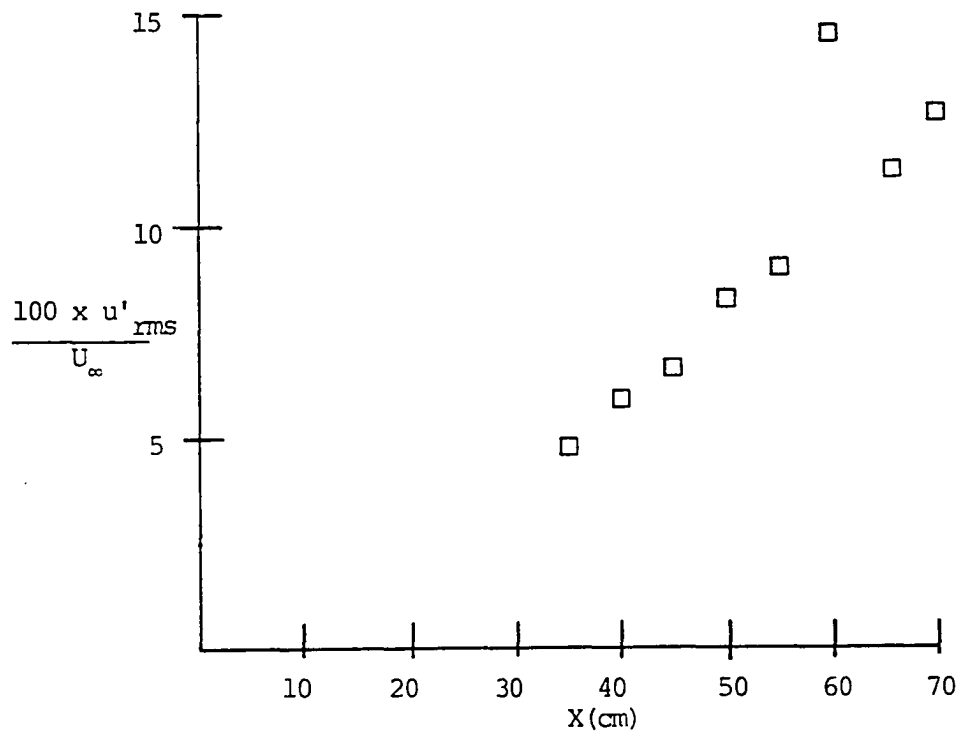

Figure 1.4: Variation of u'_{rms} maxima in the streamwise direction measured at the fixed spanwise location, Z = 0.5 cm. The point Z=0 corresponds to the center of the flat plate. The point Z = 0.5 cm seems to correspond to the location of the "head" of the vortex loop observed at X = 60 cm. Note the rapid growth in u'_{rms} between X=50 and X=60 cm.
(data taken from Figure 8 of Williams et al. (1984))

A rapid increase in u'_{rms} fluctuation values can be seen in Figure 1.4. These results are similar to those measured by Klebanoff et al. and are shown in Figure 1.3. Furthermore, Williams et al. measure inflectional high-shear layer velocity profiles at X = 60 cm, the point of breakdown, and report similar results slightly upstream of X = 60 cm. Such profiles are also observed by Klebanoff et al. in the vicinity of breakdown. Hence, we feel that breakdown occurs in the work of Williams et al. close to the downstream position, X = 60 cm. Later we will use the instantaneous velocity profiles measured at X = 60 cm to see if Landahl's theory predicts breakdown at this location. It is unfortunate that instantaneous velocity profiles upstream of X = 60 cm are not provided in the Williams et al. paper. Because of this, we will not be able to show that upstream of the neighborhood of X = 60 cm, breakdown cannot occur.

To show that Landahl's condition for breakdown holds in the work of Williams et al. will provide further coaberration of his theory. If space-time focussing occurs for the results of Williams et al., then we can argue that constructive interference in a superposition of linear shear waves is just as important to laminar-turbulent transition as the exponential amplification of an individual Fourier component making up that superposition. That is, the behavior of a shear wave packet is important to the transition process.

The second major question this dissertation proposes to answer is concerned with the applicability of the kinematic wave equations to non-conservative systems. The kinematic wave equations can be solved by means of the method of characteristics, and no problem arises for strictly real dispersion relations. Shear flow instability waves have complex dispersion relations, found as solutions of the Orr-Sommerfeld or Rayleigh equations. Consequently, group velocity and position become complex valued for the characteristic form of the kinematic wave equations. We will implement a filtering scheme to eliminate the imaginary part of group velocity and position. We plan to show this filtering scheme gives good results for the propagation of the secondary wave packet. We will examine a large number of secondary wave packet trajectories, both in the vicinity of the primary wave crest and also far from the primary wave crest in order to better understand the focussing phenomenon.

The final question discussed in this work is independent of Landahl's breakdown theory. A small-wavenumber approximation to the Rayleigh equation will be used to define the local dispersion relation. In the derivation of this dispersion relation no assumption about the realness of wavenumber was made, so the dispersion relation can describe both temporally and spatially growing waves. We refer to this as the "mixed" spatial-temporal instability problem. We propose to examine the mixed spatial-temporal problem for a Falkner-Skan-like family of velocity profiles. In boundary-layer geometry for the mixed instability problem, there appears to be an analog to the Rayleigh

inflection point theorem for temporal instability. We will derive the analog in the mixed spatial-temporal instability problem of a well-known result due to Tollmien (1935) in the temporal instability problem. There is little literature on the mixed temporal-spatial instability problem, especially for boundary-layer geometry, so the results of the Falkner-Skan-like family of velocity profiles in the mixed instability case represent a novel contribution to the area of hydrodynamic stability theory.

This dissertation is divided into five chapters. Chapter One presents an introduction to Landahl's theory of breakdown. Chapter Two is a "glorified bibliography" of equations and contains no original work of the author. The kinematic wave theory is presented with modifications for non-conservative wave systems. Landahl's theory of breakdown is derived in detail. The final part of Chapter Two presents Russell's (1985) derivation of the amplitude propagation equation for shear flow instability waves. Russell's derivation is included since it begins with the familiar linearized small-disturbance equations of fluid mechanics, rather than Whitham's kinematic wave theory.

Chapter Three begins with several derivations of classical hydrodynamic stability theory. The small-wavenumber approximation to the Rayleigh equation is solved in the temporal instability case for a

Falkner-Skan-like family of velocity profiles and the results are compared with classical stability theories. The last section of Chapter Three contains novel results for the mixed temporal-spatial instability problem in the case of a Falkner-Skan-like family of velocity profiles. The analog in the mixed spatial-temporal instability problem of a well-known result of Tollmien's in the temporal instability problem is derived at the close of Chapter 3.

Chapter Four presents Landahl's theory of breakdown applied to the experimental results of Klebanoff et al. and Williams et al. The chapter is fairly self-contained so that the reader familiar with the past research of Landahl's concerning breakdown can skip Chapter Two without much difficulty. The trajectories of one-dimensional secondary wave packets traveling through a weakly non-uniform bakcground flow are presented. Results indicating th· effect of focussing and exponential amplification of the wave packets are presented.

Chapter Five summarizes the results and offers an explanation for the appearance of the hairpin vortices after breakdown based on focussing of the secondary wave packets. The Appendix contains a derivation of the equations for three dimensional shear waves. This is included in order to set up the next logical step in research efforts.

CHAPTER TWO

LANDAHL'S THEORY CONCERNING THE WAVE MECHANICS OF BREAKDOWN AND SUBSEQUENT MODIFICATIONS TO ACCOUNT FOR NON-CONSERVATIVE SYSTEMS

Landahl had observed in the experiments of Klebanoff, Tidstrom, and Sargent (1962) that the secondary disturbances appearing at breakdown have a length scale much smaller than that of the primary instability wave. Hence relative to the secondary wave packet, the primary wave's only effect is to alter the background flow that the secondary wave packet "feels". Thus Landahl began his analysis of breakdown by using the basic ideas of kinematic wave theory developed by Whitham (1965).

This chapter outlines Whitham's kinematic wave theory and Landahl's early formulation of the problem. Subsequent modifications of Landahl's theory that place it on a firmer mathematical foundation are then presented.

2.1 Whitham's Kinematic Wave Theory.

Whitham's kinematic wave theory holds for strictly dispersive waves travelling through a weakly non-uniform background flow. Following his derivation in Chapter 11 of his text (1974), the starting point is a slowly varying wave with a phase function Θ such that $\Theta = \Theta(\vec{x},t)$ where $\vec{x} = (x_1,x_2,x_3)$. Then local frequency and local wavenumber vector k are defined by

$$\omega = -\frac{\partial \Theta}{\partial t} \qquad k_i = \frac{\partial \Theta}{\partial x_i} \tag{2.1}$$

The wave is also governed by the real dispersion relation

$$\omega = \Omega(\vec{k},\vec{x},t) \tag{2.2}$$

Eliminating Θ from (2.1) gives

$$\frac{\partial k_i}{\partial t} + \frac{\partial \omega}{\partial x_i} = 0 \tag{2.3}$$

with the consistency expression

$$\frac{\partial k_i}{\partial x_j} - \frac{\partial k_j}{\partial x_i} = 0 \tag{2.4}$$

Whitham points out that if k is the density of waves, and ω the flux of waves, then equation (3.2) is a statement of the conservation of waves.

From the dispersion relation $\omega = \Omega(\vec{k},\vec{x},t)$ and for a slowly varying wavenumber $\vec{k} = \vec{k}(\vec{x},t)$

$$\frac{\partial \omega}{\partial x_i} = \Omega_{x_i} + \Omega_{k_i} \frac{\partial k_i}{\partial x_i} \tag{2.5}$$

Substituting (2.5) into (2.3) and making use of (2.4) gives

$$\frac{\partial k_i}{\partial t} + \Omega_{k_j} \frac{\partial k_i}{\partial x_j} = -\Omega_{x_i} \tag{2.6}$$

Noting Ω_{k_j} has units of velocity we define the group velocity $c_{g_j} = \Omega_{k_j}$ so that

$$\frac{dk_i}{dt} = -\Omega_{x_i} \qquad \text{on} \tag{2.7}$$

$$\frac{dx_i}{dt} = c_{g_i} \tag{2.8}$$

Equations (2.7) and (2.8) are the wave trajectory equations for a given dispersion relation, equation (2.2). Their solution gives the trajectory of a slowly varying wave packet and the change in wavenumber along the trajectory.

Group velocity

$$c_{g_j} = \Omega_{k_j} \tag{2.9}$$

is the velocity that "falls out" of the equation for wavenumber propagation. There are several physical interpretations for group velocity which indicate it is the relevant velocity for wave packet propagation.

2.1.1 Several Interpretations of Group Velocity

One physical explanation for group velocity is given by Rayleigh for ripples in a pool of water. Consider a small stone dropped into a pool of still water. The ensuing behavoir of the "ripple train" is described by Rayleigh:

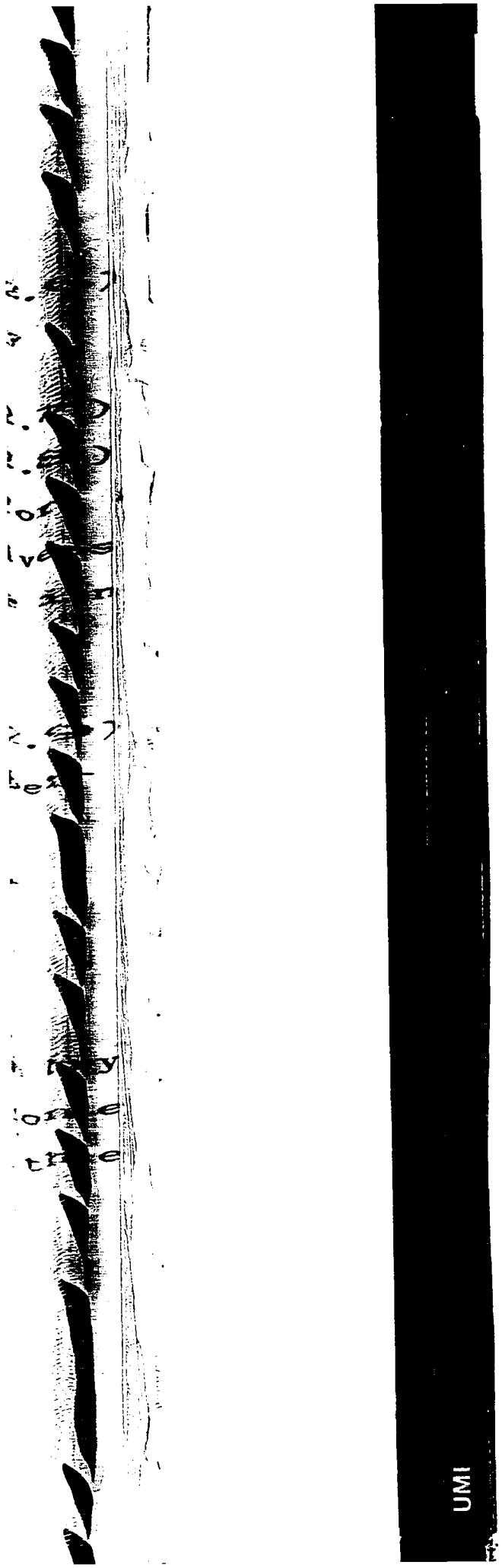

"It has often been remarked that, when a group of waves advanced into still water, the velocity of the group is less than that of the individual waves of which it is composed; the waves appear to advance through the group, dying away as they approach its anterior limit."

Paraphrasing, the phase velocity of the individual ripples is greater than the velocity of the overall group.

The classical analytical explanation of group velocity was given by Stokes (1876). Consider two waves of equal amplitude but different wavelength. Furthermore let the waves be dispersive so frequency will be a function of wavelength. Combining the two

$$a \cos 2\pi(k_1 x - \omega_1 t) + a \cos 2\pi(k_2 x - \omega_2 t) =$$

$$\{2a \cos 2\pi[(k_2-k_1)x - (\omega_2-\omega_1)t]\} \cos 2\pi[(k_1+k_2)x - (\omega_1+\omega_2)t]$$

The first term on the right is lower frequency and may be thought of as a slowly varying amplitude for the more rapidly varying second term. The amplitude term forms an envelope which surrounds the wave packet.

Vol I,pp. 474 Rayleigh, J.W.S."The Theory of Sound',vols.I and II Dover Publications, New York (1945).

UMI

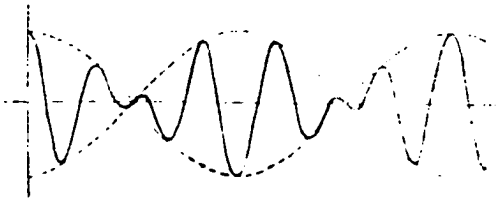

Figure 2.1:

------- amplitude envelope.

_____ wave packet, linear combination of two cosine waves.

The envelope travels with the velocity

$$C_g = \frac{\omega_2 - \omega_1}{k_2 - k_1}$$

In the limit where $\Delta\omega = (\omega_2 - \omega_1) \to 0$ and $\Delta k = (k_2 - k_1) \to 0$, we have the standard definition of the group velocity

$$c_g = \frac{\Delta\omega}{\Delta K} = \frac{d\omega}{dK}$$

Hence the group velocity can be thought of as the velocity of an envelope surrounding the wave packet. Individual waves within the packet travel with phase velocity $c_1 = \frac{\omega_1}{K_1}, c_2 = \frac{\omega_2}{k_2}$.

Lighthill [(1978), especially problem 5, pp. 433-434] presents yet another interpretation for the group velocity in terms of a variational formulation. Consider the phase function

$$\Theta = \Theta(\vec{x}, t)$$

$$d\Theta = \nabla\Theta \cdot d\vec{x} + \frac{\partial\Theta}{\partial t} dt$$

Using definitions for local frequency and wavenumber given by (2.1) yields

$$d\Theta = \vec{K} \cdot d\vec{x} - \omega dt$$

Since the dispersion relation requires $\omega = \Omega(\vec{x}, \vec{K}, t)$, then

$$d\Theta = [\vec{K} \cdot \frac{d\vec{x}}{dt} - \Omega(\vec{x}, \vec{K}, t)] dt$$

Integrating yields

$$\Theta(t_2) - \Theta(t_1) = \int_{t_1}^{t_2} (\vec{K} \cdot \frac{d\vec{x}}{dt} - \Omega(\vec{x}, \vec{K}, t)) dt$$

Take the first variation of both sides

$$\delta[\Theta(t_2) - \Theta(t_1)] = \int_{t_1}^{t_2} [(\frac{d\vec{x}}{dt} - \Omega_{\vec{K}}) \cdot \delta\vec{K} + (\vec{K} \cdot \frac{d(\delta\vec{x})}{dt} - \Omega_{\vec{x}} \cdot \delta\vec{x})] dt$$

Integrating by parts and assuming $\vec{x}(t)$ is prescribed at the endpoints as $\delta\vec{x}(t_1) = \delta\vec{x}(t_2) = 0$ gives

$$\delta[\Theta(t_2)-\Theta(t_1)] = \int_{t_1}^{t_2} [(\frac{d\vec{x}}{dt} - \Omega_{\vec{k}})\cdot\delta\vec{k} - (\frac{d\vec{k}}{dt} + \Omega_{\vec{x}})\cdot\delta\vec{x}]\,dt$$

For $\delta[\Theta(t_2) - \Theta(t_1)] = 0$ we have the requirement

$$\frac{d\vec{x}}{dt} = \Omega_{\vec{k}}$$

and

$$\frac{d\vec{k}}{dt} = -\Omega_{\vec{x}}$$

Thus an observer moving at the group velocity will see the smallest change in the phase function between neighboring components. For a multi-component wave packet this results in the greatest constructive interference among wave components. Referring back to Stokes' example for a linear combination of two cosine waves

$$\text{wave 1} = a\cos 2\pi(k_1x - \omega_1t)$$

$$\text{wave 2} = a\cos 2\pi(k_2x - \omega_2t)$$

we see that maximum constructive interference will occur when $k_1x - \omega_1t = k_2x - \omega_2t$. This is true only for $\frac{x}{t} = \frac{\omega_2-\omega_1}{k_2-k_1}$. Hence, the group velocity is the only velocity that maximizes the constructive interference between these two cosine waves.

A final interpretation of group velocity will be the one used by Whitham. For the case of a uniform medium, equation (2.7)

becomes

$$\frac{dk_i}{dt} = 0$$

Whitham then distinguishes between the phase velocity of a particular wave crest, $c = \frac{\omega}{k}$, and the group velocity of a wave packet, $c_{g_j} = \frac{\partial \omega}{\partial k_j}$. An observer following any particular crest moves with the local phase velocity, c, but sees local wavenumber and frequency changing so that neighboring crests move farther away. An observer moving with the group velocity sees the same local wavenumber and frequency, but crests keep passing the observer. In the case of a non-uniform medium an observer moving with the group velocity no longer sees the same local wavenumber. The wavenumber will change slowly with position. However crests will continue to pass the observer as in the uniform medium case.

2.2 Whitham's Variational Principle and Wave Action Density

Besides wavenumber propagation along a trajectory (equations (2.7) and (2.8)), we are also interested in amplitude propagation. Whitham used a variational principle in order to derive an expression for the "wave action density", a term with dimensions of energy density times time, which scales with square-amplitude for linear problems.

We will present a very simplified derivation of Whitham's equation for wave action density by assuming linear waves. The reader is referred to Chapter 14 of Whitham's text (1975) or his 1970 article for a detailed derivation whichapplies to both linear and non-linear waves. The crux of Whitham's derivation involves a "two timing" technique which distinguishes between two time scales -- one time scale to account for slow k and ω variations, the other time scale to account for the relatively fast oscillations of the wave train. We will apply this "two timing" technique informally.

Begin with the variational principle

$$\delta J = \delta \iint L(\varphi_t, \varphi_{\vec{x}}, \varphi)\, d\vec{x}\, dt = 0$$

for a Lagrangian, L. Suppose we have a slowly varying wave train of the form

$$\varphi \sim Re\left[\hat{A} e^{i\theta}\right]$$
$$= a \cos(\theta + \sigma)$$

where $a = |\hat{A}|$ and $\sigma = \arg(A)$. Substitute this into the variational principle and average over one period

$$\frac{1}{2\pi} \int_0^{2\pi} L(\varphi_t, \varphi_{\vec{x}}, \varphi)\, d\theta = \mathcal{L}(-\theta_t, \theta_{\vec{x}}, a)$$

for $a(\vec{x},t)$ and $\theta(\vec{x},t)$. This is the step where Whitham employed the "two-timing" scale analysis to eliminate terms that vary

slowly with x and t. So to lowest approximation

$$\delta \iint \mathcal{L}(-\theta_t, \theta_{\vec{x}}, a)\, dt\, dx = 0 \tag{2.10}$$

Here $-\theta_t$ is used to preserve symmetry between x and t rather than $+\theta_t$.

Taking variations of (2.10) yields

$$\delta a: \qquad \mathcal{L}_a = 0$$

$$\delta\theta: \qquad \frac{\partial}{\partial t}(\mathcal{L}_{\theta_t}) + \frac{\partial}{\partial x_j}(\mathcal{L}_{\theta_j}) = 0$$

Using definitions of wavenumber and frequency, we have

$$\mathcal{L}_a = 0 \tag{2.11}$$

$$\frac{\partial}{\partial t}(\mathcal{L}_\omega) - \frac{\partial}{\partial x_j}(\mathcal{L}_{k_j}) = 0 \tag{2.12}$$

Whitham then argues the Lagrangian involves energy terms. For linear problems the L must be quadratic in ϕ and its derivatives so that

$$\mathcal{L} = G(\omega, \vec{k})\, a^2 \tag{2.13}$$

Thus (2.11) becomes

$$G(\omega, \vec{k}) = 0 \tag{2.14}$$

which is simply the dispersion relation. Hence for linear problems we do not need to calculate the average Lagrangian, the dispersion relation times square-amplitude will provide $\mathcal{L}$.

Noting that equation (2.12) can be written

$$\frac{\partial}{\partial t}(\mathcal{A}_\omega) - \frac{\partial}{\partial x_j}\left(\mathcal{A}_\omega \frac{\partial \omega}{\partial k_j}\right) = 0 \qquad (2.12a)$$

by the chain rule and using the definition of group velocity, we get

$$\frac{\partial}{\partial t}(\mathcal{A}_\omega) - \frac{\partial}{\partial x_j}(\mathcal{A}_\omega\, c_{gj}) = 0$$

Substituting (2.13) into the above expression yields

$$\frac{\partial}{\partial t}(G_\omega a^2) - \frac{\partial}{\partial x_j}(G_\omega a^2\, c_{gj}) = 0$$

Expanding gives

$$G_\omega\left[\frac{\partial a^2}{\partial t} - \frac{\partial}{\partial x_j}(a^2 c_{gj})\right] + a^2 \frac{\partial G_\omega}{\partial t} + c_{gj} a^2 \frac{\partial G_\omega}{\partial x_j} = 0$$

and then using (2.3) and (2.4) to eliminate $a^2\left[\frac{\partial G_\omega}{\partial t} + c_{gj}\frac{\partial G_\omega}{\partial x_j}\right]$ yields

$$\frac{\partial}{\partial t}(a^2) - \frac{\partial}{\partial x_j}(a^2 c_{gj}) = 0 \qquad (2.15)$$

which is the expression for square-amplitude propagation for linear waves.

2.3 Landahl's Formulation of the Wave Action Density Equation and His Breakdown Theory.

The above derivation for equation (2.15) will be adequate for now since we are trying to briefly present Whitham's kinematic wave theory. However, we will return to the derivation of the wave action density equation later in this chapter. In general, Whitham's results hold for dispersive "local" waves in a conservative system propagating through a weakly non-uniform background flow. Instability waves in shear flows are termed "modal" waves rather than "local" waves. "Local" waves typically propagate in x,y,z, and t space. "Modal" waves typically propogate in x,z, and t space while their behavoir in the cross space, y-direction, is governed by an eigen solution of an eigenvalue problem such as the Rayleigh or Orr-Sommerfeld equation. Since shear flow instability waves are not conservative, their amplitude undergoes exponential amplification or decay. Finally, this is a doctoral dissertation in fluid mechanics. We are well into Chapter 2 but nowhere have the familiar equations for mass and momentum appeared. Later we will present a derivation of equation (2.15) for non-conservative modal shear flow instability waves that begins with the beloved Euler equations. For now we will continue with Landahl's application of kinematic wave theory.

In 1972 Landahl formulated his theory to describe the conditions of breakdown of laminar flow into high frequency oscillations. He began with Whitham's kinematic wave theory as derived by Hayes (1970). Hayes' analysis allowed for modal as well as local waves. Landahl assumed that instability waves in shear flow are modal waves which propogate in the x,z,t space. Their behavior with y is given by the solution of the Orr-Sommerfeld problem for a local instantaneous velocity profile.

He also noted that shear flow instability waves are non-conservative.* In Whitham's formulation, dispersive waves of the general form

$$\varphi(\vec{x},t) = A \exp\left[i \vec{k}\cdot\vec{x} - i\omega t \right]$$

propagate in a conservative system where $\vec{k}$ and ω are real values, governed by a strictly real dispersion relation. Rayleigh or Orr-Sommerfeld waves have complex dispersion relations where both k and ω may be complex valued so that their amplitude

---

*Landahl referred to shear instability waves as dissipative. This term is often associated with viscosity so we will use the term "non-conservative" to avoid ambiguity.

experiences exponential growth or damping. Landahl reformulated the square-amplitude equation (2.15) to allow for a slightly non-conservative system.

Begin with a complex dispersion relation

$$\Omega = \Omega_r + i\,\Omega_i$$

where $|\Omega_i| \ll |\Omega_r|$. Assume a strictly real wavenumber k but a complex phase velocity c (a typical eigensolution of the Orr-Sommerfeld equation). Now assume that total wave amplitude, A, is composed of two parts

$$A = a \exp(\Omega_i t) \tag{2.16}$$

where $\exp(\Omega_i t)$ is the non-conservative exponential amplification contribution, and a is the contribution due to dispersion and focussing of waves. Substituting (2.16) into the square-amplitude equation (2.15) gives

$$\frac{1}{A^2}\,\frac{dA^2}{dt} = -\nabla\cdot\vec{c}_g + 2\,\Omega_i \tag{2.17}$$

The term $\nabla\cdot\vec{c}_g$ in equation (2.17) must be evaluted carefully. Great care must be taken to distinguish between the "physical space" variables and the "characteristic space" variables.

(1) Let the symbols $\frac{\partial}{\partial x}$, $\frac{\partial}{\partial y}$, $\frac{\partial}{\partial z}$, $\frac{\partial}{\partial t}$, and ∇ be used for partial derivatives in the "physical space" whose variables are (x,y,z,t). For example, partial differentiation with respect to x in "physical space" is done keeping y,z, and t constant. Wavenumber components are allowed to vary with $\vec{x}$ or t.

(2) Let the symbols $(\ )_x$, $(\ )_y$, $(\ )_z$, $(\ )_\alpha$, $(\ )_\beta$, $(\ )_t$ by used for partial derivatives in the "characteristic space" whose variables are (x,y,z,α,β,t), where $\vec{k} = k(\alpha\hat{i}_1 + \beta\hat{i}_3)$. Partial differentiation with respect to one variable in this space requires the other 5 variables be held constant.

When we write the expression for $\nabla \cdot c_g$ in the above notation, we have

$$\nabla \cdot \vec{c}_g = \Omega_{\alpha x} + \Omega_{\alpha\alpha}\frac{\partial \alpha}{\partial x} + \Omega_{\alpha\beta}\frac{\partial \beta}{\partial x} + \Omega_{\beta z} + \Omega_{\alpha\beta}\frac{\partial \alpha}{\partial z} + \Omega_{\beta\beta}\frac{\partial \beta}{\partial z}$$

The right hand side of the above equation gives us calculable derivatives on a single ray provided propagation equations for the terms $\frac{\partial \alpha}{\partial x}$, $\frac{\partial \beta}{\partial x}$, $\frac{\partial \alpha}{\partial z}$, and $\frac{\partial \beta}{\partial z}$ along a wave packet trajectory can be formulated.

Hayes formulated a propagation equation for the "wavenumber gradient" term. He applied the operator $\frac{\partial (\ )}{\partial x_j}$

(the "physical space" operator) to (2.7) using the complete chain rule expansion whenever the operand involved Ω. For example, applying the operator $\frac{\partial(\ )}{\partial x_1}$ to the x_1-component of (2.7) gives

$$\left[\frac{\partial}{\partial t}\left(\frac{\partial K_1}{\partial x_1}\right) + \Omega_{K_1}\frac{\partial}{\partial x_1}\left(\frac{\partial K_1}{\partial x_1}\right) + \Omega_{K_3}\frac{\partial}{\partial x_3}\left(\frac{\partial K_1}{\partial x_1}\right)\right]$$

$$= -\frac{\partial K_1}{\partial x_1}\Omega_{K_1 K_1}\frac{\partial K_1}{\partial x_1} - \frac{\partial K_1}{\partial x_3}\Omega_{K_3 K_1}\frac{\partial K_1}{\partial x_1}$$

$$-\frac{\partial K_1}{\partial x_1}\Omega_{K_1 K_3}\frac{\partial K_3}{\partial x_1} - \frac{\partial K_1}{\partial x_3}\Omega_{K_3 K_3}\frac{\partial K_3}{\partial x_1}$$

$$-\frac{\partial K_1}{\partial x_1}\Omega_{K_1 x_1} - \frac{\partial K_1}{\partial x_3}\Omega_{K_3 x_1} - \Omega_{x_1 x_1}$$

The result of this laborious calculation is compactly expressed in matrix notation as a propagation equation

$$\frac{d[B]}{dt} = -[B][C][B] - [D]^T[B] - [B][D] - [E] \qquad (2.18)$$

where

$$[G] = \begin{bmatrix} \frac{\partial K_1}{\partial x_1} & \frac{\partial K_1}{\partial x_3} \\ \frac{\partial K_3}{\partial x_1} & \frac{\partial K_3}{\partial x_3} \end{bmatrix} \qquad [C] = \begin{bmatrix} \Omega_{K_1 K_1} & \Omega_{K_1 K_3} \\ \Omega_{K_3 K_1} & \Omega_{K_3 K_3} \end{bmatrix}$$

$$[D] = \begin{bmatrix} \Omega_{K_1 x_1} & \Omega_{K_1 x_3} \\ \Omega_{K_3 x_1} & \Omega_{K_3 x_3} \end{bmatrix} \qquad [E] = \begin{bmatrix} \Omega_{x_1 x_1} & \Omega_{x_1 x_3} \\ \Omega_{x_3 x_1} & \Omega_{x_3 x_3} \end{bmatrix} \qquad (2.19)$$

[B] is symmetric and thus (2.18) represents 3 equations for 3 independent solutions.

Hence Landahl had a system of seven equations that would give the trajectories of shear flow instability waves travelling through slightly non-uniform background flow. The change in wavenumber along a trajectory is given by

$$\frac{dk_i}{dt} = Re\,(-\Omega_{x_i}) \qquad i \in \{1,3\} \qquad (2.20)$$

on

$$\frac{dx_i}{dt} = c_{g_i} \qquad i \in \{1,3\} \qquad (2.21)$$

where

$$c_{g_i} = Re\,(\Omega_{K_i}) \qquad i \in \{1,3\} \qquad (2.22)$$

for the complex dispersion relation

$$\Omega = \Omega_r + i\,\Omega_i$$

The amplitude propagation is given by

$$\frac{1}{A^2}\frac{dA^2}{dt} = -\nabla\cdot\vec{c}_g + 2\Omega_i \qquad i\in\{1,3\} \tag{2.23}$$

where the wavenumber gradient term appearing in (2.23) is given by (2.18). The seven equations, (2.20,21,23,and 18) require initial conditions

$$\left.\begin{aligned} [B] &= [B_o]\,(x_{o_1}, x_{o_3}) \\ x_i &= x_{o_i}\;; \quad k_i = k_{o_i} \end{aligned}\right\} \text{for } t=0,\ i\in\{1,3\} \tag{2.24}$$

It is possible to eliminate $\nabla\cdot\vec{c}_g$ from (2.23) if a Jacobian determinant J is defined. Let (x_1,x_3) be the coordinates (x,z). Along a trajectory the "present" position coordinates (x,z) are given as

$$x = x(x_o, z_o, t) \;; \quad (x)_{t=o} = x_o$$

$$z = z(x_o, z_o, t) \;; \quad (z)_{t=o} = z_o$$

We can write an expression relating "present" position coordinates to initial position coordinates as

$$\begin{bmatrix} \frac{\partial}{\partial x_o} \\ \frac{\partial}{\partial z_o} \end{bmatrix} = \begin{bmatrix} \frac{\partial x}{\partial x_o} & \frac{\partial z}{\partial z_o} \\ \frac{\partial x}{\partial z_o} & \frac{\partial z}{\partial z_o} \end{bmatrix} \begin{bmatrix} \frac{\partial}{\partial x} \\ \frac{\partial}{\partial z} \end{bmatrix}$$

Inverting the above expression gives

$$\begin{bmatrix} \frac{\partial}{\partial x} \\ \frac{\partial}{\partial z} \end{bmatrix} = \frac{1}{J}\begin{bmatrix} \frac{\partial z}{\partial z_o} & -\frac{\partial z}{\partial x_o} \\ -\frac{\partial x}{\partial z_o} & \frac{\partial x}{\partial x_o} \end{bmatrix} \begin{bmatrix} \frac{\partial}{\partial x_o} \\ \frac{\partial}{\partial z_o} \end{bmatrix} \tag{2.25}$$

where

$$J = \frac{\partial x}{\partial x_o}\frac{\partial z}{\partial z_o} - \frac{\partial z}{\partial x_o}\frac{\partial x}{\partial z_o} \tag{2.26}$$

An expression for $\frac{1}{J}\frac{dJ}{dt}$ is

$$\frac{1}{J}\frac{dJ}{dt} = \frac{1}{J}\left[\frac{\partial}{\partial x_o}\left[\frac{dx}{dt}\right]\frac{\partial z}{\partial z_o} + \frac{\partial x}{\partial x_o}\frac{\partial}{\partial z_o}\left[\frac{dz}{dt}\right]\right.$$

$$\left. - \frac{\partial}{\partial x_o}\left[\frac{dz}{dt}\right]\frac{dx}{dz_o} - \frac{\partial z}{\partial x_o}\frac{\partial}{\partial z_o}\left[\frac{dx}{dt}\right]\right] \tag{2.27}$$

From (2.21), we have

$$\frac{dx}{dt} = Re(\Omega_\alpha)$$

$$\frac{dz}{dt} = Re(\Omega_\beta)$$

so that (2.27) becomes

$$\frac{1}{J}\frac{dJ}{dt} = \frac{1}{J}\left[\frac{\partial}{\partial x_o}(Re(\Omega_\alpha))\frac{\partial z}{\partial z_o} + \frac{\partial x}{\partial x_o}\frac{\partial}{\partial z_o}(Re(\Omega_\beta))\right.$$

$$\left. - \frac{\partial}{\partial x_o}[Re(\Omega_\beta)]\frac{\partial x}{\partial z_o} - \frac{\partial}{\partial z_o}[Re(\Omega_\alpha)]\frac{\partial z}{\partial x_o}\right]$$

Using (2.25) gives

$$\frac{1}{J}\frac{dJ}{dt} = \nabla\cdot\vec{c}_g \tag{2.28}$$

The point where J becomes zero is known as a focus. J can be thought of as a "group area" which changes as the trajectories change. One can visualize J through the use of a geoemetrical model. In Figure 4.2 the "group area" is formed by two incremental changes in the trajectories, dx_o and dz_o. The incremental area is given as

$$dAr = |\vec{OQ} \times \vec{OP}|$$

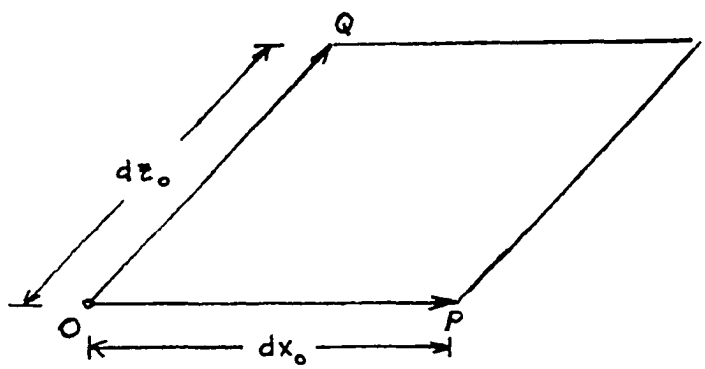

Figure 2.2: A geometrical interpretation of the Jacobian J.

Noting that

$$\vec{OP} = \frac{\partial \vec{x}}{\partial x_o} dx_o$$
$$= \left(\frac{\partial x}{\partial x_o} \hat{i}_1 + \frac{\partial z}{\partial z_o} \hat{i}_3 \right) dx_o$$
$$\vec{OQ} = \frac{\partial \vec{x}}{\partial z_o} dz_o$$
$$= \left(\frac{\partial x}{\partial z_o} \hat{i}_1 + \frac{\partial z}{\partial z_o} \hat{i}_3 \right) dz_o$$

Then

$$d(Ar) = \left| \hat{\imath}_2 \frac{\partial z}{\partial z_0} \frac{\partial x}{\partial x_0} - \hat{\imath}_2 \frac{\partial x}{\partial z_0} \frac{\partial z}{\partial z_0} \right| = J$$

There are two ways for J to become zero. $\vec{OQ}$ and $\vec{OP}$ may become parallel to one another or either $\vec{OQ}$ or $\vec{OP}$ shrinks to zero.

Combination of (2.23) and (2.28) gives

$$A = \frac{\text{constant}}{J} \exp\left[2 \int \Omega_i \, dt \right]$$

which shows for a focus, J = 0, A will become infinitely large provided $\int \Omega_i \, dt \neq -\infty$. Since A is proportional to amplitude-squared, at a focus the wave amplitude becomes infinite. Landahl points out that in reality the wave amplitude will never become infinitely large since the kinetic wave theory becomes invalid near a focus. A more complete theory involving diffraction and non-linear effects should be considered near a focus.

Based on the above analysis, Landahl argued a focus will result in a tremendous build-up of wave amplitude. Thus locating the focus is an essential step in determining the breakdown location. Consider the propagation of a wave packet through an inhomogeneous background flow. The inhomogeneity is caused by a plane travelling primary wave moving with the phase velocity c_0. Furthermore assume that we are near a peak in the experiment of Klebanoff et al. (1962). Due to local symmetry we

expect the tangential component of $\vec{c}_g$ to have an extremum so that

$$\nabla \cdot \vec{c}_g \propto \frac{\partial c_g^{(n)}}{d\xi} \tag{2.2}$$

where $\xi = x - c_o t$ is the coordinate normal to the primary wave front, moving with the primary wave. $c_g^{(n)}$ is the component of the group velocity normal to the wave front so that

$$c_g^{(n)} = \Omega_\alpha \tag{2.30}$$

The equation (2.13) becomes

$$\frac{1}{J} \frac{dJ}{dt} = \frac{\partial c_g^{(n)}}{\partial \xi} \tag{2.31}$$

or

$$\frac{1}{J} \left[\frac{\partial J}{\partial t} + c_g^{(n)} \frac{\partial J}{\partial \xi} \right] = \frac{\partial c_g^{(n)}}{\partial \xi} \tag{2.32}$$

Since the inhomogeneity caused by the primary wave is a frozen pattern moving at c_o, we have

$$\begin{aligned} \frac{\partial J}{\partial t} &= \frac{\partial J}{\partial \xi} \frac{\partial \xi}{\partial t} \\ &= \frac{\partial J}{\partial \xi} (-c_o) \end{aligned} \tag{2.33}$$

Substituting into (2.30) yields

$$\frac{1}{J} (-c_o + c_g^{(n)}) \frac{\partial J}{\partial \xi} = \frac{\partial c_g^{(n)}}{\partial \xi} \tag{2.34}$$

Therefore

$$\frac{\frac{\partial J}{\partial \xi}}{J} = \frac{\frac{\partial c_g^{(n)}}{\partial \xi}}{c_g^{(n)} - c_o} \qquad (2.35)$$

J will be zero whenever the component of the secondary wave packet group velocity normal to the primary wave, $c_g^{(n)}$, becomes equal to the normal component of the phase velocity of the primary wave. Physically, secondary wave packets become trapped at a peak of the primary wave until there is such a build up of energy that nonlinear effects dominate and the flow breaksdown to a new configuration.

The comparison between Landahl's theory and experiments on boundary layer transition by Klebanoff et al (1962) was good to within experimental uncertainty. Landahl fit polynomial expressions to mean and instantaneous velocity profiles measured by Klebanoff et al. Figure 2.3 shows the fitted velocity profiles for station C, upstream of where breakdown occurred. Using a numerical solution of the Orr-Sommerfeld equations (Landahl 1969) for the dispersion relation for the instantaneous velocity profile at station C, Landahl then determined group velocities by graphical differentiation. These results are shown in Figure 2.4a. The group velocity for all unstable wavenumbers shown is greater than the phase velocity of the primary wave, c_o, as measured by Klebanoff et al. At station D, the dispersion relation for the instantaneous profile indicated the phase velocity of the primary

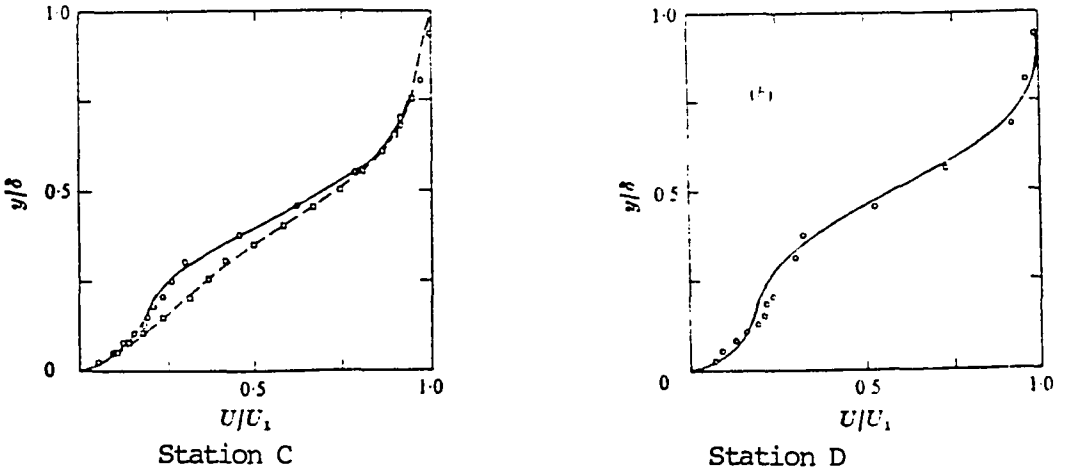

Figure 2.3: Fitted velocity profiles to the instantaneous velocity profiles at station C and station D (from Landahl (1972), figures 6 and 8).

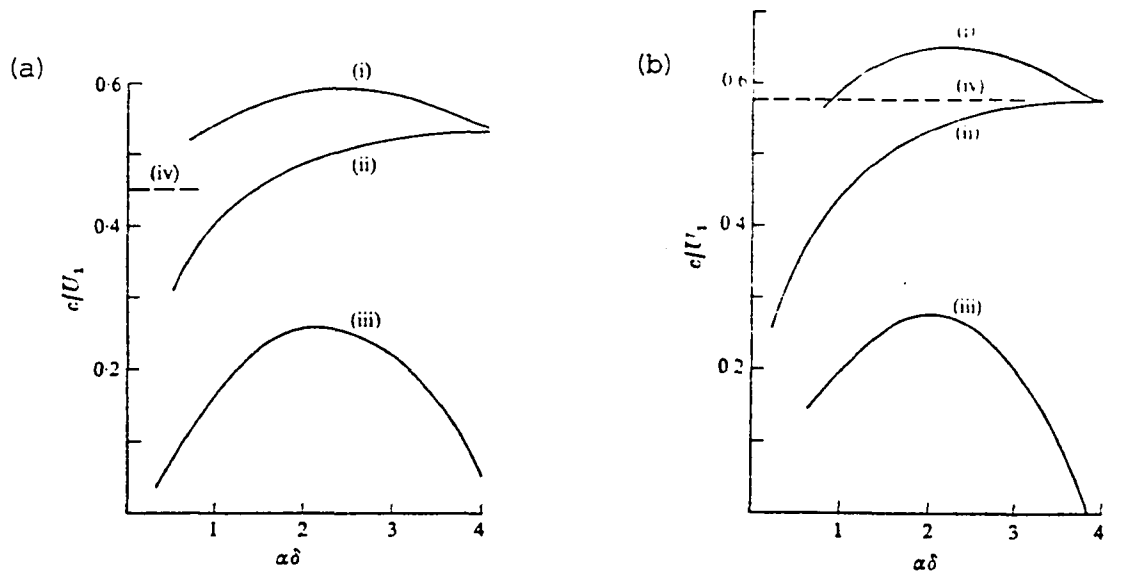

Figure 2.4 (a) Dispersion diagram for instantaneous profile at station C, (i) group velocity, (ii) phase velocity, (iii) growth rate Ω_i, (iv) primary wave phase velocity, c_o

(b) Dispersion diagram for instantaneous profile at station D. Same legend as above.
(from Landahl (1972), Figures 7 and 9)

wave was equal to the group velocity at the shortwave cut off, as shown in figure 2.4b. At station D breakdown to secondary higher frequency oscillations should occur based on Landahl's analysis since $c_g = c_o$ in equation (2.35). Klebanoff et al. observed breakdown at station D giving good quantititave agreement with Landahl's theory. It should be noted that Landahl did not trace the trajectories of wave packets by solving equations (2.18,20,21,23).

2.4 Criticisms of Landahl's Work and Subsequent Modifications.

Landahl received sharp criticism for his derivation of (2.23). Stewartson (1972) argued the equation was limited in validity to waves which were much more dispersive than non-conservative -- not generally the case for Tollmien-Schlichting instability waves. By using a centered wavenumber expansion for the dispersion relation, Stewartson further argued that Ω_i is not small compared to Ω_r. In addition, Stewartson felt the focussing phenomenon is of secondary importance in non-conservative systems.* Nonlinear effects are more important in the breakdown process in Stewartson's opinion.

---

*though Stewartson's evidence for this was based entirely on analysis of the "far field" wave pattern (where $J \rightarrow \infty$) rather than of a focus (where $J \rightarrow 0$), the case actually considered by Landahl.

Because of Stewartson's criticisms, subsequent researchers have used different approaches to put the theory of non-conservative wave trains on firmer foundation. Chin (1980) and Landahl (1982) began with the complex dispersion relation expressing frequency as a function of wavenumber. By applying the Fourier integral theorem, they found a relationship between an initial wavenumber distribution function and a dependent variable Ψ may be written down. Expanding the dispersion relation in a complete Taylor series in the wavenumber allows an infinite term partial differential equation for Ψ to be derived. Chin then applied the WKBJ method to the solution of the equation for Ψ. To a few orders in the WKBJ expansion Chin was able to analytically sum the infinite series associated with the original power series expansion in wavenumber. One result of Chin's was an equation for the propogation of square-amplitude for a slowly varying wave train.

Landahl (1982) applied Chin's method. By selecting a complex wavenumber that makes the group velocity real, he modified Chin's theory to improve the accuracy of the approximation in the far field. The 1982 work by Landahl addressed the earlier criticisms of Stewartson.

Nayfeh (1980) applied a multiple scale expansion to the solution of the small disturbance equations of motion. Itoh (1980,1981) also began with the small disturbance equations and used a WKBJ approximation. In both cases, the lower order

balance in the equations of motion ignored non-uniformity of the parameters (such as wavenumber) of the wave train. The next higher order balance involved the solution of an inhomogeneous equation whose homogeneous operator was the same as the lowest order problem. A necessary condition for the existence of nontrivial solutions of the inhomogeneous problem was that a certain solvability condition be satisified. When this solvability condition was manipulated by Itoh and Nayfeh, the result was a propagation equation for the local square-amplitude of the wave train.

Russell (1985) uses yet another approach to derive the amplitude propagation equation. Recall shear flow instabiity waves are modal, they do not propagate in a direction transverse to the undisturbed flow. Shear flow instability waves are non-conservative, propagating through a weakly non-uniform background flow. Using ideas of Hayes (1970a) for the theory of conservative modal waves and the theory of Jiemenez and Whitham (1976) for nonconservative local waves, Russell found an amplitude propagation equation compatible with those of Itoh (1980), Nayfeh (1980), and Landahl (1982). The last part of this chapter will involve a brief account of Russell's derivation.

2.5 Russell's Derivation of the Wave Action Density Equation.

Beginning with the disturbance equation that results from subtracting the equations satisfied by a reference flow solution (U_1,U_2,U_3) from those satisfied by a neighboring flow solution $(U_1 + u_1, U_2 + u_2, U_3 + u_3)$ and linearizing for small amplitude, we get

$$\left(\frac{\partial}{\partial t} + U_1 \frac{\partial}{\partial x_1} + U_3 \frac{\partial}{\partial x_3}\right) u_i + u_2 \left(\frac{\partial U_1}{\partial x_2}\delta_{1i} + \frac{\partial U_3}{\partial x_2}\delta_{3i}\right) = -\frac{1}{\rho}\frac{\partial p}{\partial x_i} + \mathcal{O}(\epsilon_{rf}, \epsilon_\beta^2) \tag{2.36}$$

$$\frac{\partial u_j}{\partial x_j} = 0 \tag{2.37}$$

Here ϵ_{rf} is a small parameter associated with the "flatness" of the reference flow. If (l_1,l_2,l_3) are typical length scales in the (x_1,x_2,x_3) directions then we define

$$\epsilon_{rf} \equiv l_2 \left[l_1^{-2} + l_3^{-2}\right]^{1/2}$$

for thin shear layer flows

$$\epsilon_{rf} << 1$$

If (Q_1,Q_2,Q_3) denote the magnitude of the velocity components (U_1,U_2,U_3) and

$$\epsilon_\beta^2 \equiv \frac{\max(u_j\, u_j)}{(Q_1^2 + Q_3^2)}$$

then ϵ_β^2 measures the smallness of the disturbance amplitude.

We will change the dependent variables in (2.36) and (2.37) so we can write these equations as Euler equations for a variational principle. The appropriate change of variable is

$$u_i = -\ell sd\,(b_i) + b_2\left[\frac{\partial U_1}{\partial x_2}\,\delta_{1i} + \frac{\partial U_3}{\partial x_2}\,\delta_{3i}\right] \tag{2.38}$$

where

$$\ell sd(\;) = \left(\frac{\partial}{\partial t} + U_1\frac{\partial}{\partial x_1} + U_3\frac{\partial}{\partial x_3}\right)(\;) \tag{2.39}$$

$$b_i \equiv a_i + a_2\left(\frac{\partial U_1}{\partial x_2}\,\delta_{1i} + \frac{\partial U_3}{\partial x_2}\,\delta_{3i}\right)t \tag{2.40}$$

and the a_i's are solution of

$$\ell sd\,(a_i) = -u_i + u_2\left(\frac{\partial U_1}{\partial x_2}\,\delta_{1i} + \frac{\partial U_3}{\partial x_2}\,\delta_{3i}\right)t + \Theta(\epsilon_{rf}, \epsilon_{q_0}^2)$$

where

$$a_i = 0 \qquad \text{at} \qquad t=0$$

Hence

$$b_i = 0 \qquad \text{at} \qquad t=0$$

in light of (2.40). Applying the change of variable to (2.36) and (2.37) gives

$$\ell sd^2(b_i) - \frac{\partial}{\partial x_i}\left(\frac{p}{\rho}\right) = \mathcal{O}(\epsilon_{rf}, \epsilon_{q_0}^2) \tag{2.41}$$

$$\frac{\partial b_j}{\partial x_j} = \mathcal{O}(\epsilon_{rf}, \epsilon_{q_0}^2) \tag{2.42}$$

Russell's formulation used a bilinear variational principle. This formulation will be useful when substituting trial solutions of the form of slowly varying wave trains which may experience exponential growth or decay along a ray. The bilinear variational principle is

$$\delta \iiint_D \int_{t_0}^{t_1} \left[\ell_{sd}(b_j)\, \ell_{sd}(\underline{b}_j) - (p/\rho)\frac{d\underline{b}_j}{dx_j} - (\underline{p}/\rho)\frac{db_j}{dx_j} \right] dt\, d\vec{x}$$

$$= \mathcal{O}(\epsilon_{rf}, \epsilon_\theta^2) \tag{2.43}$$

The eight quantities (b_1, b_2, b_3), $(\underline{b}_1, \underline{b}_2, \underline{b}_3)$, p and $\underline{p}$ are all treated as independently variable. Assume b_j and $\underline{b}_j$ have prescribed values on the surfaces $x_1 = 0$, $x_3 = 0$, $x_2 = 0$, $x_2 = h$, and at times t_0 and t_1.

Taking variations of the underlined variables $\delta(\underline{b}_j)$ and $\delta(\underline{p})$ give equations (2.41) and (2.42), respectively. Taking variation of the nonunderlined variables

$$\delta(b_j): \qquad \ell_{sd}^2(\underline{b}_i) - \frac{\partial}{\partial x_i}\left(\frac{p}{\rho}\right) = \mathcal{O}(\epsilon_{rf}, \epsilon_\theta^2)$$

$$\delta(p): \qquad \frac{\partial}{\partial x_j}\left(\underline{b}_j/\rho\right) = \mathcal{O}(\epsilon_{rf}, \epsilon_\theta^2)$$

Before proceeding with trial functions for (2.43), a definition of "slowly varying" is needed. Let

$$\Theta = \Theta(x_1, x_3, t)$$

where Θ may be complexed valued. We will say a quantity H is "slowly varying" relative to a wave train with phase function Θ if for

$$\frac{\partial}{\partial t}\left[H e^{\pm i\Theta}\right] = \pm i \frac{\partial \Theta}{\partial t} H e^{\pm i\Theta} + \frac{\partial H}{\partial t} e^{\pm i\Theta}$$

$$\frac{\partial}{\partial x_i}\left[H e^{\pm i\Theta}\right] = \pm i \frac{\partial \Theta}{\partial x} H e^{\pm i\Theta} + \frac{\partial H}{\partial x_i} e^{\pm i\Theta}$$

$$i \in \{1, 3\}$$

the second term on the right hand side is small compared to the first quantity. Let ϵ_w be a wave train nonuniformity parameter that measures the smallness of $\frac{\partial H}{\partial t} e^{\pm i\Theta}$ or $\frac{\partial H}{\partial x_i} e^{\pm i\Theta}$. Furthermore, we assume that wavenumber and frequency change slowly in the x_1 or x_3 direction or with time and are of order ϵ_w. The phase function Θ will be allowed relatively fast oscillations.

Now formulate trial functions in the form of slowly varying wave trains. Let

$$b_i = 2\,\mathrm{Re}\left[\tilde{b}_i\, e^{i\Theta}\right] = \tilde{b}_i\, e^{i\Theta} + \tilde{b}_i^*\, e^{-i\Theta^*} \tag{2.44a}$$

$$p = 2\,\mathrm{Re}\left[\tilde{p}\, e^{i\Theta}\right] = \tilde{p}\, e^{i\Theta} + \tilde{p}^*\, e^{-i\Theta^*} \tag{2.44b}$$

$$\underline{b_i} = 2\,\mathrm{Re}\left[\underline{\tilde{b}_i}\, e^{-i\Theta}\right] = \underline{\tilde{b}_i}\, e^{-i\Theta} + \underline{\tilde{b}}^*\, e^{i\Theta^*} \tag{2.44c}$$

$$\underline{p} = 2\,\mathrm{Re}\left[\underline{\tilde{p}}\, e^{-i\Theta}\right] = \underline{\tilde{p}}\, e^{-i\Theta} + \underline{\tilde{p}}^*\, e^{i\Theta^*} \tag{2.44d}$$

in which the overhead tilde quantities may be complex valued and are functions of x_1, x_2, x_3, and t. The asterisks denote the complex conjugate. Now the use of the bilinear variational principle becomes clearer, for if (b_i, p) represents an amplified wave then $(\underline{b_i}, \underline{p})$ represents a damped wave or vice versa.

Substitute the trial functions (2.44) into (2.43) and eliminate terms of order ϵ_w or smaller. Following Whitham (1970) take the phase average over a 2π cycle of (2.43). The resulting "phase average bilinear variational principle" is

$$\delta \iiint_D \int_{t_0}^{t} 2\,\mathrm{Re}\{\tilde{L}\}\,dt\,d\vec{x} = \mathcal{O}(\epsilon_{rf}, \epsilon_q^2, \epsilon_w) \qquad (2.45)$$

where

$$\tilde{L} = \tilde{b}_j \underline{\tilde{b}}_j (\ell s d\,\theta)^2 - (\tilde{p}/\rho)\left[\underline{\tilde{b}}_1 \frac{\partial(-i\theta)}{\partial x_1} + \frac{\partial \underline{\tilde{b}}_2}{\partial x_2} + \underline{\tilde{b}}_3 \frac{\partial}{\partial x_3}(-i\theta)\right] - \left(\frac{\tilde{p}}{\rho}\right)\left[\tilde{b}_1 \frac{\partial}{\partial x_1}(i\theta) + \frac{\partial \underline{\tilde{b}}_2}{\partial x_2} + \tilde{b}_3 \frac{\partial(i\theta)}{\partial x_3}\right] + \mathcal{O}(\epsilon_w)$$

Then the Euler equations become

$$\delta \underline{\tilde{b}}_j: \quad \tilde{L}_{\underline{\tilde{b}}_j} - \delta_{2j} \frac{\partial}{\partial x_2}\left(\tilde{L}_{(\partial \underline{\tilde{b}}_2/\partial x_2)}\right) = \mathcal{O}(\epsilon_{rf}, \epsilon_q^2, \epsilon_w) \qquad (2.46)$$

$$\delta \underline{\tilde{p}}: \quad \tilde{L}_{\underline{\tilde{p}}} = \mathcal{O}(\epsilon_{rf}, \epsilon_q^2, \epsilon_w) \qquad (2.47)$$

$$\delta \tilde{b}_j: \quad \tilde{L}_{\tilde{b}_j} - \delta_{2j} \frac{\partial}{\partial x_2}\left(\tilde{L}_{(\partial \tilde{b}_2/\partial x_2)}\right) = \mathcal{O}(\epsilon_{rf}, \epsilon_q^2, \epsilon_w) \qquad (2.48)$$

$$\delta \tilde{p}: \quad \tilde{L}_{\tilde{p}} = \mathcal{O}(\epsilon_{rf}, \epsilon_q^2, \epsilon_w) \qquad (2.49)$$

$$\delta(\epsilon_w \theta): \quad \frac{1}{\epsilon_w}\left[-\frac{\partial}{\partial t}\left(\tilde{L}_{(-\partial\theta/\partial t)}\right) + \frac{\partial}{\partial x_1}\left(\tilde{L}_{(\partial\theta/\partial x_1)}\right) + \frac{\partial}{\partial x_3}\left(\tilde{L}_{(\partial\theta/\partial x_3)}\right)\right] = \mathcal{O}(\epsilon_{rf}, \epsilon_q^3, \epsilon_w) \qquad (2.50)$$

Equation (2.50) results from rescaling terms with $\delta\theta$ to $\delta(\epsilon_w\theta)$ in order to avoid trivial solutions as $\epsilon_w \to 0$. Without the factor $\frac{1}{\epsilon_w}$ terms in the equation such as

$$\frac{\partial}{\partial t}\left(\tilde{L}_{(-\partial\theta/\partial t)}\right)$$

would vanish as $\epsilon_w \to 0$ and the Euler equation corresponding to would reduce to triviality. Note that equations (2.46) and (2.47) for the underlined variables are uncoupled from the equations for nonunderlined variables (2.48) and (2.49).

Recalling the definition of wavenumber and frequency, we can write

$$\omega = -\frac{\partial\theta}{\partial t} \qquad k_i = \frac{\partial\theta_i}{\partial x_i}$$

Applying the above definitions, allows us to combine equations (2.46) and (2.47) to give

$$\frac{\partial}{\partial x_2}\left[(-\omega + \vec{k}\cdot\vec{U})^2 \frac{\partial\tilde{b}_2}{\partial x_2}\right] - \vec{k}\cdot\vec{k}\,(-\omega + \vec{k}\cdot\vec{U})^2 \tilde{b}_2 = \mathcal{O}(\epsilon_{rf}, \epsilon_g^2, \epsilon_w)$$

which is a form of the Rayleigh stability equation. Manipulating (2.48) and (2.49) would have given an analogous result.

Integrating (2.50) over the cross space from $y_2 = 0$ to $y_2 = h$ and multiplying by ϵ_w gives

$$-\frac{\partial}{\partial t}(\mathcal{A}_\omega) + \frac{\partial}{\partial x_1}(\mathcal{A}_{k_1}) + \frac{\partial}{\partial x_3}(\mathcal{A}_{k_3}) = \mathcal{O}(\epsilon_{rf}, \epsilon_g^3, \epsilon_w^2) \qquad (2.51)$$

where

$$\int_0^h \tilde{L}\, dx_2 \equiv \mathcal{L}$$

The above definition follows if equations (2.46) - (2.49) are substituted back into the definition of L given below (2.45).

Then we see that

$\tilde{L} = \frac{\partial}{\partial x_2}$ [a quantity that vanishes as x_2=0 and at x_2=h]

Thus we have

$$\mathcal{L} = \int_0^h \tilde{L}\, dx_2 = \mathcal{O}(\epsilon_{rf}, \epsilon_q^2, \epsilon_w)$$

for solutions of (2.46) - (2.49).

Furthermore, we can write

$$\mathcal{L}_\omega\, d\omega + \mathcal{L}_{k_1}\, dk_1 + \mathcal{L}_{k_3}\, dk_3 = \mathcal{O}(\epsilon_{rf}, \epsilon_q^2, \epsilon_w)$$

Expanding the term $d\omega$ gives us the following expression

$$\mathcal{L}_\omega \left[\Omega_{k_1} dk_1 + \Omega_{k_3} dk_3\right] + \mathcal{L}_{k_1} dk_1 + \mathcal{L}_{k_3} dk_3 = \mathcal{O}(\epsilon_{rf}, \epsilon_q^2, \epsilon_w)$$

Noting the term in square brackets is zero, we then have the following expression

$$\mathcal{L}_{k_1} dk_1 + \mathcal{L}_{k_3} dk_3 = \mathcal{O}(\epsilon_{rf}, \epsilon_q^2, \epsilon_w)$$

One final expansion yields

$$dk_1 \left[\Omega_{k_1} \mathcal{L}_\omega + \mathcal{L}_{k_1}\right] + dk_3 \left[\Omega_{k_3} \mathcal{L}_\omega + \mathcal{L}_{k_3}\right] = \mathcal{O}(\epsilon_{rf}, \epsilon_q^2, \epsilon_w)$$

Finally, it follows that

$$\mathcal{L}_{k_1} = -\Omega_{k_1} \mathcal{L}_\omega$$

$$\mathcal{L}_{k_3} = -\Omega_{k_3} \mathcal{L}_\omega$$

Then we can write (2.51) in final form

$$\frac{\partial}{\partial t}(\mathcal{L}_\omega) + \frac{\partial}{\partial x_1}(\Omega_{k_1} \mathcal{L}_\omega) + \frac{\partial}{\partial x_3}(\Omega_{k_3} \mathcal{L}_\omega) = \mathcal{O}(\epsilon_{rf}, \epsilon_q^3, \epsilon_w^2) \tag{2.52}$$

The group velocity terms Ω_{K_1} and Ω_{K_3} appear as propagation terms for $\mathcal{A}_\omega$. Equation (2.52) is identical to Whitham's law of conservation of wave action density, equation (12a) presented earlier.

Hence an amplitude propagation equation can be derived for shear flow instability waves beginning with familiar linearized equations of motion. $\mathcal{A}_\omega$ does not contain information about exponential growth or decay. Returning to the trial solutions (44 a,b,c,d) we see that if either of the sets of variables (b_i,p) or $(\underline{b_i},\underline{p})$ represents an amplified wave, then the other represents a damped one. By forming products of underlined and nonunderlined terms in the variational formulation, we eliminated the exponential growth factor. Hence $\mathcal{A}_\omega$ represents only part of the observed square-amplitude. The exponential amplification factor has the form

$$\exp\left[-\mathrm{Im}\{\theta\}\right]$$

so that observed square-amplitude has the form

$$A^2 = \mathcal{A}_\omega \exp\left[-2\,\mathrm{Im}\{\theta\}\right] \qquad (2.53)$$

where $\mathcal{A}_\omega$ represents amplitude change due to focussing and dispersion while $\exp[-\mathrm{Im}\{\theta\}]$ describes exponential amplification. The factor of 2 is a mathematical convenience. Eliminating $\mathcal{A}_\omega$ between (2.52) and (2.53) gives the

"non-conservative" law for A^2

$$\frac{\partial}{\partial t}(A^2) + \frac{\partial}{\partial x_1}(\Omega_{k_1} A^2) + \frac{\partial}{\partial x_3}(\Omega_{k_3} A^2)$$
$$= 2 A^2 [\mathrm{Im}\{\Omega\} - \Omega_{k_1} \mathrm{Im}\{k_1\} \qquad (2.54)$$
$$- \Omega_{k_3} \mathrm{Im}\{k_3\}] \quad + \mathcal{O}(\epsilon_{rf}, \epsilon_0^3, \epsilon_w^2)$$

with the hypotheses:

a flat reference flow

$$\epsilon_{rf} << 1$$

slowly varying wave train

$$\epsilon_w << 1$$

and small disturbances

$$\epsilon_0^2 << 1$$

Equations (2.55) was also derived by Landahl in his 1982 paper by a procedure described earlier. Feeling confident that the trajectories of shear flow instability waves can be traced by equations

$$\frac{dk_i}{dt} = -\Omega_{x_i} \qquad \text{on} \qquad \frac{dx_i}{dt} = c_{gi}$$

and that equation (2.55) describes amplitude propagation along a trajectory we conclude this chapter. For shear flow instability waves the dispersion relation is complex. Consequently both Ω_{x_i} and c_{gi} in the above equations will be complex. Chapter 4 will

deal extensively with the solution of these characteristic equations for complex values. For now it is important to note that the fundamental equation governing wavenumber propagation derived at the beginning of this chapter, equation (2.6), can be written in the form

$$\frac{\partial \vec{k}}{\partial t} = \frac{\partial}{\partial \vec{x}} \left[\Omega(\vec{k}, \vec{x}, t) \right]$$

The above equation can be solved using a step-by-step method (in the case of complex dispersion relations) for complex k_i keeping x_j and t real. Only when equation (2.6) is rewritten in characteristic form does difficulty arise.

Landahl's original claim remains unchanged. A focus will still occur when J = 0 since from (2.55) and (2.28)

$$A = \frac{\text{constant}}{J} \exp \left[2 \int \left[\mathrm{Im}(\Omega) - \Omega_{k_1} \mathrm{Im}(k_1) - \Omega_{k_3} \mathrm{Im}(k_3) \right] dt \right.$$

And from arguments made earlier, J = 0 corresponds to a situation where $c_g = c_o$, when the phase velocity of the primary wave is equal to the group velocity of the secondary wave packet.

CHAPTER THREE

DERIVATION OF CLASSICAL TEMPORAL STABILITY RESULTS AND INTRODUCTION TO THE MIXED STABILITY PROBLEM

Before ray tracing is possible the dispersion relation must be known. In this work we have assumed the local dispersion relation can be found as a solution of the Rayleigh equation. Russell has found an asymptotic small wave number approximate solution of the Rayleigh equation for a family of cubic-tanh profiles. In order to verify the accuracy of Russell's solution a comparison with known results is necessary. Thus one point of this chapter is to derive several fundamental results of classical stability theory, derive Russell's solution to the Rayleigh equation, and then compare Russell's results with the classical results.

In addition to verifying the accuracy of Russell's approximate solution, this chapter explores the "mixed" problem in hydrodynamic stability theory. There is a large volume of literature concerned with the temporal instability problem where the wave grows in time. Analysis of the spatial instability problem has also been

performed, especially for free shear layers. The spatial instability problem is attractive since most disturbances grow as they propagate downstream. Less literature exists on the "mixed" problem -- a temporally and spatially growing traveling wave. The filtering scheme used for the ray tracing equations requires a real group velocity, which results in both a complex phase velocity and a complex wavenumber. Hence an interesting by-product of this work is the possibility of a mixed instability problem. This chapter will present several novel results of a mixed stability analysis for a Falkner-Skan-like family of velocity profiles.

3.1 Derivation of Several Results from Classical Stability Theory

Throughout this work a typical dimensionless scheme has been used. Choose a reference velocity U_1 of the main flow. Choose a reference length, δ in the y-direction of the flow where (x,y,z) are member of a right-handed coordinate system. The coordinate x is in the free stream direction. Let the * denote dimensional quantities. Then the dimensionless time, position, velocity, pressure are

$$t = \frac{t_* U_1}{\delta} \qquad \vec{r} = \frac{\vec{r}_*}{\delta} \qquad \vec{u} = \frac{\vec{u}_*}{U_1} \qquad p = \frac{p_*}{\rho U_1^2}$$

3.1.1 Derivation of the Rayleigh Stability Equation

We begin with the cornerstone of classical stability theory, derivation of the Rayleigh stability equation. Consider the stability of a planar, parallel flow of inviscid fluid. The

unperturbed flow is known and described by the velocity

$$\vec{u} = (\bar{u}(y), 0, 0)$$

over the region $y_1 \leq y \leq y_2$. We assume this flow satisfies the Euler equations of motion and continuity. In general the boundaries y_1 and y_2 can be rigid or free so that either the normal velocity of the fluid is zero at the boundary or the pressure is constant. Either, or both, boundaries may be at infinity. Furthermore assume the fluid is incompressible and homogeneous.

To study the possibile instability of the flow, the known reference flow is perturbed slightly so that the new velocity and pressure are given by

$$\vec{u}(\vec{r},t) = \bar{u}(y) + \vec{u}'(\vec{r},t)$$

$$p(\vec{r},t) = \bar{p} + p'(\vec{r},t)$$

where the primes denote the perturbed quantities and overbar denotes the reference flow quantity. This neighboring flow is substituted into the equations of motion and continuity. Subtracting the equations of motion for the reference flow from the corresponding ones for the neighboring flow, and then neglecting quadratic terms in the perturbation equations gives the linearized equations

$$\frac{\partial u'}{\partial t} + \bar{u}\frac{\partial u'}{\partial x} + v'\frac{d\bar{u}}{dy} = -\frac{\partial p'}{\partial x} \qquad (3.1a)$$

$$\frac{\partial v'}{\partial t} + \bar{u}\frac{\partial v'}{\partial x} = -\frac{\partial p'}{\partial y} \qquad (3.1b)$$

$$\frac{\partial w'}{\partial t} + \bar{u}\frac{\partial w'}{\partial x} = -\frac{\partial p'}{\partial z} \qquad (3.1c)$$

$$\frac{\partial u'}{\partial x} + \frac{\partial v'}{\partial y} + \frac{\partial w'}{\partial z} = 0 \qquad (3.1d)$$

Taking the "horizontal divergence" of equation (3.1a) and (3.1c) and using continuity (3.1d) gives

$$\left[\frac{\partial}{\partial t} + U\frac{\partial}{\partial x}\right]\left(-\frac{\partial v'}{\partial y}\right) + \frac{dU}{dy}\frac{\partial v'}{\partial x} = -\left(\frac{\partial^2}{\partial x^2} + \frac{\partial^2}{\partial z^2}\right)\frac{p}{\rho}$$

$$= -\nabla_H^2\left(\frac{p}{\rho}\right)$$

Eliminating pressure between this equation and the y-momentum equation (3.1b) gives

$$\left(\frac{\partial}{\partial t} + U\frac{\partial}{\partial x}\right)\nabla^2 v' - \frac{d^2U}{dy^2}\frac{\partial v'}{\partial x} = 0 \qquad (3.2)$$

which is called the "Rayleigh equation in physical variables".

To arrive at the more familiar form of the Rayleigh equation, employ the fundamental assumption of stability theory. That is assume the velocity perturbation can be resolved into wave-like components of the form

$$v'_{\text{normal mode}} = \tilde{v}(y)\exp(i(\alpha x + \beta z - \alpha c t)) \qquad (3.3)$$

The normal modes are assumed to be completely discrete. After the components of an initial disturbance experience a time of exponential growth or damping, the theory assumes the most unstable mode will dominate the linear stability problem. Analysis has shown that for the initial value problem of plane

parallel flow, a continuous spectrum of eigenvalues can also be found but that the exponentially growing or damping contribution is due to the discrete spectrum of normal modes. A more thorough discussion of "proper" and "improper" modes can be found in the review article by Drazin and Howard (1966) pp.29-31 or Russell's Sc.D. dissertation (1981).

The temporal stability problem assumes α and β are real so that the wave grows or decays in time like $\exp(\alpha c_i t)$. An unstable wave occurs when $\alpha c_i > 0$ and a stable wave requires $\alpha c_i \leq 0$. A neutrally stable wave is defined by $\alpha c_i = 0$. Similarly a spatial stability problem is possible for complex wavenumbers α and β and real c. If both wave numbers α and β and phase velocity c are complex, a mixed instability problem arises where temporally and spatially growing waves are possible.

Substituting the normal mode assumption, equation (3.3), into the Rayleigh equation in physical variables, equation (3.2); cancelling the exponential factor; and introducing the notation $k^2 = \alpha^2 + \beta^2$ gives

$$(U-c)(\tilde{v}'' - k^2\tilde{v}) - U''\tilde{v} = 0 \tag{3.4}$$

The above equation is the familiar form of the Rayleigh equation. With rigid boundary conditions

$$\tilde{v}(y_1, y_2) = 0 \tag{3.5}$$

For boundary-layer geometry, the boundary condition is the free stream region are given as follows. In boundary-layer geometry, U(y) approaches the free stream velocity U_∞ = constant as y approaches the outer edge $y_{o.e}$ of the boundary layer. For $y > y_{o.e.}$, $U'' = 0$ so that (3.4) becomes

$$(U - c)(\tilde{v}'' - k^2\tilde{v}) = 0 \qquad y > y_{o.e.}$$

which yields two solutions

$$\tilde{v} \rightarrow (e^{ky}, e^{-ky}) \qquad k > 0$$

An exponentially growing disturbance is physically unrealistic for $ky >> 1$. To rule out the unrealistic solution the free stream boundary condition is rewritten as

$$\frac{d\tilde{v}}{dy} + k\tilde{v} = 0 \qquad \text{for} \quad Y \geq Y_{o.e.} \tag{3.8a}$$

The wall boundary condition is

$$\tilde{v}(Y_1) = 0 \tag{3.8b}$$

The solution of the Rayleigh equation for a known U(y) with the application of the impermeable wall boundary condition

$$\tilde{v}(y_1) = 0$$

gives rise to the secular equation

$$F(k,c) = 0$$

The eigenvalue c is found for a known value of k.

3.1.2 Derivation of the Rayleigh Inflection Point Theorem

The well-known Rayleigh inflection point theorem is a direct consequence of equation (3.4) for real k. Multiply equation (3.4) by $\tilde{v}^*$ and integrate from y_1 to y_2:

$$\int_{y_1}^{y_2} \left(\frac{d^2|\tilde{v}|^2}{dy^2} - k^2 |\tilde{v}|^2 \right) dy = \int_{y_1}^{y_2} \frac{d^2U}{dy^2} \frac{|\tilde{v}|^2}{(U-c)} \, dy$$

The imaginary part of this equation gives

$$c_i \int_{y_1}^{y_2} \frac{d^2U}{dy^2} \frac{|\tilde{v}|^2}{|U-c|^2} \, dy = 0 \qquad (3.6)$$

since k is strictly real. For temporally unstable waves $c_i > 0$. In order for the integral to be zero, $\frac{d^2U}{dy^2}$ must change signs at least once across the interval (y_1, y_2). Thus in the inviscid case, for real wave number, a velocity profile must have at least one inflection point for instability. Later in this chapter, some comment on the Rayleigh inflection point theorem for complex k and c, the mixed problem, will be made.

The Rayleigh inflection point theorem is an immediate consequence of Rayleigh's equation for real k. It provides a necessary condition for determining an unstable velocity profile under the inviscid assumption . In order to know the range of unstable wave numbers and associated phase velocities for a particular velocity profile, the Rayleigh equation must be solved, which in general is a difficult problem.

In the era of computational fluid dynamics, a numerical solution of Rayleigh's equation may seem the obvious choice.* The Rayleigh equation poses an eigenvalue problem of a singular second-order linear differential equation and a two-point boundary condition. The region close to U = c can present numerical difficulties if not handled properly. Since the main intent of this dissertation is to trace the trajectories of secondary wave packets where the local dispersion relation is a necessity, an asymptotic approximate solution of the Rayleigh equation will provide the dispersion relation instead of a numerical solution. Since the small wave number approximate solution is valid for both complex k and c, an exact method is available for defining a strictly real group velocity for the mixed stability problem. A numerical solution involving the constraint of real group velocity would be more difficult.

3.1.3 Derivation of the Small-Wavenumber Approximation to the Rayleigh Equation.

Rayleigh (1913) and Heisenberg (1924) both considered solutions of the Rayleigh equation for small wave number. A

---

*The viscous form of the stability equation, the Orr-Sommerfeld equation, is probably a better choice for numerical solution. The reader is referred to the book by Drazin and Reid (1981), pages 202-211 for a description of numerical methods of solution.

uniformly valid small wave number expansion for boundary-layer geometry was given by Lighthill (1957) and applied by Benjamin (1959). Following the method of Benjamin, rewrite (3.7) as

$$\frac{d}{dy}\left[(U-c)^2\ \frac{d}{dy}\left(\frac{\tilde{v}}{U-c}\right)\right] = k^2(U-c)\tilde{v} \tag{3.9}$$

which suggests a change of variable. Let

$$\frac{\tilde{v}}{(U-c)} = e^{-ky}\,G(y) \tag{3.10}$$

$$G_\infty = \lim_{Y\to\infty}\{G(y)\}$$

$G_\infty(y)$ may be viewed as a dimensionless amplitude measure. Substituting (3.10) into (3.9) and multiplying by e^{ky} gives

$$\frac{d}{dy}\left[(U-c)^2\ \frac{dG}{dy}\right] = k\left\{\frac{d}{dy}\left[(U-c)^2 G\right] + (U-c)^2\ \frac{dG}{dy}\right\} \tag{3.11}$$

with boundary conditions

$$G(0) = 0 \tag{3.12a}$$

$$G \to G_\infty = \text{constant for } y > y_{o.e.} \tag{3.12b}$$

Integration, application of boundary conditions, and rearrangement gives

$$\frac{G(y)}{G_\infty} = 1 + k\int_y^\infty\left\{\left[\frac{U_\infty - c}{U-c}\right]^2 - \frac{G}{G_\infty} + \frac{1}{(U-c)^2}\int_{y'}^\infty (U-c)^2\ \frac{dG}{dy''}\,dy''\right\}dy'$$

Making explicit the non-dimensionalization, let δ = a typical cross-stream length scale of the boundary layer

and let the quantities with * be dimensional:

$$\frac{G}{G_\infty}(y_*/\delta) = 1 + k\delta \int_{y_*/\delta}^{\infty} \left\{ \left(\frac{U_\infty - c}{U - c} \right)^2 - \frac{G(y_*'/\delta)}{G_\infty} + \right.$$

$$\left. \frac{1}{(U(\frac{y_*'}{\delta}) - c)^2} \int_{\frac{y_*'}{\delta}}^{\infty} \left[U(\frac{y_*''}{\delta}) - c \right]^2 \frac{dG}{d(y_*''/\delta)} \, d\left(\frac{y_*''}{\delta}\right) \right\} d\left(\frac{y_*'}{\delta}\right) \tag{3.13}$$

A "long wave" will be defined by the condition $k\delta \ll 1$.

Assume a small wave number expansion for G of the form

$$\frac{G}{G_\infty} = \frac{G^{(0)}}{G_\infty} + k\delta \frac{G^{(1)}}{G_\infty} + (k\delta)^2 \frac{G^{(2)}}{G_\infty} + \cdots$$

For "long waves", the zeroth order approximation to (3.13) is

$$\frac{G^{(0)}}{G_\infty}(y_*/\delta) = 1 + \mathcal{O}(k\delta)$$

Note: for the zeroth-order approximation. Substituting this zeroth approximation back into (3.13) gives the first order result

$$\frac{G^{(0)}}{G_\infty} + k\delta \frac{G^{(1)}}{G_\infty}(y_*/\delta) = 1$$

$$+ k\delta \int_{\frac{y_*}{\delta}}^{\infty} \left[\left(\frac{U_\infty - c}{U(y_*/\delta) - c} \right)^2 - 1 \right] d\left(\frac{y_*'}{\delta}\right) + \mathcal{O}[(k\delta)^2] \tag{3.14}$$

This process can be continued to any order of accuracy in a systematic way. Knowing the nth-order approximation gives

$$\frac{G^{(n+1)}}{G_\infty} = \int_{\frac{y_*}{\delta}}^{\infty} \left\{ \frac{-G^{(n)}}{G_\infty} + \frac{1}{(U-c)^2} \int_{\frac{y_*'}{\delta}}^{\infty} (U-c)^2 \frac{d}{d\left(\frac{y_*''}{\delta}\right)} \left(\frac{G^{(n)}}{G_\infty} \right) d\left(\frac{y_*''}{\delta}\right) \right\} d\left(\frac{y_*'}{\delta}\right)$$

Drazin and Howard (1962) proved the convergence of this series.

For the purpose of this work, the first order approximation will be sufficient. Substituting (3.14) into (3.10) gives

$$\tilde{v} = (U-c)\left\{e^{-KY}\, G_\infty \left[1 + K\delta \int_{y_*/\delta}^{\infty} \left[\left(\frac{U_\infty - c}{U-c}\right)^2 - 1\right] d(y_*'/\delta) + \mathcal{O}[(K\delta)^2]\right]\right\} \tag{3.15}$$

The impermeable wall boundary condition v(0) = 0 together with the assumption U(0) = 0 gives

$$0 = -c\, G_\infty \left[1 + K\delta \int_0^{\infty} \left\{\left(\frac{U_\infty - c}{U-c}\right)^2 - 1\right\} d(y_*/\delta) + \mathcal{O}[(K\delta)^2]\right] \tag{3.16}$$

Equation (3.16) is called the secular equation. For a known k and U(y), the corresponding eigenvalue c can be found provided the integral can be evaluated. Hence for small wave numbers, the Rayleigh equation has been reduced to the evaluation of the integral expression in (3.16).

3.1.4 Derivation of Tollmien's Vanishingly Small-Wavenumber Expression

Before solving (3.16) for a special family of velocity profiles, consider the solutions which neighbor the trivial solution c = k = 0. First rewrite (3.16)

$$0 = -c\, G_\infty \left[1 + K(U_\infty - c)^2 \int_0^{Y_{o.e.}} \left[\frac{1}{U-c}\right]^2 dy_* - K y_{o.e.} + \mathcal{O}[(K\delta)^2]\right] \tag{3.16a}$$

Here $y_{o.e.}$ corresponds to the y-position where $U = U_\infty$. We note that

$$\frac{1}{(U-c)^2} = \frac{d}{dy}\left(\frac{-1}{U-c}\right)\frac{1}{U'} = \frac{d}{dy}\left[\frac{-1}{(U-c)U'}\right] - \left(\frac{-1}{U-c}\right)\left(\frac{-U''}{(U')^2}\right)$$

$$= \frac{d}{dy}\left[\frac{-1}{(U-c)U'} - \frac{U''}{(U')^3}\log A(U-c)\right] + \left(\frac{U''}{(U')^3}\right)'\log A(U-c)$$

where A is an arbitrary positive constant. Let y_{j*} be finite and within the interval $(0, y_{o.e.})$. Then

$$\int_0^{y_{o.e.}} \frac{dy_*}{(U-c)^2} = \left[\frac{-1}{(U-c)U'} - \frac{U''}{(U')^3}\log A(U-c)\right]\Bigg|_0^{y_{j*}} + \int_0^{y_{j*}} \left(\frac{U''}{(U')^3}\right)'\log A(U-c)\,dy_* + \int_{y_{j*}}^{y_{o.e.}} \frac{dy_*}{(U-c)^2}$$

Evaluating the real and imaginary parts gives

$$\mathrm{Re}\left\{\int_0^{y_{o.e.}} \frac{dy_*}{(U-c)^2}\right\} = \frac{-c_r}{U'_w|c|^2} + \frac{U''_w}{(U'_w)^3}\log A|c| + \Theta\left[\frac{1}{U(y_{j*})U'(y_{j*})}\right]$$

$$\mathrm{Im}\left\{\int_0^{y_{o.e.}} \frac{dy_*}{(U-c)^2}\right\} = \frac{c_i}{U'_w|c|^2} + \frac{U''_w}{(U'_w)^3}(-\pi) + \left(\frac{U''}{(U')^3}\right)'\Bigg|_w \frac{c_r}{U'_w}(-\pi) + \Theta\left[\frac{c_i}{U^2(y_{j*})U'(y_{j*})}\right]$$

Here it is assumed that $c_i > 0$ for all values of y so that

$$\lim_{|c|\to 0^+} (\arg(U-c)_{y_*=0}) = -\pi$$

The assumption $c_i > 0$ is consistant with temporarily amplified disturbances.

For real k, as $k \to 0^+$, $|c| \to 0^+$, the imaginary part of equation (3.16) gives

$$c_i = \pi \frac{U''_w}{(U'_w)^2} |c|^2 + \cdots \tag{3.17}$$

It follows that c_i is proportional to c_r^2. Thus the real part of (3.16) gives

$$c_r = \frac{k U_\infty^2}{U'_w} + \cdots \tag{3.18}$$

to leading order. These results were first derived by Tollmien (1935) for boundary-layer profiles in the small wavenumber limit. In order for equation (3.17) to be consistent with the assumption $c_i > 0$, $U''_w > 0$ is required. This condition is satisfied by Falkner-Skan type profiles (i.e., self similar laminar boundary layers with an adverse pressure gradient.)

Equation (3.17) and (3.18) are important within the context of this work because they serve as well-known solutions in the small wave number limit for the dispersion relation c = c(k). The results of our calculations for c = c(k) should agree with Tollmien's results for small |c| and small real k if we satisfy the condition $U''_w > 0$.

3.1.5 Derivation of Tollmien's Neutral Mode Solution

Another well known result of classical stability theory is the existence of neutral solutions ($c_i = 0$) at some point $k=k_s$, $c=c_s>0$. This point will be referred to as the short wave cutoff. Tollmein must be given credit for initially proving the existence of neutral-mode solutions. The following argument for describing the value of c_s can be found in Drazin and Howard.

Define the phase averaged Reynolds stress

$$-\rho \langle u'v' \rangle = (-\rho) \frac{1}{2\pi} \int_0^{2\pi} (u'v') d\theta \qquad (3.19)$$

where u' and v' are defined by the normal mode assumption written in terms of a stream function

$$\psi = Re \{ \tilde{\varphi}(y) \, e^{ik(x-ct)} \}$$

Substituting the stream function form of u' and v' into (3.19) and integrating gives

$$\tau \equiv -\rho \langle u'v' \rangle = \rho k \frac{e^{2kc_i t}}{2} \, Im \{ \tilde{\varphi}' \tilde{\varphi}^* \} \qquad (3.20)$$

The phase averaged Reynolds stress, τ, must be zero at $y=y_1$ and $y=y_2$ to satisfy the boundary conditions given by (3.5).

Tollmien derived an expression for jump in Reynolds stress across the "critical layer", i.e. the thin layer in the neighborhood of the singular point U=c. This result will help us define the shortwave cut off point. For strictly real k write the Rayleigh equation and the complex conjugate of the Rayleigh

equation

$$\mathcal{L}(\tilde{v}) = \tilde{v}'' - k^2 \tilde{v} - \frac{U''}{(U-c)} \tilde{v} = 0$$

$$\mathcal{L}^*(\tilde{v}^*) = \tilde{v}^{*\prime\prime} - k^2 \tilde{v}^* - \frac{U''}{(U-c^*)} \tilde{v}^* = 0$$

Form the quantity $\tilde{v}^* \mathcal{L}(\tilde{v}) - \tilde{v} \mathcal{L}^*(\tilde{v}^*) = 0$ and manipulate terms to give

$$\frac{d}{dy}\left[\mathrm{Im}(\tilde{v}'\tilde{v}^*)\right] - \frac{U''}{U'} |\tilde{v}|^2 \frac{d}{dy}\left[\arg(U-c)\right] = 0$$

Let y_c be the value of y at the critical layer. Integrate across this thin layer:

$$\lim_{\epsilon \to 0} \left\{ \int_{y_c-\epsilon}^{y_c+\epsilon} \left[\frac{d}{dy}\left(\mathrm{Im}(\tilde{v}'\tilde{v}^*)\right) - \frac{U''}{U'} |\tilde{v}|^2 \frac{d}{dy}\left(\arg(U-c)\right)\right] dy = 0 \right.$$

It must be noted that arg(U-c) tends to a step function as c_i approaches zero. In particular, we note that

$$\frac{d}{dy}\left[\arg(U-c)\right] = \text{a small quantity}, \quad y \neq y_c$$

so that

$\arg(U-c) \to -\pi$ for $y < y_c$

$\arg(U-c) \to 0$ for $y > y_c$

Let $c_i \to 0^+$ so that $\arg(U-c) \to -\pi$. The final result is the jump in $(\tilde{v}'\tilde{v}^*)$ across the critical layer

$$\left[\mathrm{Im}(\tilde{v}'\tilde{v}^*)\right]_{y=y_{critical}} = \pi \frac{U_c''}{U_c'} |\tilde{v}_c|^2 \qquad (3.21)$$

Noting that $\mathrm{Im}(\tilde{v}'\tilde{v}^*) = k^2 \mathrm{Im}(\tilde{\varphi}'\tilde{\varphi}^*)$ allows (3.21) to be written in terms of the jump in Reynolds stress, equation (3.20), across the critical layer.

$$[\tau]_{y=y_c} = \frac{\rho}{2k} \pi \frac{U_c^*}{U_c'} |\tilde{v}_c|^2 \qquad (3.22)$$

Since the Reynolds stess is zero at the boundaries, it follows that for monotonic velocity profiles the jump in Reynolds stress across the critical layer must be zero. If $[\quad]_{yc} = 0$, then U''_c vanishes at y_c according to equation (3.22). (It can be shown $|\tilde{v}_c|^2 \neq 0$ at $y = y_c$.) Thus the value of the velocity at the point U''_c must correspond to the phase velocity $c = c_s$ at the short wave cut off point for monotonic profiles. This result will serve as another benchmark for Russell's solution.

Returning focus to the secular equation (3.16), we see the dispersion relation $c = c(k)$ can be known for a particular velocity profile $U(y)$, provided the integral can be evaluated. No assumption was made about the realness of k in the derivation of (3.16) so a dispersion relation for complex k and c is possible.

3.2 Russell's Small Wavenumber Approximation Solution of the Rayleigh Equation

Russell (1983) has found a solution of (3.16) for a particular family of velocity profiles of the form

$$U(y/\delta) = U_1 \left[\tanh^3 \left(\frac{y-y_0}{\delta} \right) + A_2 \tanh^2 \left(\frac{y-y_0}{\delta} \right) + A_1 \tanh \left(\frac{y-y_0}{\delta} \right) + A_0 \right] \qquad (3.23)$$

where U_1 is a velocity scale, δ a length scale, and A_2, A_1, A_0, and y_0/δ are non-dimensional parameters. Introducing the change of variable

$$r = \tanh \left(\frac{y-y_0}{\delta} \right) + \frac{A_2}{3} \qquad (3.24a)$$

$$r_e = \sqrt{\left(\frac{A_2}{3} \right)^2 - \frac{A_1}{3}} \qquad (3.24b)$$

$$U_s = U_1 \left[\frac{2}{27} A_2^3 - \frac{A_1 A_2}{3} + A_0 \right] \qquad (3.24c)$$

allows equation (3.23) to be written more compactly in the form

$$U - U_s = U_1 (r^3 - 3 r_e^2 r) \qquad (3.25)$$

Note $\frac{dU}{dr}$, and likewise $\frac{dU}{dy}$, are zero at $r = \pm r_e$. Equation (3.25) represents a fairly wide class of velocity profiles.

At the wall, $y = 0$, define the variable

$$r_w = - \tanh \left(\frac{y_0}{\delta} \right) + \frac{A_2}{3} \qquad (3.26)$$

Then four different types of velocity profiles can be defined which give rise to four different classes of modes. Class one and two correspond to $r_e > 0$, that is, the profile has an extremum point. Class one corresponds to $r_e > 0$ and $r_w < r_e$ -- the extrumums located above the "wall". Class two corresponds to both extremums located above the "wall", that is $r_e > r_w$ and $-r_e > r_w$. These two classes could be used to model jet flow, wake flow, or rotating flow cases, to list a few examples. Class three corresponds to $r_e = 0$ and $r_w < 0$. In this case U_s represents a point on the profile where $\frac{dU}{dr}\Big|_{r=r_e} = 0$ across which $\frac{d^2U}{dy^2}$ changes sign. This could represent a profile with a steep shear layer. Class 4 has no extremums and could represent monotonic profiles such as the Falkner-Skan profiles. Example profiles are shown in figure 3.1.

Substituting (3.24a), (3.25) into (3.16) with the appropriate change of variable, Russell was able to evaluate the integral. Briefly outlining his procedure, we write the denominator of the integral expression $\int \frac{1}{[U-c]^2}\,dr$ as

$$U(r)-c = U_1(r^3 - 3r_e^2 r) + U_s - c \qquad (3.27)$$

Assume the above expression can be factors as

$$U(r) - c = U_1(r-r_{c_1})(r-r_{c_2})(r-r_{c_3}) \qquad (3.28)$$

Comparing like coefficients of r between (3.27) and (3.28) gives

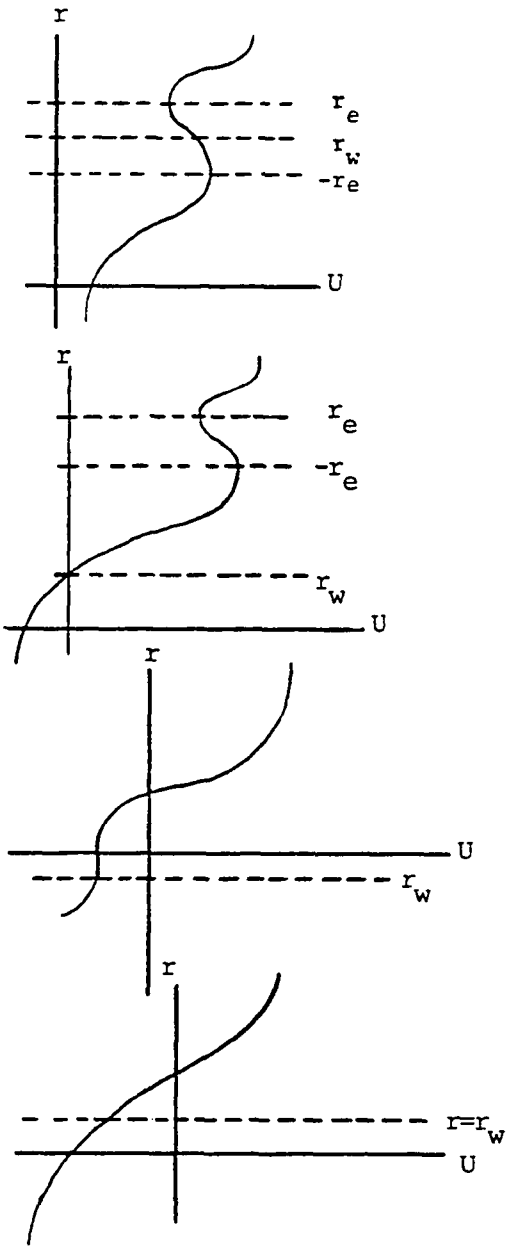

Class One
$r_w < r_e < r_\infty$

Class 2 (also admits a Class 1 mode)
$r_w < -r_e < r_\infty$

Class Three
$r_e = 0$, $r_w < 0 < r_\infty$

Class Four
$d^2U/dy^2 > 0$ at $r=r_w$

Figure 3.1 Schematic diagram illustrating the four profiles admitting four classes of modes from Russell's solution of the small wavenumber approximation to the Rayleigh equation.

$$r_{c_1} + r_{c_2} + r_{c_3} = 0 \tag{3.29a}$$

$$r_{c_1} r_{c_2} + r_{c_2} r_{c_3} + r_{c_3} r_{c_1} = -3r_e^2 \tag{3.29b}$$

$$r_{c_1} r_{c_2} r_{c_3} = \frac{c-U_s}{U_1} \tag{3.29c}$$

The first two equations (3.29a,b) can be satisfied identically by

$$r_{c_2} = \frac{-r_{c_1}}{2} + \sqrt{(2r_e^2)^2 - r_{c_1}^2}\,\frac{\sqrt{3}}{2} \tag{3.30a}$$

$$r_{c_3} = \frac{-r_{c_1}}{2} - \sqrt{(2r_e^2)^2 - r_{c_1}^2}\,\frac{\sqrt{3}}{2} \tag{3.30b}$$

The remaining equation

$$r_{c_1}(r_{c_1}^2 - 3r_e^2) = \frac{c-U_s}{U_1} \tag{3.31}$$

contains two unknowns, c and r_{c1}. Substitute the "partial fraction" expression

$$\frac{1}{(U-c)^2} = \sum_{m=1}^{3} \left[\frac{Q_m}{(r-r_{cm})^2} + \frac{L_m}{(r-r_{cm})} \right]$$

into (3.16). By writing the coefficients of a Laurent series expansion for $(U(r)-c)^{-2}$, Russell was able to determine the Q_m's and L_m's. Then the integral expression involves terms that are easily integrated.

The resulting equation is

$$1 = -K\delta(U_\infty - c)^2 \sum_{m=1}^{3} \frac{1}{[3U_1(r_{cm}^2 - r_e^2)]^2 [1-(r_{cm}-r_\infty+1)^2]} \left[\left(\frac{1}{r_w - r_{cm}} - \frac{1}{r_\infty - r_{cm}} \right) - 2 \left\{ \frac{r_{cm}}{r_{cm}^2 - r_e^2} - \frac{r_{cm} - r_\infty + 1}{1-(r_{cm}-r_\infty+1)^2} \right\} \ln \left[\frac{r_\infty - r_{cm}}{r_w - r_{cm}} \, \frac{2 + r_w - r_\infty}{2} \right] \right] \tag{3.32}$$

Substitute a given velocity profile of the form of equation (3.25); a known value of $k\delta$ (real or complex); and the expression for c, r_{c2}, and r_{c3} from equations (3.30) and (3.28) into equation (3.32). Then equation (3.32) represents a transcendental expression for r_{c1}. Once r_{c1} is known, equation (3.31) can be solved for c.

3.3 Comparison of Stability Results for Cubic-Tanh Family of Profiles with Known Results

In order to verify the accuracy of Russell's solution, a Falkner-Skan-like family of profiles was considered. Define δ to be the height of the boundary layer, $U(y = \delta) = 0.99\ U_\infty$. Fix

$$A_2 = 0$$

$$\frac{y_o}{\delta} = -0.01$$

in the profile equation (3.23). The choice of $\frac{y_o}{\delta} = -0.01$ results in $(d^2U/dy^2)_{wall} > 0$, but only barely greater than zero. Allow A_1 to vary but rewrite in terms of a new parameter n,

$$A_1 = n/(1-n)$$

Then (3.23) can be written

$$\frac{u}{u_1} = \tanh^3\left(\frac{y-y_o}{\delta}\right) + \frac{n}{1-n}\tanh\left(\frac{y-y_o}{\delta}\right) + A_o$$

Choose A_0 to satisfy the wall condition $\frac{u}{u_1} = 0$ at $y = 0$,

$$A_o = \tanh^3\left(\frac{y_o}{\delta}\right) + \frac{n}{1-n}\tanh\left(\frac{y_o}{\delta}\right)$$

The free stream condition that $u \to U_\infty$ as $y \to \infty$ is written

$$\frac{u_\infty}{u_1} = 1 + \frac{n}{1-n} + A_0$$

so that the form of equation (3.23) used to model a Falkner-Skan-like family of profiles is

$$\frac{u}{u_\infty} = \frac{\tanh^3\left(\frac{y-y_0}{\delta}\right) + \frac{n}{1-n}\tanh\left(\frac{y-y_0}{\delta}\right) + A_0}{1 + \frac{n}{1-n} + A_0}$$

Variations in n/(1-n) will model the adverse pressure gradient effect. Increasing values of n, $0 \leq n \leq 0.75$, provide a fuller profile with less steepening due to an adverse pressure gradient.

Figure 3.2 shows the family of profiles and their second derivatives, $\frac{d^2U}{dy^2}$. Profiles (a) through (e) have $U''_w > 0$, but it is difficult to see this on the graphs, since U''_w is close to zero. Recall a necessary condition for Tollmien's vanishingly small wavenumber approximation, equations (3.17) and (3.18), is $U''_w > 0$. Profiles (a) through (e) are singly inflectional, with $U'' = 0$ only once over the y-interval $(0, \delta)$. We let $U'' \to 0$ at the outer edge of the boundary layer. Profile (f) represents the zero pressure gradient member of this Falkner-Skan-like family. Figure 3.3 shows a comparison between profile (f) and the Blasius profile. Note that for this one profile, $\frac{y_0}{\delta} = -0.02$ to insure $U''_w = 0$ and $U'' < 0$ for all y on the open interval $(0, \delta)$.

From previous discussion in this chapter, we can anticipate the results of solving for $c = c(k)$ using Russell's

(a) n = 0.1

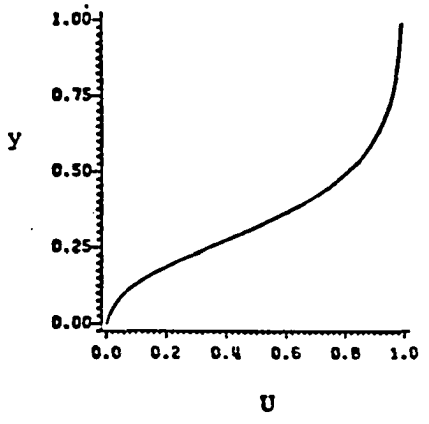

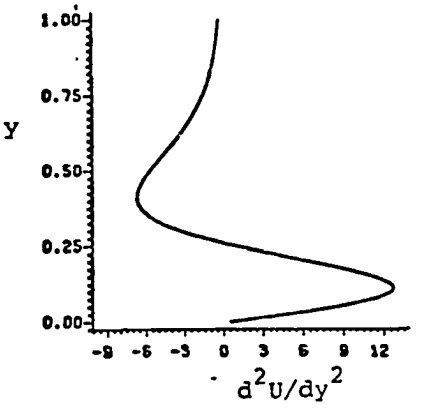

(b) n = 0.2

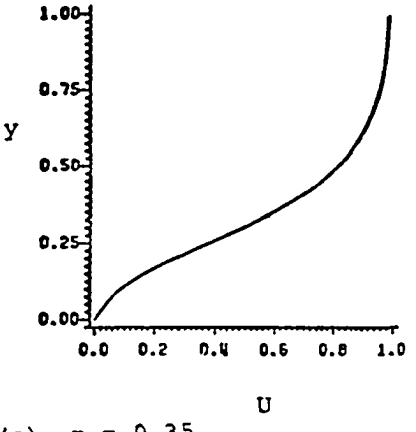

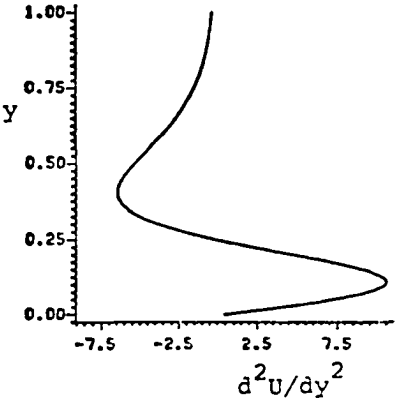

(c) n = 0.35

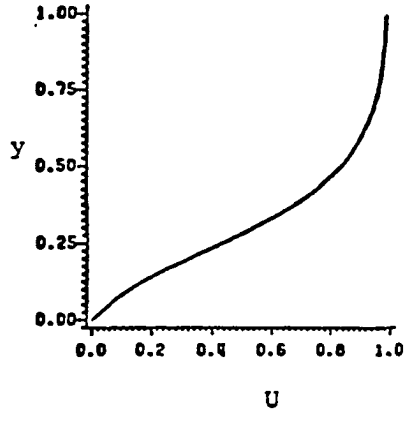

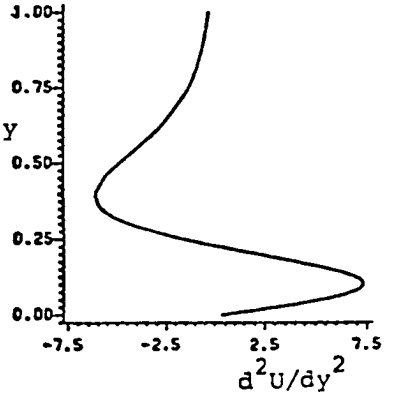

(d) n = 0.5

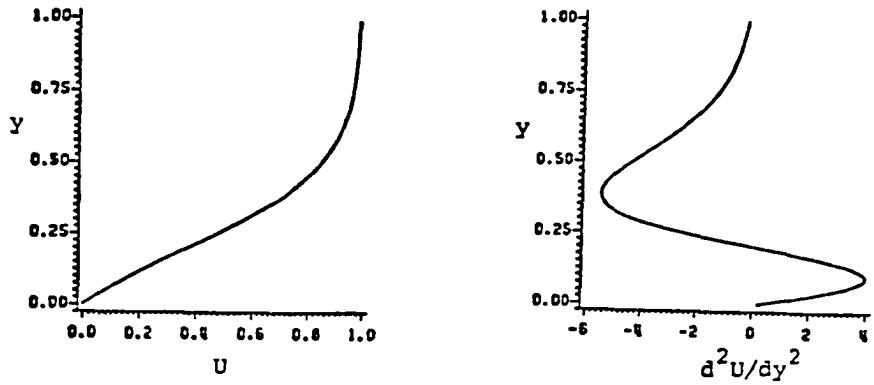

(e) n = 0.7

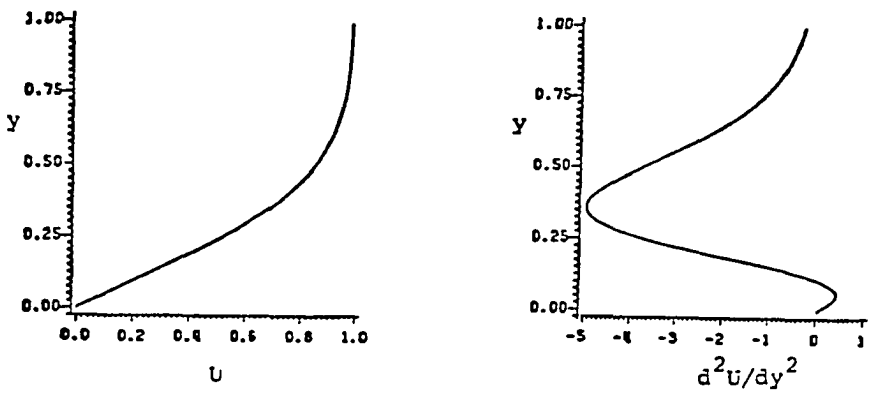

(f) n = 0.74985

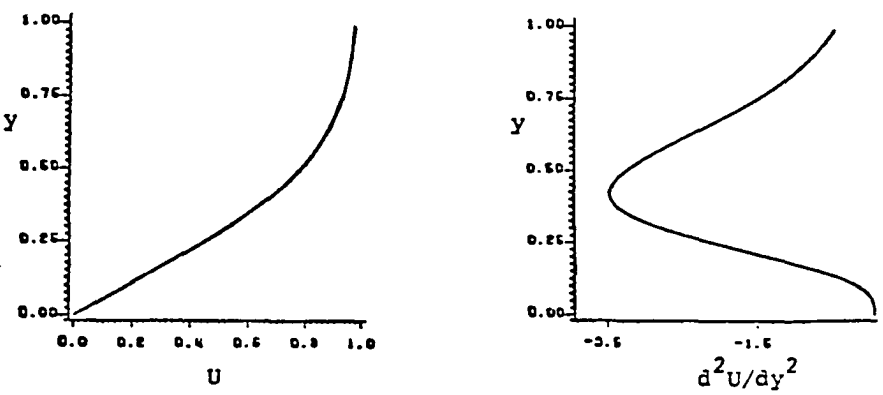

Figure 3.2: The left graph shows a member of the Falkner-Skan-like family of velocity profiles, the corresponding graph on the right indicates d^2U/dy^2 as a function of y. The second derivatives are extremely small for y=0, but not exactly zero. y_o/δ=-0.01 with (a) n=0.1; (b) n=0.2; (c) n=0.35; (d) n=0.5; (e) n=0.7. Profile (f) represents the Blasius profile with n=0.74985 and y_o/δ = 0.02

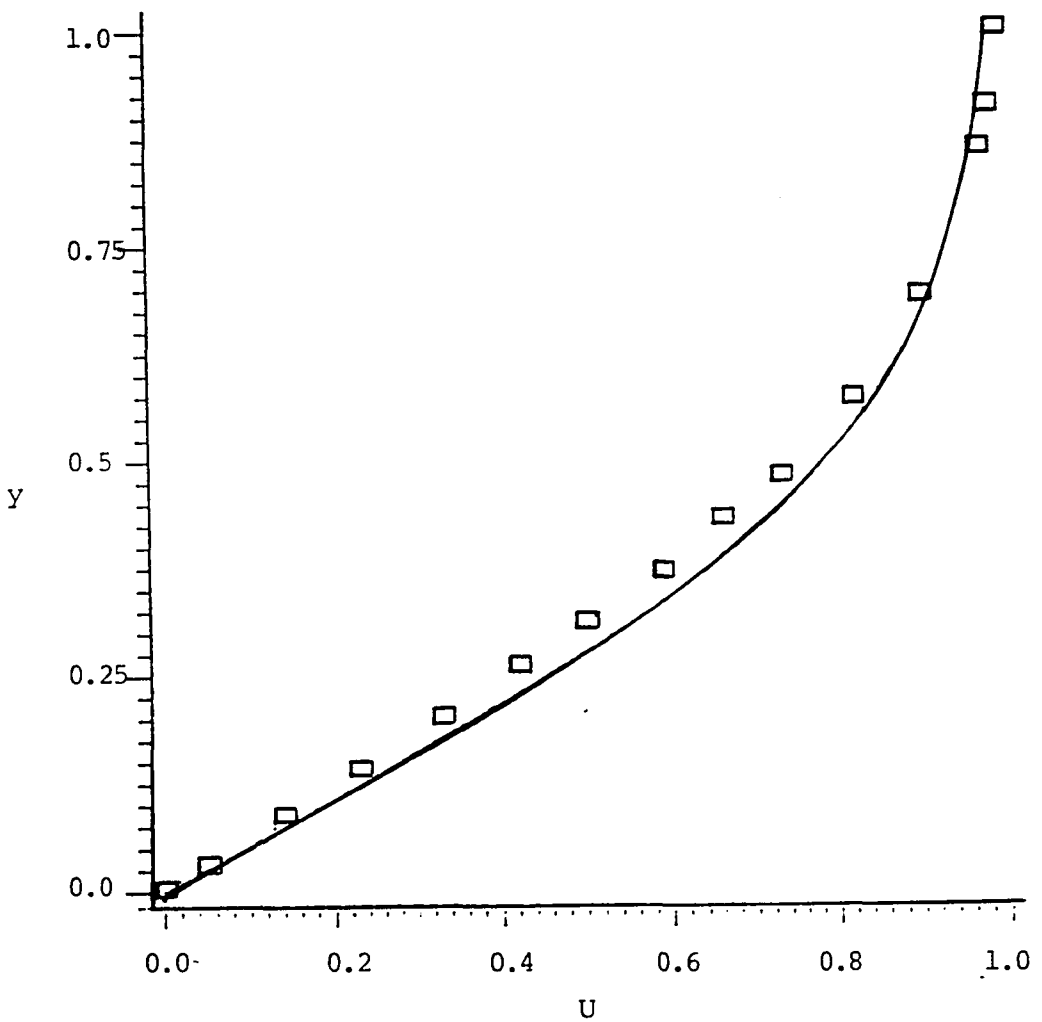

Figure 3.3 Comparison between profile (f) of the Falkner-Skan-like family of profiles and the Blasius profile. The Blasius results are shown as □ with the solid line indicating the result of setting n=0.74985 and y_o/δ=0.02 in the cubic tanh profile.

approximate solution (3.31) and (3.32). Profiles (a) through (e) are singly inflectional. Rayleigh's inflection point theorem says an inflection point is a necessary condition for temporal instability. Thus we might expect a range of unstable wave numbers, although we are not necessarily guaranteed instability. Likewise Russell's results should not yield an instability curve for the Blasius profile (f). Tollmien's relations

$$c_i = \pi \frac{U''_w}{(U'_w)^2} |c|^2 + \cdots \tag{3.17}$$

and

$$c_r = K \frac{U_\infty^2}{U'_w} + \cdots \tag{3.18}$$

should hold for small values of c and k for profiles (a) through (f). In the normal mode assumption, for real k temporal instability results from the term exp(-ckt) (see equation 3.3) having positive imaginary values for c. A comparable way of stating the temporal instability problem is to insist on positive imaginary values for the term $\omega_i = k\, c_i$ for various given k. When equation (3.17) is written in terms of ω_i, we have

$$\omega_i \sim k c_r^2$$

and from (3.18)

$$c_r \sim k$$

so that

$$\omega_i \sim k^3$$

in the limit $k \to 0^+$, $|c| \to 0^+$.

Figure 3.4 shows the solution of Russell's small wave number approximation for real k. Briefly, the solution technique was to choose a particular velocity profile, for example profile (a). Once the profile is defined, the values of $\frac{U_\infty}{v_i}$, r_e^2, r_ω, and r_w are known in equation (3.32). For a given input value of $k\delta$, equation (3.32) can be numerically solved for r_{cl} by means of a complex root finding technique called Mueller's method. (Mueller's method is available as an IMSL routine). The value of r_{cl} was found to 5 significant digits and then substituted into (3.31) to give the corresponding value for c. An entire dispersion curve was generated by slowly incrementing the value of $k\delta$.

Overall the results in Figure 3.4 are pleasing. The most unstable flow, profile (a) has the widest range of unstable wave numbers and the largest maximum growth term , ω_i. As the flow becomes progressively more stable the range of $k\delta$ decreases as does the maximum value of ω_i. Finally for the case of the Blasius profile (f), Mueller's technique would not converge to a vallue of r_{cl}. These results agree quantititavely with the work of Obremski et al. (1969) for the stability of Falkner-Skan flow in the viscous case as Re=Reynolds number $\rightarrow \infty$.

Figure 4.4, profile (a) is the most unstable as seen by the range of unstable wave numbers. For profiles with steeper

(a) n = 0.1

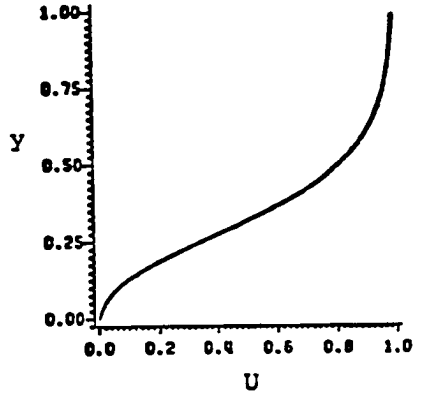

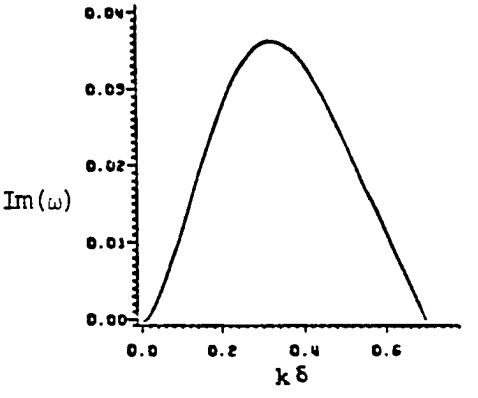

(b) n = 0.2

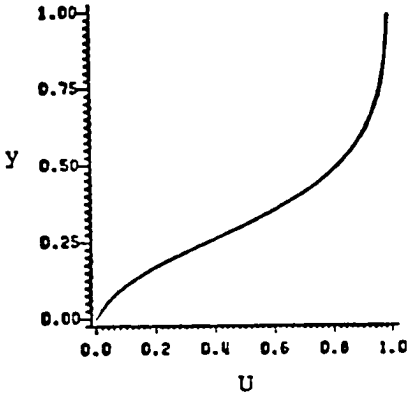

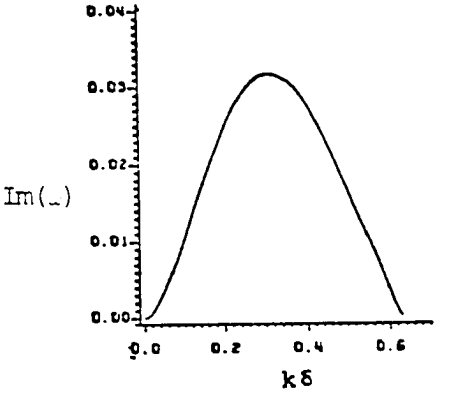

(c) n = 0.35

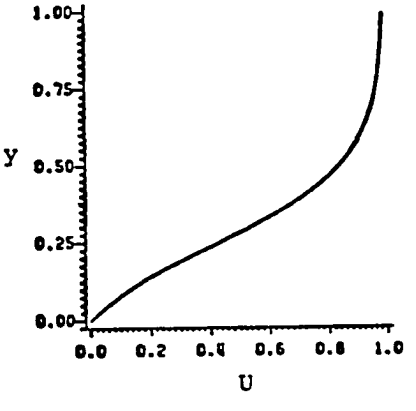

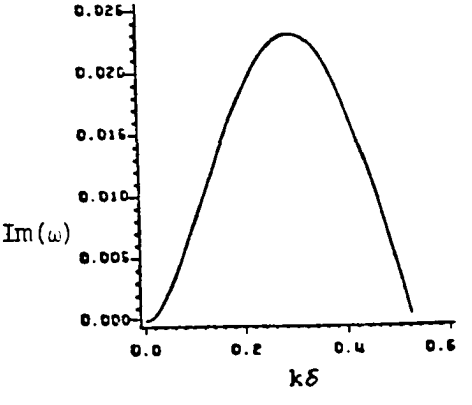

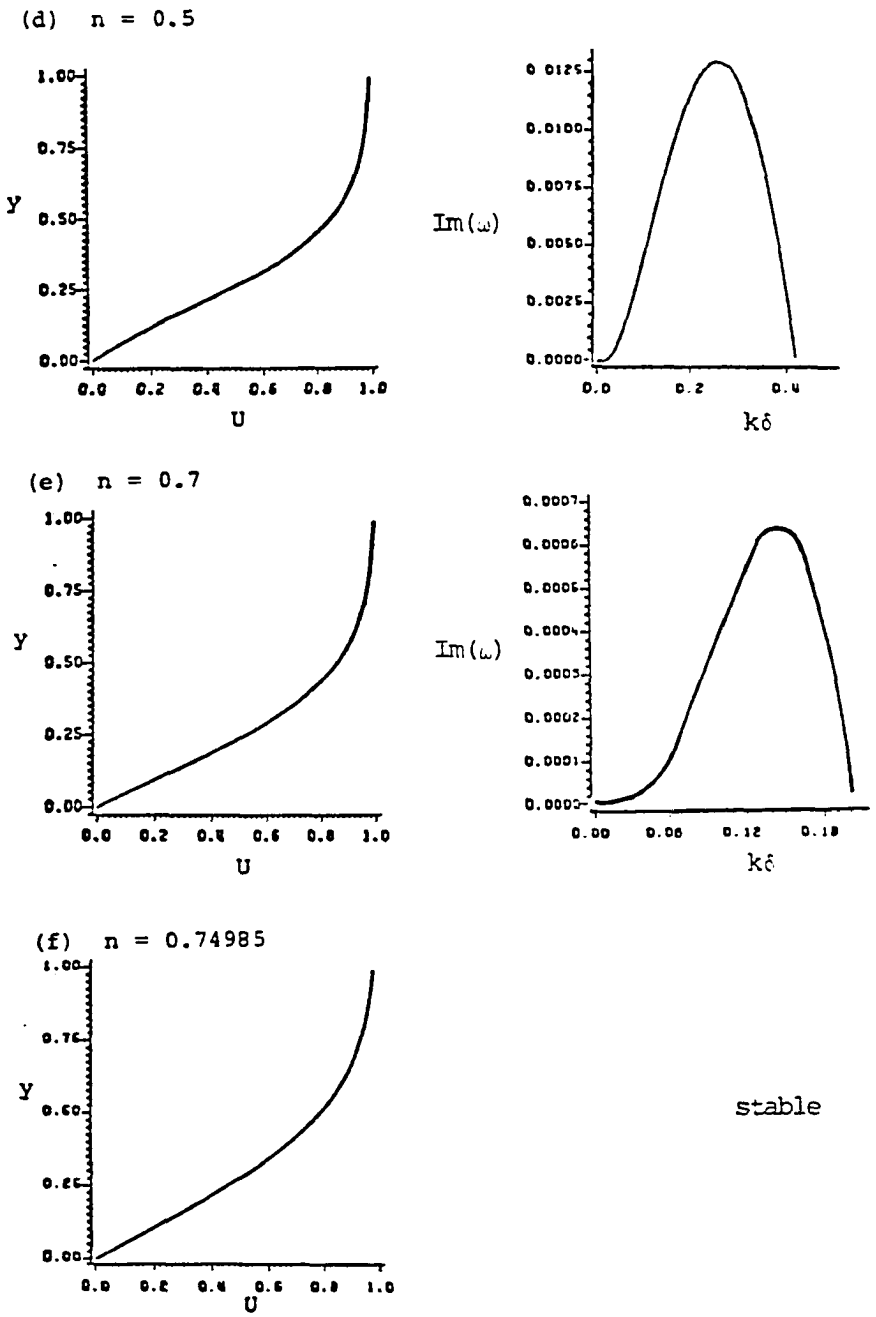

Figure 3.4: A member of the Falkner-Skan-like family of velocity profiles is shown to the left with the corresponding temporal dispersion relation to the right. In all cases, strictly real kδ was the input parameter, giving complex value of c. $y_o/\delta = -0.01$ with variable values of n to model the effect of the adverse pressure gradient. (a) n=0.1; (b) n=0.2; (c) n=0.35; (d) n=0.5; (e) n=0.7 .
Profile (f) corresponds to the Blasius profile with n=0.74985, $y_o/\delta = 0.02$.

slope at the wall ($U'_w \to 0$), the dispersion relation would not converge to the short wave cut-off point. Thus for highly unstable flows, with a large range of unstable $k\delta$, for example $\beta = -0.1988$ in the Falkner-Skan family, Russell's approximate solution will not converge to the short wave cut-off. This is not unexpected since the solution is a first-order small wave number approximation.

For $k\delta \to 0$, profiles (a) through (e) exhibit Tollmien's result

$$\omega_i \sim (k\delta)^3$$

This can be seen especially in profile (e) where the range of unstable wave numbers is sufficiently small.

The short wave cutoff results derived earlier also hold for this Falkner-Skan like family of profiles. Recall that the phase velocity, c_r, of the neutral wave at the short wave cutoff point should correspond to the velocity of the profile at the inflection point. Table One lists these results for profiles (a) through (e).

Profile (e) is also interesting because it appears Blasius-like at first glance. The flow changes curvature slightly. Experimentally what appears Blasius-like may have a slight inflection point. These results indicate a small range of unstable wave numbers is possible.

Table One

Short wave cut off results

n	c/Uinf	$U(y_{inflection})/Uinf$
0.1	0.3711	0.3697
0.166667	0.3785	0.3766
0.2	0.3807	0.3828
0.35	0.3889	0.3929
0.5	0.3762	0.3815
0.7	0.2342	0.2390

3.4 The Mixed Stability Problem for the Falkner-Skan-like Family of Profiles

Encouraged by the temporal stability results, we decided to explore the mixed stability problem. Since derivation of the small wavenumber approximation to solution of the Rayleigh equation (3.16) made no assumption about the realness of k, it is possible to define a complex $k\delta$, and then solve the secular equation for complex c.

Both C.C. Lin (1955) and Drazin and Reid (1981) express concern about the formulation of the stability problem for complex k. A mathematical requirement of normal modes

$$\vec{u}'(\vec{x},t) = \tilde{\vec{u}}(y)\exp[i(\alpha x + \beta z - \alpha c t)]$$

is that they be bounded as $x,z \to \pm\infty$. In order to satisfy the boundedness at infinity requirement, α and β must be real.

Despite the mathematical constraint numerous researchers have considered spatially growing waves because experimental results of boundary-layer flow show growing waves convected downstream. The primary rationale for using spatially growing waves in boundary-layer geometry is that the waves are fairly localized, and nonlinear effects become important long before the waves travel a great distance in the x,z direction. Crimanale and Kovasznay (1962) examined the behavior of wave pulses propagating downstream. Stuart (1960), Watson (1960), and Watson (1962) studied spatially growing finite amplitude waves in plane Poiseuille flow. Gaster (1965) studied spatially growing waves in a boundary layer where the initial disturbance was chosen to represent a vibrating ribbon used to force disturbances in experimental studies of boundary-layer flow. Drazin and Reid (1981) devote a small section of their book to the spatial stability problem, (pp. 349-353) in light of the experimental results and the number of theoretical results concerned with the spatial instability problem.

This dissertation is not concerned simply with the spatial instability problem, but rather the mixed stability problem, where waves grow as they are convected downstream and in addition are allowed to grow locally in time. Pierrehumbart (1984) has discussed the mixed problem for shear flows. Gaster (1965) suggested the solution to a linear boundary-layer stability problem is the mixed problem. To the best of our knowledge, the mixed problem has not been solved for boundary-layer geometry.

Group velocity plays an important role in the mixed problem. The normal modes vary with respect to wavenumber. The most unstable mode is neighbored by modes only slightly less unstable. So this group of most unstable modes may be thought to propagate downstream. Hence a wave packet better characterizes spatial motion than a single traveling wave, and the group velocity describes the packet's motion better than a single phase velocity. Gaster (1962) used group velocity to relate spatial growth to temporal growth when the rates of growth are small ($|k_i| \ll 1$). In this work we use group velocity to relate a complex wavenumber to a specific complex phase velocity.

Two important questions come to mind when posing the mixed stability problem. First, what variable(s) describe the total growth rate of the wave? Should $k_i < 0$ be the measure,

or $(kc_i) > 0$, or some combination of both be the measure of amplification? Second, we must somehow address the boundedness at infinity requirement for the spatially growing part of the mixed stability problem. The answer to these two questions will be to define the "total" instability of a wave packet as follows.

In general, the normal-mode assumption for a one dimensional wave is of the form

$$\varphi(x,t) = A(y)\, e^{i\theta}$$

where the quantity θ, the phase, is given by

$$\theta = kx - \omega t$$

Variations in phase with respect to time, following the trajectory of a wave packet are given by

$$\frac{d\theta}{dt} = \frac{\partial\theta}{\partial t} + c_g \frac{\partial\theta}{\partial x}$$

Using the definitions

$$\frac{\partial\theta}{\partial t} = -\omega$$

$$\frac{\partial\theta}{\partial x} = k$$

we have

$$\frac{d\theta}{dt} = -\omega + c_g k$$

or

$$\frac{d\theta}{dt} = k(c_g - c) \tag{3.33}$$

Equation (3.33) will determine the total amplification of a wave packet in the mixed problem. If

$$Im\left[\frac{d\theta}{dt}\right] < 0$$

the wave packet experiences exponential amplification. By

following the trajectories of wave packets, we argue both local temporal and spatial instabilities "felt" by the wave packets can be accounted for.

Equation 3.33 describes a change of reference frame so that in the new frame time derivatives are taken following the wave packet. While the wave packet may experience exponential amplifications relative to the new coordinate system, far upstream or downstream of the wavepacket in laboratory coordinates we assume the disturbances die out, thus answering the boundedness at infinity requirement. Thus equation 3.33 is the appropriate quantity to answer the two question posed above.

The application of Russell's small wavenumber approximation to the mixed problem is now described. By definition the group velocity is given by

$$\vec{c}_g \equiv \Omega_{\vec{k}}$$

where for the one-dimensional wave

$$c_g = c + k \frac{dc}{dk} \tag{3.34}$$

Equation (3.31) provides the relationship between c and k via the intermediate value r_{cl}

$$c_g = c + k \frac{dc}{dr_{cl}} \frac{dr_{cl}}{dk}$$

But from (3.32) we can find $\frac{dr_{c_1}}{dK}$, although it is more convenient to solve (3.32) for k and find $\frac{dK}{dr_{c_1}}$. Writing in more compact notation, we obtain

$$K\delta = \frac{-1}{(U_\infty - C)^2} \left[\sum_{m=1}^{3} B_m (C_m - D_m \log E_m) \right]^{-1}$$

where

$$B_m = \frac{1}{[3U_1(r_{cm}^2 - r_e^2)]^2 \, [1-(r_{cm} - r_\infty + 1)^2]} \tag{3.35a}$$

$$C_m = \frac{1}{r_w - r_{cm}} - \frac{1}{r_\infty - r_{cm}} \tag{3.35b}$$

$$D_m = 2 \left[\frac{r_{cm}}{r_{cm}^2 - r_e^2} - \frac{r_{cm} - r_\infty + 1}{1-(r_{cm} - r_\infty + 1)^2} \right] \tag{3.35c}$$

$$E_m = \frac{r_\infty - r_{cm}}{r_w - r_{cm}} \quad \frac{2 + r_w + r_\infty}{2} \tag{3.35d}$$

$\frac{dK}{dr_{c_1}}$ is given as

$$\begin{aligned} \frac{dK}{dr_{c_1}} = {} & \frac{-2(3r_{c_1}^2 - 3r_e^2)}{(U_\infty - C)^3} \left[\sum_{m=1}^{3} B_m (C_m - D_m \log E_m) \right]^{-1} \\ & + \frac{1}{(U_\infty - C)^2} \left[\sum_{m=1}^{3} B_m (C_m - D_m \log E_m) \right]^{-2} \textcircled{x} \\ & \left\{ \sum_{m=1}^{3} \left[\frac{dB_m}{dr_{cm}} (C_m - D_m \log E_m) \right. \right. \\ & \left. \left. + B_m \left(\frac{dC_m}{dr_{cm}} - \frac{D_m}{E_m} \frac{dE_m}{dr_{cm}} - \frac{dD_m}{dr_{cm}} \log E_m \right) \right] \frac{dr_{cm}}{dr_{c_1}} \right\} \end{aligned} \tag{3.36}$$

where

$$\frac{dB_m}{dr_{cm}} = \frac{-1}{\left\{[3U_1(r_{cm}^2 - r_e^2)]^2\,[1-(r_{cm}-r_\infty+1)^2]\right\}^2} \circledast$$

$$\left\{2[3U_1(r_{cm}^2-r_e^2)][3U_1(2r_{cm})][1-(r_{cm}-r_\infty+1)^2] + [3U_1(r_{cm}^2-r_e^2)]^2\,[-2(r_{cm}-r_\infty+1)]\right\}$$

$$\frac{dC_m}{dr_{cm}} = \frac{1}{(r_w-r_{cm})^2} + \frac{1}{(r_\infty-r_{cm})^2}$$

$$\frac{dD_m}{dr_{cm}} = 2\left[\frac{-(r_{cm}^2-r_e^2)}{(r_{cm}^2-r_e^2)^2} - \frac{1+(r_{cm}-r_\infty+1)^2}{1-(r_{cm}-r_\infty+1)^2}\right]$$

$$\frac{dE_m}{dr_{cm}} = \left[\frac{r_\infty-r_w}{(r_w-r_{cm})^2}\right]\left[\frac{2+r_w-r_\infty}{2}\right]$$

Since (3.31) represents the first order small wavenumber approximate solution to the Rayleigh equation , it depends linearly on k. Noting (3.36) is independent of k, we solve (3.34) for k

$$k = \frac{(c_g - c)\frac{dk}{dr_{c_1}}}{[3r_{c_1}^2 - 3r_e^2]} \tag{3.37}$$

and substitute this expression for k into (3.32) giving

$$1 = \frac{(c_g - c)\frac{dk}{dr_{c_1}}}{(3r_{c_1}^2 - 3r_e^2)} (U_\infty - c)^2 \sum_{m=1}^{3} B_m (C_m - D_m \log E_m) \tag{3.38}$$

The above transcendental equation can be solved for r_{c1} given U(y) and c_g, where c_g is a real group velocity. Then equation 3.31 determines the corresponding complex phase velocity c for these given values of c_g and U(y). Likewise, equation 3.37 determines the corresponding complex wavenumber.

In summary, for the temporal stability problem a real wavenumber kδ and known profile U(y) were input to find the corresponding complex phase velocity c. For the mixed problem a real group velocity c_g and a known velocity profile U(y) were

input to find the corresponding complex phase velocity c. Then the relationship between c_g, c, and k determines the appropriate complex wavenumber.

Using the same family of Falkner-Skan-like flows as in the temporal stability case, we considered the mixed stability problem. Figure 3.5 presents the stability results. First, we plotted Im($\frac{d\theta}{dt}$), the imaginary part of the frequency as seen by an observer moving with the group velocity, versus the real part of the wavenumber. This was done in order to compare with the temporal problem where we have plotted imaginary frequency as seen by a stationary observer, ω_i, versus strictly real wavenumber. The maximum amplification for the mixed problem is only slightly larger than in the temporal problem. As the Falkner-Skan profile feels less adverse pressure gradient, the magnitude of Im($\frac{d\theta}{dt}$) decreases, similarly to the behavior for the temporal problem. For the Blasius profile, the mixed stability results converged to solutions unlike the temporal stability case. The solutions were damped, however, which indicates the Blasius profile does not produce instability in the mixed problem.

In the temporal case, strictly real k was the input, giving complex c as output. In the mixed problem, strictly real group velocity was the input, giving complex $d\theta/dt$ as output.

(a) n = 0.1

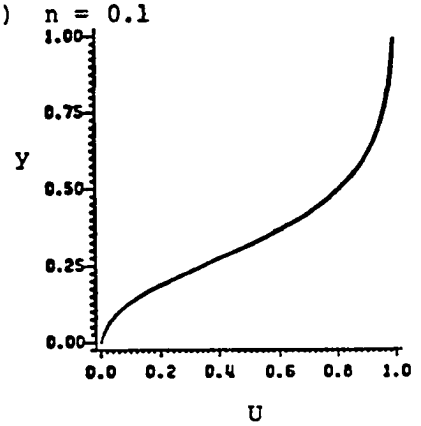

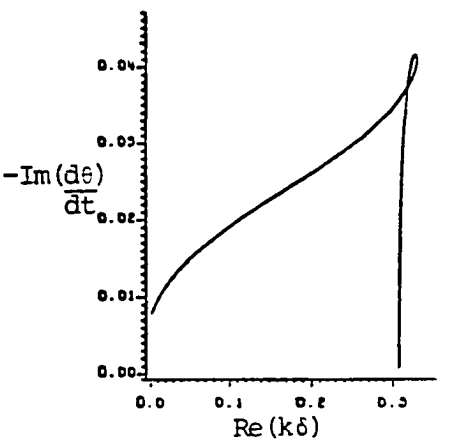

(b) n = 0.2

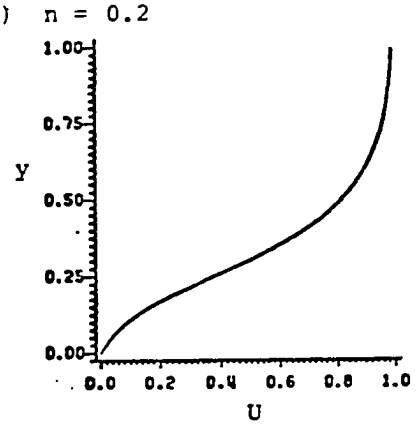

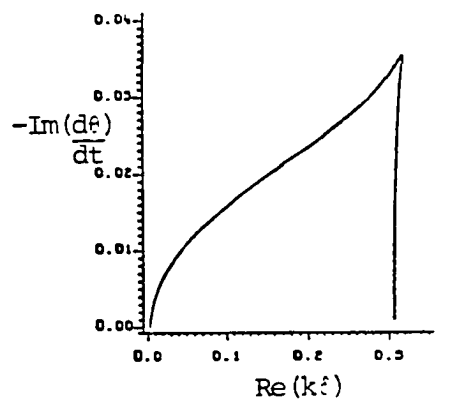

(c) n = 0.35

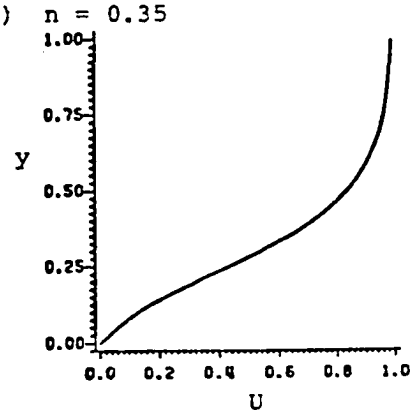

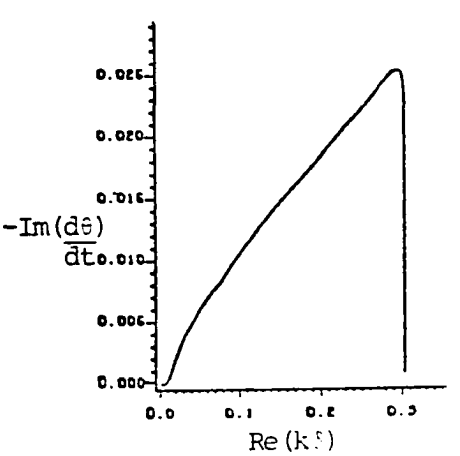

(d) n = 0.5

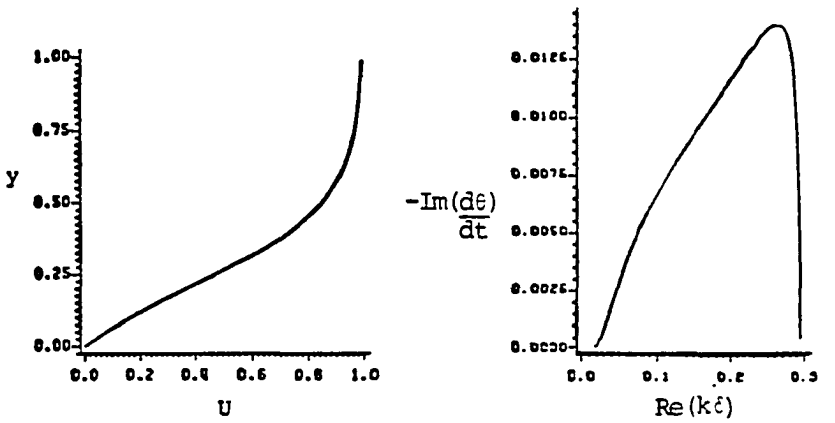

(e) n = 0.7

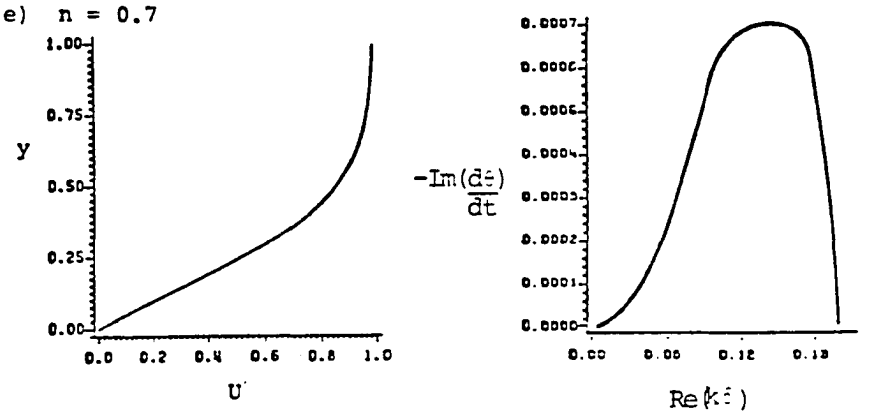

(f) n = 0.74985

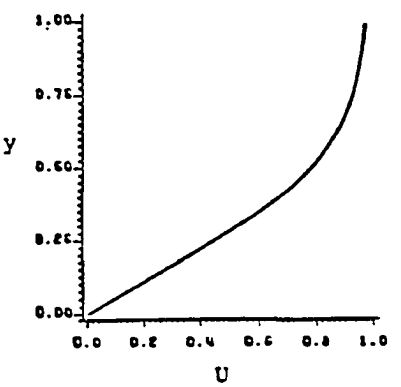

stable

Figure 3.5: A member of the Falkner-Skan-like family of velocity profiles is shown to the left with the corresponding "mixed" dispersion relation to the right. In all cases, strictly real group velocity, c_g, was the input parameter, giving complex values of k and c. $y_o/\delta = -0.01$ with variable values of n. (a) n=0.1; (b) n=0.2; (c) n=0.3; (d) n=0.5; (e) n=0.7. Profile (f) corresponds to the Blasius profile with n=0.74985, $y_o/\delta = 0.02$.

Hence another way to plot the mixed problem results is to mimic the temporal problem and plot output versus input, i.e., Imag($\frac{d\theta}{dt}$) versus c_g. These results graphically appear similar to the temporal problem as shown in figure 3.6. In the region of small c_g and small Im($\frac{d\theta}{dt}$), the curve takes on behavior similar to that predicted by Tollmien for the temporal problem.

3.4.1 Derivation of Vanishingly Small-Wavenumber Expression for the Mixed Stability Problem

We begin with the definition of group velocity for a one-dimensional wave

$$c_g = c + k\frac{dc}{dk}$$

and assume for vanishingly small c and k

$$\frac{dc}{dk} \approx \frac{c}{k} \approx \text{constant}$$

Then

$$c_g \approx 2c \tag{3.39}$$

Thus for small c and k, $c_i \to 0$. This result can be found in the Appendix of Rayleigh's The Theory of Sound, Vol. I for "flexural waves". The definition of $\frac{d\theta}{dt}$ gives

$$\frac{d\theta}{dt} = k(c_g - c)$$

Substituting 3.39 gives

$$\frac{d\theta}{dt} \approx k\frac{c_g}{2}$$

$$\mathrm{Im}\left(\frac{d\theta}{dt}\right) \approx \frac{c_g}{2}\,\mathrm{Im}(k) \tag{3.40}$$

The expression for k_i can be found from Tollmien's analysis.

Recall the small wavenumber approximation gave first order results

$$0 = -c\,G_\infty \left[1 + K(U_\infty - c)^2 \int_0^\delta \left[\frac{1}{U-c}\right]^2 dy_* - K\delta + \Theta\left[(K\delta)^2\right]\right] \tag{3.16a}$$

(3.16a)

We write the real and imaginary parts for $|c| \to 0^+$ and $|k| \to 0^+$

$$\text{Real:}\quad 0 = 1 + K_r U_\infty^2\, \mathrm{Re}\left[\int_0^\delta \left[\frac{1}{U-c}\right]^2 dy_*\right] - K_i U_\infty^2\, \mathrm{Im}\left[\int_0^\delta \left[\frac{1}{U-c}\right]^2 dy_*\right] \tag{3.41}$$

$$\text{Imag:}\quad 0 = K_i U_\infty^2\, \mathrm{Re}\left[\int_0^\delta \left[\frac{1}{U-c}\right]^2 dy_*\right] + K_r U_\infty^2\, \mathrm{Im}\left[\int_0^\delta \left[\frac{1}{U-c}\right]^2 dy_*\right] \tag{3.42}$$

Use Tollmien's results

$$\mathrm{Re}\left\{\int_0^\delta \frac{dy_*}{(U-c)^2}\right\} = \frac{-c_r}{U'_w |c|^2} + \frac{U''_w}{(U'_w)^3} \log A|c| + \Theta\left[\frac{1}{U(y_{j*})U'(y_{j*})}\right]$$

$$\mathrm{Im}\left\{\int_0^\delta \frac{dy_*}{(U-c)^2}\right\} = \frac{c_i}{U'_w |c|^2} + \frac{U''_w}{(U'_w)^3}(-\pi) + \left(\frac{U''}{(U')^3}\right)\Big|_w \frac{c_r}{U'_w}(-\pi) + \Theta\left[\frac{c_i}{U^2(y_{j*})U'(y_{j*})}\right]$$

(a) n = 0.1

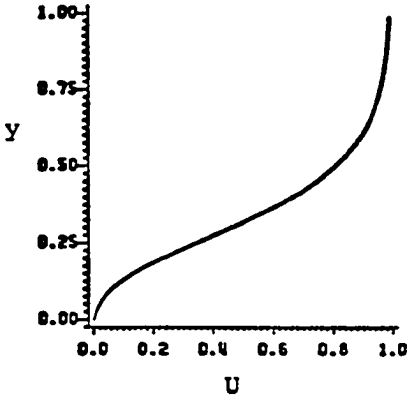

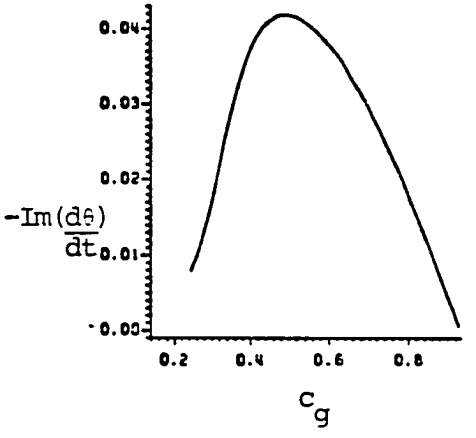

(b) n = 0.2

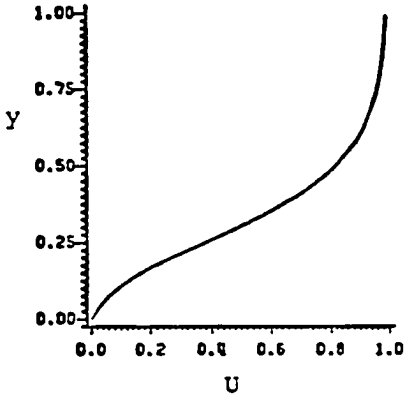

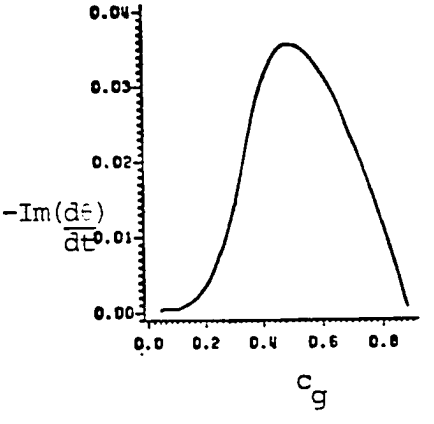

(c) n = 0.35

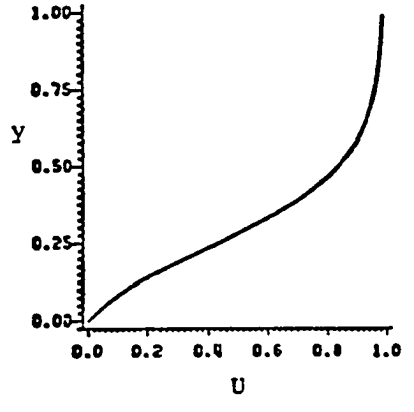

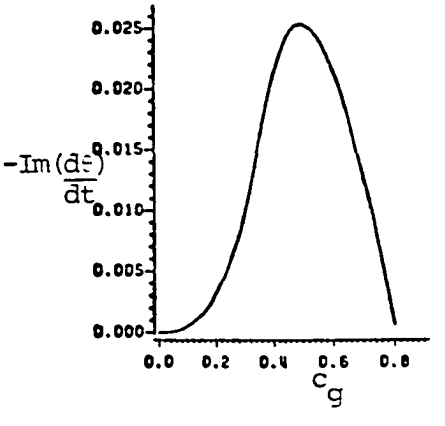

(d) n = 0.5

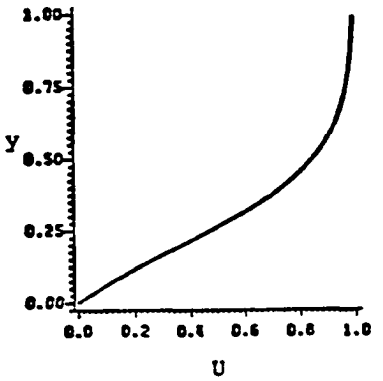

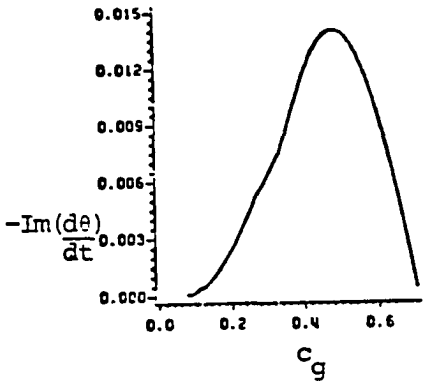

(e) n = 0.7

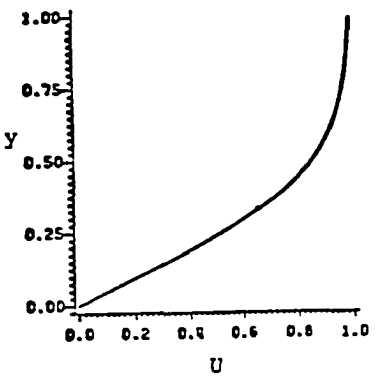

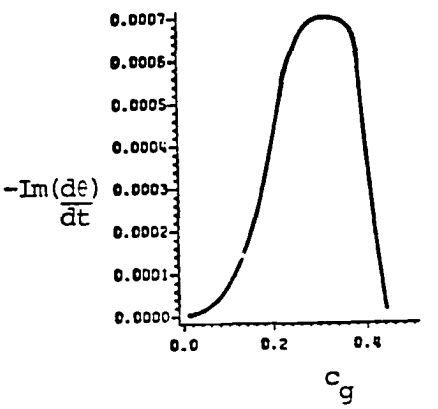

(f) n = 0.74985

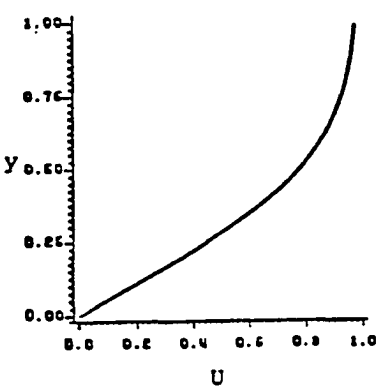

stable

Figure 3.6: A member of the Falkner-Skan-like family of velocity profiles is shown to the left with the corresponding "mixed" dispersion to the right. -Im(dθ/dt) represents the total rate of growth of a disturbance, both in space and time. In all cases, strictly real group velocity, c_g, was the input parameter, giving complex values for dθ/dt. y_o/δ=-0.01 with variable values of n. (a) n=0.1; (b) n=0.2; (c) n=0.3; (d) n=0.5; (e) n=0.7. Profile (f) corresponds to the Blasius profile with n=0.74985, y_o/δ=0.02.

Substitute the leading order terms into (3.40) and (3.41) and neglect terms that involve c_i since $c_i \sim \mathcal{O}(k^2)$ for this family of curves as $|c| \to 0^+$, $|k| \to 0^+$.

Real:
$$0 = 1 + K_r U_\infty^2 \left(\frac{-c_r}{U'_w c_r^2}\right) - K_i U_\infty^2 \left[\frac{U''_w}{(U'_w)^3}(-\pi)\right] \tag{3.43}$$

Imag:
$$0 = K_i U_\infty^2 \left(\frac{-c_r}{U'_w c_r^2}\right) + K_r U_\infty^2 \left[\frac{U''_w}{(U'_w)^3}(-\pi)\right] \tag{3.44}$$

Solving (3.43) for $k_r U^2$ yields

$$K_r U_\infty^2 = \frac{1 + K_i U_\infty^2 \left[\frac{U''_w}{(U'_w)^3}\pi\right]}{\frac{c_r}{U'_w c_r^2}}$$

Substituting this result into (3.44) gives

$$K_i U_\infty^2 = \frac{\frac{-\pi c_r^2 U''_w}{U'_w}}{1 + \frac{\pi^2 c_r^2}{(U''_w)^2}}$$

Assume in the limit $|c| \to 0^+$ that

$$\frac{\pi^2 c_r^2}{(U''_w)^2} << 1$$

Then

$$K_i \sim -\pi \frac{c_r^2}{U_\infty^2} \frac{U''_w}{U'_w} \tag{3.45}$$

For a given profile in the Falkner-Skan-like family, U''_w and U'_w are constants, and thus

$$K_i \sim c_r^2 \tag{3.46}$$

Substituting this result into (3.40) along with $c_r \sim \frac{c_g}{2}$ gives

$$Im\left(\frac{d\theta}{dt}\right) \approx \left(\frac{c_g}{2}\right)^3 \tag{3.47}$$

For small c_g and Im($\frac{d\theta}{dt}$) the curves shown in Figure 3.5 reflect this cubic behavior.

The curious result of this mixed stability problem is the possible existence of a generalized Rayleigh Inflection Point Theorem. Recall equation 3.6 was derived for real k only. The previous equation

$$\int_{y_1}^{y_2} \left(\frac{d^2|\tilde{v}|^2}{dy^2} - k^2 |\tilde{v}|^2 \right) dy = \int_{y_1}^{y_2} \frac{d^2U}{dy^2} \frac{|\tilde{v}|^2}{(U-c)} dy$$

holds for complex k. By observing this result, the best one can say is that the quantity

$$2 k_r k_i - \frac{c_i}{|U-c|^2} \frac{d^2U}{dy^2}$$

must change sign at least once across the interval (y_1,y_2). Since k_i and c_i, in addition to $U''(y)$, may change sign across the interval, little can be said about the requirements of the existence of an inflection point for instability.

Yet the results of this study point to the necessary condition of at least one inflection point for mixed instability. It seems the proof must begin with an expression of the Rayleigh equation that involves group velocity. This author has made little head way in such a proof.

To summarize this chapter, we covered Russell's solution of the Rayleigh equation using a small wavenumber approximation which holds for a cubic-tanh family of velocity profiles. The

temporal stability results for a Falkner-Skan-like group of velocity profiles agree well with existing theories provided the profiles are not too unstable. A surprising bonus associated with Russell's solution is the mixed stability problem. Russell's solution permits both a complex wavenumber and associated complex phase velocity to be calculated by the method presented above with strictly real group velocity as input. The final section of this chapter involved plotting stability diagrams for the mixed problem and examining the relationship between frequency and group velocity for vanishingly small wavenumber and phase velocity -- a novel contribution to the area of hydrodynamic stability theory.

CHAPTER FOUR

ONE DIMENSIONAL SHEAR WAVE TRAJECTORIES

Chapter Two presented derivations of the equations for the trajectories of secondary wave packets travelling through slightly inhomogeneous background flow. Equations governing wavenumber and amplitude propagation along the trajectories were also derived. The results of Chapter Two held for shear flow waves, that is, a non-conservative system of modal waves where the local dispersion relation was given by a solution of the Rayleigh equation. Chapter Three presented a small wavenumber asymptotic approximation to the solution of the Rayleigh equation and associated eigenvalue problem for a cubic-tanh family of velocity profiles. Hence we have in hand all necessary equations in order to trace wave packet trajectories through physically realistic background flows.

4.1 Equations of One-Dimensional Shear Flow

Begin with a slowly-varying wave packet, traveling through a "slightly" inhomogeneous background flow. By "slightly" we mean that variations in the background flow are small within the distance of one wavelength or the time of one cycle of the wave packet. For a phase function $\Theta(x,t)$, the local wavenumber, k, and frequency, ω, are

$$k = \partial\Theta/\partial x \tag{4.1}$$

$$\omega = -\partial\Theta/\partial t \tag{4.2}$$

Here x is the streamwise position coordinate. Eliminating the phase function gives

$$\frac{\partial k}{\partial t} + \frac{\partial \omega}{\partial x} = 0 \tag{4.3}$$

Propose a dispersion relation

$$\omega = \Omega(k,x,t) \tag{4.4}$$

which holds for modal waves in a non-conservative system. The dispersion relation can be described locally as a solution of the Rayleigh or Orr-Sommerfeld equation.

Substituting (4.4) into (4.3) and using wavenumber dependence on x gives

$$\frac{\partial k}{\partial t} = \frac{\partial}{\partial x}\left[\Omega(k,x,t)\right] \tag{4.5}$$

subject to the initial condition

$$k = f(x) \qquad \text{at} \qquad t = 0 \tag{4.6}$$

Since the eigenvalues of the Rayleigh or Orr-Sommerfeld equation are

in general complex, $\Omega = \Omega(k,x,t)$ is complex. Hence Ω_k and Ω_x are in general complex valued and the solution to equation (4.5) will be complex. Note, however, that x and t can be real valued in the solution of (4.5) and (4.6).

Writing (4.5) and (4.6) as characteristic equations gives

$$\frac{dk}{dt} = -\Omega_x \tag{4.7}$$

on

$$\frac{dx}{dt} = c_g \tag{4.8}$$

where c_g, the group velocity, is defined as

$$c_g \equiv \Omega_k \tag{4.9}$$

with initial conditions

$$\left.\begin{aligned} k &= k_o \\ x &= x_o \end{aligned}\right\} \quad \text{at} \quad t = 0 \tag{4.10}$$

Equation (4.8) has innocently compounded the difficulties in tracing trajectories of shear flow wave packets. Since $\Omega_k = c_g$ is complex valued, the position x is now also complex valued. Since x is typically viewed as a real coordinate, let ζ be a complex position coordinate of the form

$$\zeta = x + i\eta$$

This change of notation will be helpful in describing the general solution of (4.7) and (4.8), which can be rewritten as

$$\frac{dk}{dt} = -\Omega_\zeta(k,\zeta,t) \tag{4.11a}$$

on

$$\frac{d\zeta}{dt} = \Omega_k(k,\zeta,t) \tag{4.11b}$$

The general solution is

$$\kappa = \mathbb{K}(\kappa_0, \zeta_0, t) \tag{4.12a}$$

$$\zeta = \mathbb{Z}(\kappa_0, \zeta_0, t) \tag{4.12b}$$

Here k_0 and ζ_0 are the values of k and ζ at t = 0.

Impose the initial condition

$$\kappa_0 = f(\zeta_0) \tag{4.13}$$

(which is analogous to (4.6)). Substituting (4.13) into (4.12) casts

The general solution has the form

$$\kappa = \mathbb{K}^+(\zeta_0, t) \tag{4.14a}$$

$$\zeta = \mathbb{Z}^+(\zeta_0, t) \tag{4.14b}$$

The above two equations involve four quantities, so that only two are independent. Let and t be the independent ones. This gives a functional dependency of the form

$$\kappa = \chi(\zeta, t) \tag{4.15}$$

We define a subset of all possible solution points, which we call the "physical subset", Σ, of solution points by the filtering condition

$$\mathrm{Im}(\zeta) = 0 \tag{4.16a}$$

$$\mathrm{Re}(\zeta) = x \tag{4.16b}$$

These are the features that the exact solution should have if we solved (4.5) and (4.6) by a step-by-step method. Note that (4.13) is the "analytic continuation" of the initial data function defined by (4.6).

The preceeding paragraph may appear to some readers as excessive mathematical finery. The important point is that (4.7) and (4.8) cannot be solved by the method of characteristics in a way that ensures real position coordinate x for all points on a single characteristic curve. Out of the entire family of characteristics defined by (4.7) and (4.8) it is possible to find a "physical subset" of points where x is real. To find this physical subset requires we jump from characteristic to characteristic as we progress in time, always "hopping" on the characteristic that intersects the real position axis at the particular time of interest.

The approximation of "hopping" from one characteristic to another without drastically altering the solution must be justified. This is possible if the complex trajectories that belong to the physical subset, Σ, are nearly tangent to the real axis in the complex $\mathcal{J}$-plane. That is, $\mathrm{Im}(\mathcal{J}) \ll \mathrm{Re}(\mathcal{J})$.

To deduce $\mathrm{Im}(\mathcal{J}) \ll \mathrm{Re}(\mathcal{J})$, we make an assumption about the dispersion relation. Let

$$\frac{\mathrm{Im}(\Omega)}{\mathrm{Re}(\Omega)} \doteq \Theta(\epsilon_{rf}) \tag{4.17}$$

where ϵ_{rf} is the small parameter which describes the "flatness" of the reference flow discussed in Chapter Two. Then if we consider $\frac{d}{dt}(\Omega_k)$, we have

$$\mathrm{Im}\left(\frac{d\Omega_k}{dt}\right) = \mathrm{Im}\left[\frac{dk}{dt}\,\Omega_{kk} + \frac{dx}{dt}\,\Omega_{kx} + \Omega_{kt}\right]$$

or, by applying the definitions given in (4.1) and (4.2),

$$\mathrm{Im}\left(\frac{d\Omega_k}{dt}\right) = \mathrm{Im}\left[-\Omega_x \Omega_{kk} + \Omega_k \Omega_{kx} + \Omega_{kt}\right]$$

$$= \Theta(\epsilon_{rf}^2)$$

The real part of the time rate of change of group velocity is given by

$$\mathrm{Re}\left(\frac{d\Omega_k}{dt}\right) = \mathrm{Re}\left[-\Omega_x \Omega_{kk} + \Omega_k \Omega_{kx} + \Omega_{kt}\right]$$

$$= \Theta(\epsilon_{rf})$$

Hence

$$\mathrm{Im}\left(\frac{d\Omega_k}{dt}\right) << \mathrm{Re}\left(\frac{d\Omega_k}{dt}\right) \tag{4.18}$$

By an appropriate choice of initial conditions, it follows from (4.18) that

$$\mathrm{Im}(\Omega_k) << \mathrm{Re}(\Omega_k)$$

Then from (4.8) it follows that

$$\mathrm{Im}(\mathcal{J}) << \mathrm{Re}(\mathcal{J})$$

Thus, provided we begin with a dispersion relation of the form of (4.17), the complex characteristics are nearly parallel to the real axis in the complex $\mathcal{J}$ -plane.

To numerically implement this solution technique, we propose the following. We initially select a complex wavenumber, k_o, so that the initial value of group velocity, c_g, is strictly real. After each iteration of a Runge-Kutta solution technique, the group velocity,

c_g, has a very small imaginary part. We truncate $Im(c_g)$, consequently from (4.11b) we have $Im(\mathcal{J}) = 0$. We have now "hopped" to a new characteristic which intersects the real axis of the complex $\mathcal{J}$-plane. The value of the wavenumber is then adjusted, by use of the dispersion relation (4.4), to hold for strictly real group velocity. We refer to this truncation of imaginary group velocity after each iteration as the "filtering scheme". See Figure 4.1 for a schematic diagram of the "filtering scheme".

In order to assess the accuracy of this scheme in approximating the solution of equation (4.5), we argue that the time step between location A and B is small in Figure 4.1. We have shown earlier that the characteristics are nearly parallel to the real x-axis. Thus in moving from A to B, the calculated values of $Im(\mathcal{J})$ and $Im(c_g)$ are small. When neglected, they do not introduce a large error in the approximation. Furthermore, the initial distribution of wavenumber with respect to initial position is continuous. That is, the function f in the initial condition

$$k_o = f(\mathcal{J}_o)$$

given in equation (4.13) is continuous. There are two sources of approximation relocating the characteristic position from B to C and using at C the value of $Re(c_g)$ calculated at B. The former is of the order of the slope of the characteristic relative to the real x-axis which is small because $Im(c_g) << Re(c_g)$. The

second source of approximation is of the order of the variation in the initial data from characteristic 1 to characteristic 2 , which is small because from the onset we have assumed a slowly varying wave packet. By hypothesis, we have

$$\frac{dk_o}{d\xi_o} = \theta(\epsilon_w)$$

where ϵ_w is a small parameter associated with the slowly varying wave train introduced in Chapter Two.

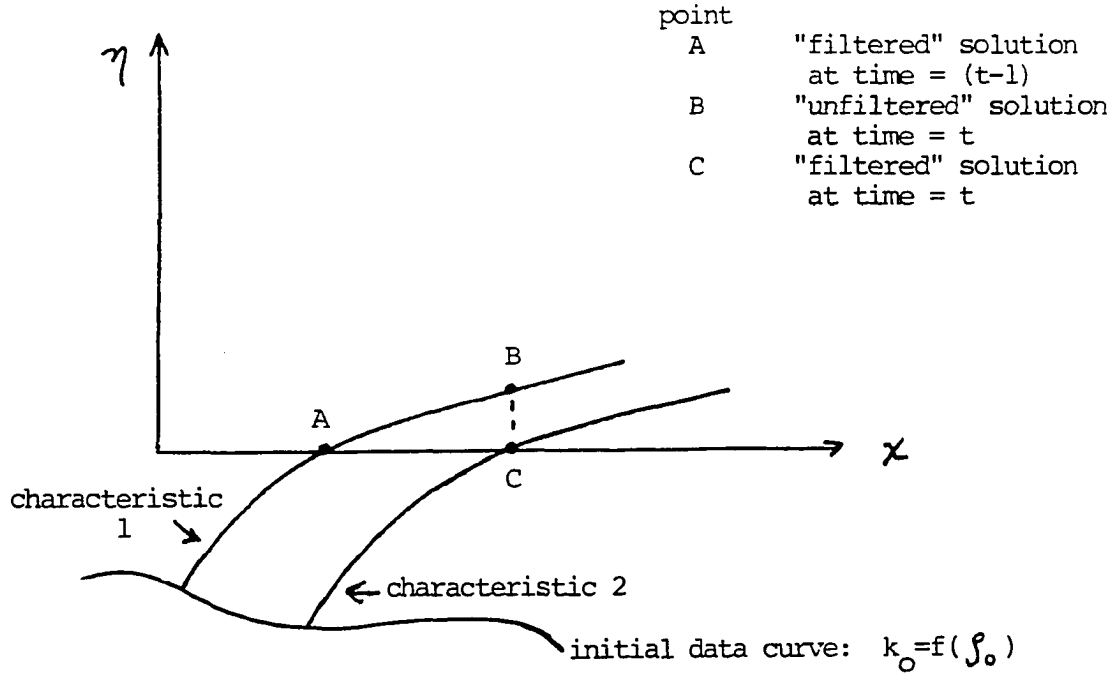

Figure 4.1: A schematic diagram showing the "filtering scheme" proposed to approximate the solution of the characteristic equations (4.11a,b)

It must be mentioned that Itoh (1981) originally suggested that complex position of the form

$$\zeta = x + i\eta$$

be used in the solution of equation (4.5). He then proposed to find the solution of (4.7) by letting $\eta = 0$. Later in this paper we will return to a discussion of Itoh's work.

Following the discussion in Chapter Two, we will define the observed square amplitude, A^2, as

$$A^2 = \mathcal{A}_\omega \quad \exp\left[-2\,\mathrm{Im}(\theta)\right] \tag{4.20}$$

Substituting this into the expression for wave action density,

$$\frac{\partial \mathcal{A}_\omega}{\partial t} + \frac{\partial}{\partial x}\left(\Omega_k \mathcal{A}_\omega\right) = h.o.t.$$

gives, after rearrangement,

$$\frac{dA^2}{dt} = -A^2\left[\Omega_{kx} + \Omega_{kk}\frac{\partial k}{\partial x}\right] + 2A^2\left[\mathrm{Im}(\Omega) - \Omega_k\,\mathrm{Im}(k)\right] \tag{4.21}$$

$\mathcal{A}_\omega$ is the wave action density, a term which represents amplitude change due to focussing or dispersion. $\exp(-2\,\mathrm{Im}\{\theta\})$ is the non-conservative wave system contribution, representing exponential

amplification or decay along a trajectory. Following Hayes (1970), we distinguish between "physical" space (x,t) with y as the cross-space variable and "characteristic" space (x,k,t). The symbols $\frac{\partial}{\partial t}$, $\frac{\partial}{\partial x}$, and ∇ are used for derivatives in "physical" space while subscripts $(\ )_x$, $(\ )_t$, and $(\ )_k$ are used for derivatives in "characteristic" space. An expression for the wavenumber gradient propagation, $\frac{d(\frac{\partial k}{\partial x})}{dt}$, is found by applying $\frac{\partial(\ )}{\partial x}$ to (4.5). The result is

$$\frac{d}{dt}\left(\frac{\partial k}{\partial x}\right) = -\Omega_{xx} - 2\Omega_{kx}\frac{\partial k}{\partial x} - \left(\frac{\partial k}{\partial x}\right)^2 \Omega_{kk} \tag{4.22}$$

which Hayes refers to as the "derived ray equation".

Assume the inhomogenities in the background flow are caused by a neutrally stable primary wave moving with constant phase velocity c_o. Let $\xi = x - c_o t$. Equations (4.7), (4.8), (4.21), and (4.22) become respectively

$$\frac{dk}{dt} = -\Omega_\xi \tag{4.23}$$

$$\frac{d\xi}{dt} = c_g - c_o \tag{4.24}$$

$$\frac{dA^2}{dt} = -A^2\left[\Omega_{\xi k} + \Omega_{kk}\frac{\partial k}{\partial \xi}\right] + 2A^2\left[Im(\Omega) - \Omega_k\, Im(k)\right] \tag{4.25}$$

$$\frac{d}{dt}\left(\frac{\partial k}{\partial \xi}\right) = -\Omega_{\xi\xi} - 2\Omega_{k\xi}\frac{\partial k}{\partial \xi} - \left(\frac{\partial k}{\partial \xi}\right)^2 \Omega_{kk} \tag{4.26}$$

subject to initial conditions

$$\left.\begin{aligned} K &= K_o \\ \xi &= \xi_o \\ A^2 &= A_o^2 \end{aligned}\right\} \quad \text{at} \quad t = 0 \tag{4.27}$$

We will select a suitable combination of A_o^2 and ξ_o to produce a localized disturbance. For example, a Gaussian-type distribution may be used. We do this to ensure that far upstream the disturbance dies out to avoid mathematical difficulties associated with unbounded normal modes at $x \to \pm\infty$. The trajectories and variation of wavenumber along a trajectory can be found from equations (4.23) and (4.24) which are coupled first order ordinary differential equations. We use a Runge-Kutta technique and apply the filtering scheme

$$Im(c_g) = 0$$

after each iteration.

4.1.1 Landahl's Breakdown Condition for One-Dimensional Waves

Equations (4.25) and (4.26) can be solved by introducing the Jacobian, J,

$$\frac{1}{J}\frac{dJ}{dt} = \nabla\cdot\vec{c_g}$$

(see equation (8) in Landahl's 1972 paper). The Jacobian, J, can be described as a measure of the volume as convected by the rays and for the one dimensional case

$$\frac{1}{J}\frac{dJ}{dt} = \left[\Omega_{kk}\frac{\partial k}{\partial \xi} + \Omega_{k\xi}\right] \tag{4.28}$$

Combining (4.28) with (4.25) and integrating gives

$$A^2 = \frac{\text{constant}}{J}\exp\left[2\int\left[\mathrm{Im}(\Omega) - \Omega_k\,\mathrm{Im}(k)\right]dt\right] \tag{4.29}$$

so that a singularity in J results in an infinite value for the square-amplitude term provided $\int[\mathrm{Im}(\Omega) - \Omega_k\,\mathrm{Im}(k)]\,dt \neq -\infty$. The place where J equals zero is called a focus, and, in Landahl's theory of breakdown, marks the location of a tremendous build-up of energy which results in the "breakdown" of the flow field to higher frequency oscillations.

For the one-dimensional case with a constant phase velocity primary wave, Landahl argued space-time focussing occurs when the phase velocity of the primary wave, c_o, is equal to the group velocity of the secondary wave, c_g. The behavior of the wavenumber gradient term $\frac{\partial k}{\partial \xi}$ at a focus can be found if we assume terms involving Ω_ξ and $\Omega_{\xi\xi}$ in equations (4.26) and (4.28) are small compared to Ω_{kk} terms. This assumption is justified for the case of a weak nonuniformity in background flow which changes with respect

to position are small. Then (4.28) becomes

$$\frac{1}{J}\frac{dJ}{dt} \simeq \Omega_{kk}\frac{\partial k}{\partial \xi} \tag{4.30}$$

and (4.26) becomes

$$\frac{d}{dt}\left(\frac{\partial k}{\partial \xi}\right) \simeq -\left(\frac{\partial k}{\partial \xi}\right)^2 \Omega_{kk} \tag{4.31}$$

Eliminating Ω_{kk} between the above two equations gives

$$-\frac{d}{dt}\left[\ln\left(\frac{\partial k}{\partial \xi}\right)\right] = \frac{d}{dt}(\ln J)$$

Thus

$$\frac{\partial k}{\partial \xi} \approx \frac{1}{J} \tag{4.32}$$

As J collapses to zero, $\frac{\partial k}{\partial \xi} \to \infty$. Physically, $\frac{\partial k}{\partial \xi} \to \infty$ can be viewed as an infinite amount of wavenumbers, i.e., an infinite collection of waves building up in a small increment of space $d\xi$. Furthermore, if we solve equations (4.23) and (4.24) for wavenumber propagation along a trajectory, we can plot k versus ξ and find the point of infinite slope which should corresond to the focus. Hence for the one-dimensional case, there is no need to solve (4.25) and (4.26) directly.

4.1.2 The Dispersion Relation for One-Dimensional Waves

The solution of (4.23) and (4.24) requires an expression for the dispersion relation. In this work the dispersion relation is found by a well-known small wavenumber asymptotic solution of the Rayleigh equation (cf. Benjamin (1959), equation 7.3)

$$\tilde{v} = (U-c)\, e^{-ky}\, G_\infty \left\{ 1 + k\delta\,(U_\infty - c)^2 \int_{y/\delta}^{\infty} \left[\frac{1}{(U-c)^2} - \frac{1}{(U_\infty - c)^2} \right] d(y/\delta)' + \Theta\left[(k\delta)^2\right] \right. \tag{4.33}$$

Here c is the phase velocity $\frac{\omega}{k}$, and k the wavenumber of a travelling wave of the form

$$\tilde{v}(y)\ \exp\left[\, i\,(kx - \omega t)\right]$$

which satisfies the free stream condition $\tilde{v} \sim e^{-ky}$ in the region where $d^2U/dy^2 = 0$. G_∞ is a dimensionless constant representing the amplitude of the mode. For a family of velocity profiles of the form

$$\frac{U}{U_1} = \tanh^3\left(\frac{y-y_0}{\delta}\right) + A_2 \tanh^2\left(\frac{y-y_0}{\delta}\right) + A_1 \tanh\left(\frac{y-y_0}{\delta}\right) + A_0 \tag{4.34}$$

Russell (1983) was able to evaluate the integral in (4.33) exactly using the method of partial fractions. In equation (4.34), U_1 represents a reference velocity, δ a reference length scale, and A_2, A_1, A_0, and y_0/δ are free parameters. The dispersion relation is found by applying the wall boundary condition and is given exactly within the limitations of the small wavenumber asymptotic approximation of (4.33). Hence the group velocity can also be found exactly. No assumption about the realness of $k\delta$ was made in the derivation of (4.33) so that the dispersion relation holds for complex values of both wavenumber and phase velocity.

4.2 Comparing Landahl's Theory of Breakdown with the Experimental Results of Klebanoff et al.

In 1972, Landahl formulated his theory of breakdown but never actually traced the trajectories of secondary wave packets traveling through a physically realistic background flow. He did approximate the behavior of the trajectories near the crest of the primary wave. In addition, he fitted polynomial expressions to the 1962 instant velocity data of Klebanoff et al. and then used a numerical procedure to solve the Orr-Sommerfeld equation with the experimental velocity profiles as input to the temporal stability problem. His numerical procedure (Landahl 1969) gave phase velocities directly, and from these group velocities were determined by graphical differentiation. His results for station C (upstream of breakdown) and station D (location of breakdown) are shown in Figure 4.2 (a) and Figure 4.3(a), respectively. He inferred the phase velocity c_o of the primary wave from Klebanoff's data. His theory for breakdown was corroborated when he observed that at station D the phase velocity, c_o, and the group velocity of the secondary wave, c_g, matched at the short wave cutoff point. Upstream of breakdown at station C, the phase velocity of the primary wave was everywhere less than the calculated group velocities.

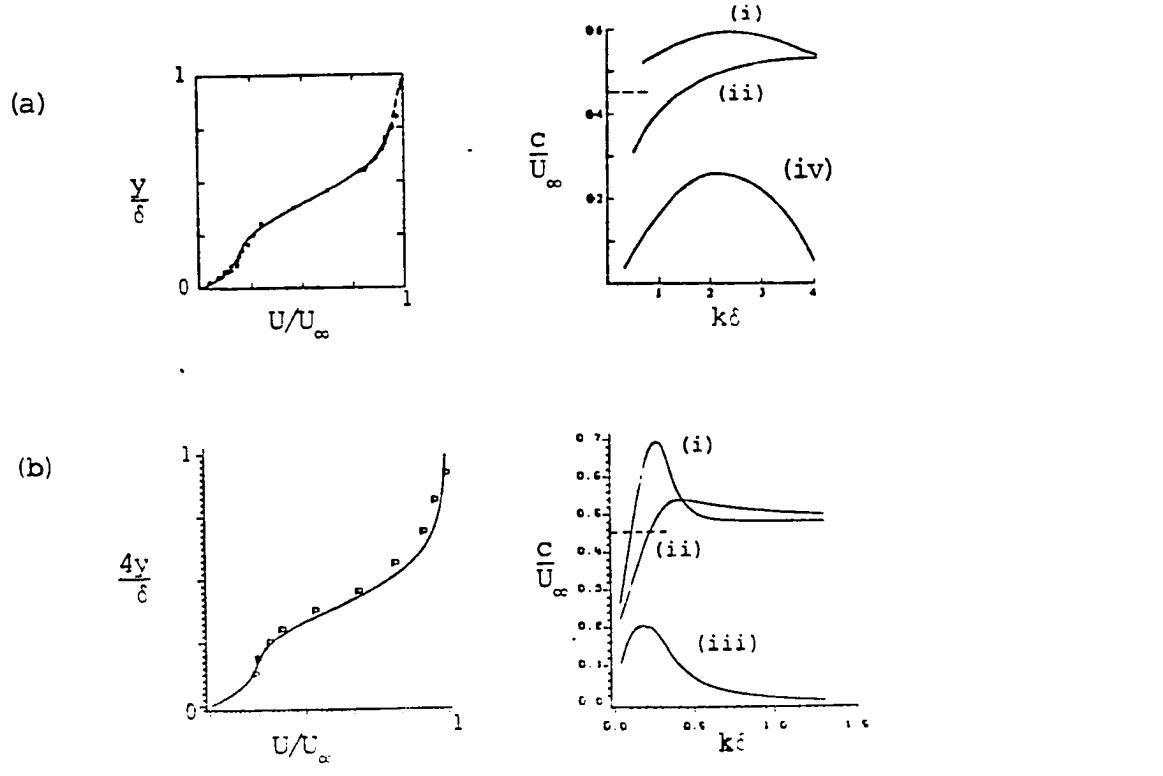

(i) $Re(c_g)$
(ii) $Re(c)$
(iii) $Im(c)$
----- c_o, primary wave velocity from Klebanoff et al. data
(iv) $Im(\Omega)$

Figure 4.2: The instantaneous velocity profiles and dispersion relations for station C of the Klebanoff et al. data (1962)
(a) Klebanoff et al. data is shown as ·, the solid line is the velocity profile that Landahl fitted to the data. The corresponding dispersion relations are shown to the right, found from a numerical solution of the Orr-Sommerfeld equation.
(b) Curve fitted using n= 0.15, yo = 0.65. Klebanoff et al. data is shown as □ . The dispersion relations for the temporal instability problem found using the small kδ approximation to the Rayleigh equation.

(a)

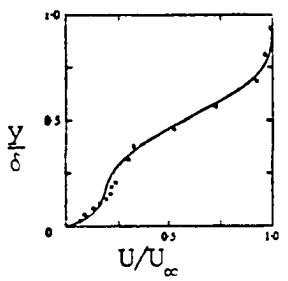

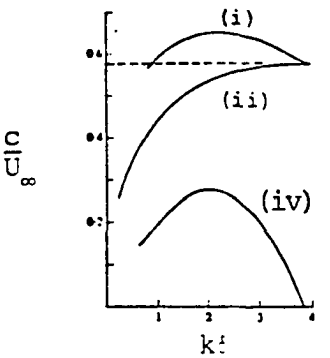

(b)

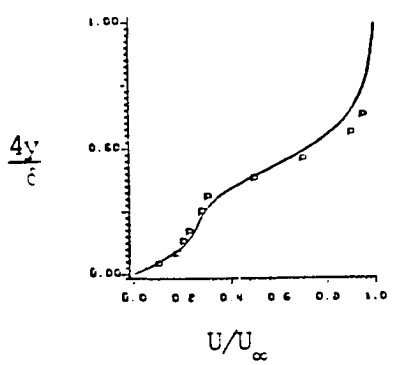

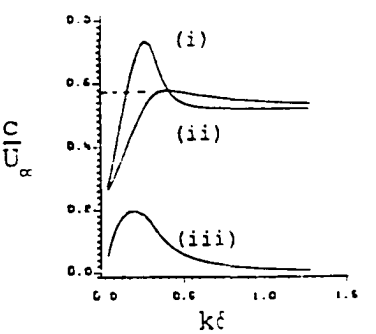

(c)

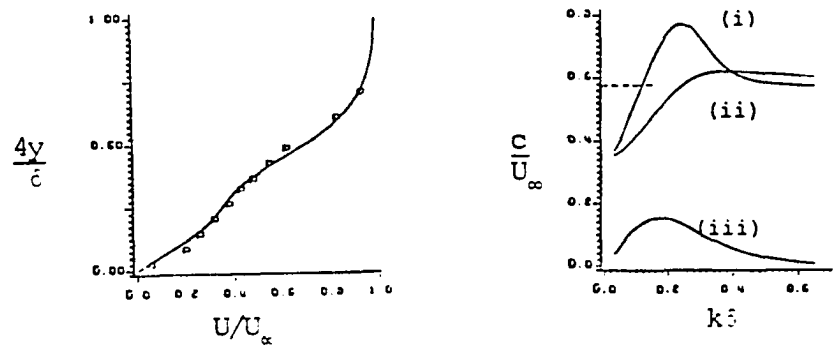

Figure 4.3: (a) Landahl's curve fit to the data of Klebanoff et al. for the instantaneous velocity profile at station D. The corresponding dispersion relations are shown to the right, found from a numerical solution of the Orr-Sommerfeld equation.

(b) Curve fitted to the instantaneous velocity data, shown as □ , at station D using yo = 0.8, n=0.15. The dispersion relations for the temporal stability problem found using the small kδ approximation are shown to the right.

(c) Curve fitted to the averag velocity data, shown as □ , at station D using yo = 1.0, n=0.3. The dispersion relations for the temporal stabilty problem found by using the small kδ approximation are shown to the right.

(i) $Re(c_g)$; (ii) Re(c); (iii) Im(c); ---- c_o, primary wave velocity

(iv) Im(α)

One novel contribution of this dissertation is to do actual ray tracing. Using the data of Klebanoff et al. to provide the physically realistic background flow, we solve equations (4.23) and (4.24) to obtain the trajectories of secondary wave packets. In the next section we use the recent data of Williams, Hama, and Fasel (1985) as background flow for ray tracing. Both Klebanoff et al. and Williams et al. have observed that in a very short distance, a rapid growth in u' fluctuations occur (as shown in figures 1.1 and 1.3). This produces a new type of oscillation whose frequencies are roughly one-order of magnitude higher than the frequency of the primary wave. In both experiments, these high frequency oscillations are associated with local instantaneous inflexional velocity profiles.

In modelling both experiments, we will use the local dispersion relation given by the small-wavenumber asymptotic solution described by equations (4.33) and (4.34), for the case of temporal and spatial instability. The use of a dispersion relation to account for both temporal and spatial instability, the "mixed" stability problem, is also novel.

Equation (4.33) is used to describe the local dispersion relation. After applying the wall boundary condition at a fixed location, a dispersion relation of the form

$$(\tilde{v})_{y=0} = F(k,c) = 0 \qquad (4.35)$$

is found, and F depends linearly on k. Therefore we may solve for k to get

$$k = K(c) \tag{4.36}$$

But since

$$c_g = (d\Omega/dk)_{F=0} \tag{4.37a}$$

and

$$\omega = kc \tag{4.37b}$$

we have

$$\begin{aligned} c_g &= (c + k\, dc/dk)_{F=0} \\ &= c + K(c)/K'(c) \\ &\equiv H(c) \end{aligned} \tag{4.38}$$

Equation (4.38) is the dispersion relation for the mixed stability problem; selecting real c_g as the input parameter gives complex c. Then the parameter c_g and complex c are substituted into

$$k = \frac{c_g - c}{\frac{dc}{d\kappa}}$$

to give the complex wavenumber.

The total rate of growth of a disturbance along a trajectory is given as

$$\frac{d\theta}{dt} = \frac{\partial\theta}{\partial t} + c_g \frac{\partial\theta}{\partial x}$$

Substituting the definitions given by (4.1) and (4.2) yields,

$$\frac{d\theta}{dt} = K(c_g - c_o) \tag{4.39}$$

Equation (4.39) describes both spatial and temporal amplification along a particular trajectory. We assume that in physical space far upstream the disturbance dies by appropriate choice of A_o^2 and ξ_o. This assumption is necessary so that the spatial amplification will not be infinite as x or z approaches infinity.

Using the expression (4.34) in order to fit velocity profiles of the Klebanoff et al. data we can compare the temporal stability results with the mixed stability results. Figures 4.2(b) and 4.3(b) and (c) show the fitted velocity profiles compared with data from Klebanoff et al. The velocity profiles were fitted with expressions of the form

$$\frac{u}{u_\infty} = \frac{\tanh^3\left(\frac{y-y_o}{\delta}\right) + \frac{n}{1-n}\tanh\left(\frac{y-y_o}{\delta}\right) + A_o}{1 + \frac{n}{1-n} + A_o}$$

In this case $y/\delta = 4$ when $u/u_\infty = 0.99$, and A_0 was chosen to satisfy no slip at the wall, that is,

$$A_o = \tanh^3\left(\frac{y_o}{\delta}\right) + \frac{n}{1-n}\tanh\left(\frac{y_o}{\delta}\right)$$

For the instantaneous velocity profiles at station D (the location of breakdown in the Klebanoff work) $y_o/\delta = 0.8$ and $n = 0.15$. The average velocity profile at station D was fitted using $y_o/\delta = 1.0$ and $n = 0.3$. Upstream of breakdown at station C the instantaneous velocity profile was fitted using $y_o/\delta = 0.65$ and $n = 0.15$.

Figures 4.2 and 4.3 show the dispersion relations for the temporal stability problem for the three velocity profiles described above. Real $k\delta$ was the input. The small wavenumber approximation gave results for real phase velocity, c_r, and imaginary phase velocity, c_i. Differentiating the dispersion relation gave complex group velocities, of which c_{gr}, the real group velocity is shown. Comparing these results with those found by Landahl as solution of the Orr-Sommerfeld equation we see overall good agreement. It must be pointed out that in our work δ is 4 times the δ value used by Landahl. The small wavenumber approximation solution is not expected to behave well for larger wavenumber and hence the behavior near the shortwave cutoff differs from Landahl's results. Because the small $k\delta$ solution does not converge rapidly to the shortwave cutoff, the group velocity at instantaneous station D at the shortwave cutoff is $c_g/U_\infty = 0.522$ while Landahl found $c_g/U_\infty = 0.575$. We differ by roughly 9% which is pleasing considering the small $k\delta$ approximation. Landahl found that the group velocity at instantaneous station C, was everywhere larger than the phase velocity $c_o/U_\infty \approx 0.45$*. We also found that

---

*In the region of small wavenumber there is the possibility of group velocities smaller than the phase velocity $c_o/U_\infty \approx 0.45$. Landahl ignored these long waves because the secondary disturbance wavelengths were very small. In fact a fundamental assumption of this work is that the secondary wavepackets are much higher frequency, larger wavenumber than the primary wave.

at station C the group velocity was larger than the phase velocity of the primary wave c_0 for larger $k\delta$.

Encouraged by the temporal stability results, we then solved the mixed stability problem. Strictly real group velocity are the input. The corresponding complex wavenumber and phase velocity were found. The results of the mixed stability calculations are shown in figure 4.4. The total rate of amplification term

$$-Im\left(\frac{d\theta}{dt}\right) = -Im\left(k(c_g - c)\right)$$

is plotted as a function of group velocity. Also shown is the variation of real and imaginary wavenumber and real and imaginary phase velocity with c_g as the input parameter. We note that the maximum value of the total rate of amplification term $-Im\left(\frac{d\theta}{dt}\right)$ for the mixed problem is roughly the same size as the maximum temporal growth value $Im(kc)$. The term $-Im\left(\frac{d\theta}{dt}\right)$ has the neutral solution $-Im\left(\frac{d\theta}{dt}\right) = 0$ for a value of group velocity greater than one in all three cases.

It was particularly surprising to find that certain values of the real group velocity resulted in negative values for the real part of the wavenumber. These results were ruled out as physically unrealistic. It appears that as the imaginary part of phase velocity approaches zero the real part of the wavenumber takes on negative values. This result may somehow be related to the small wavenumber

(a) Average Station D

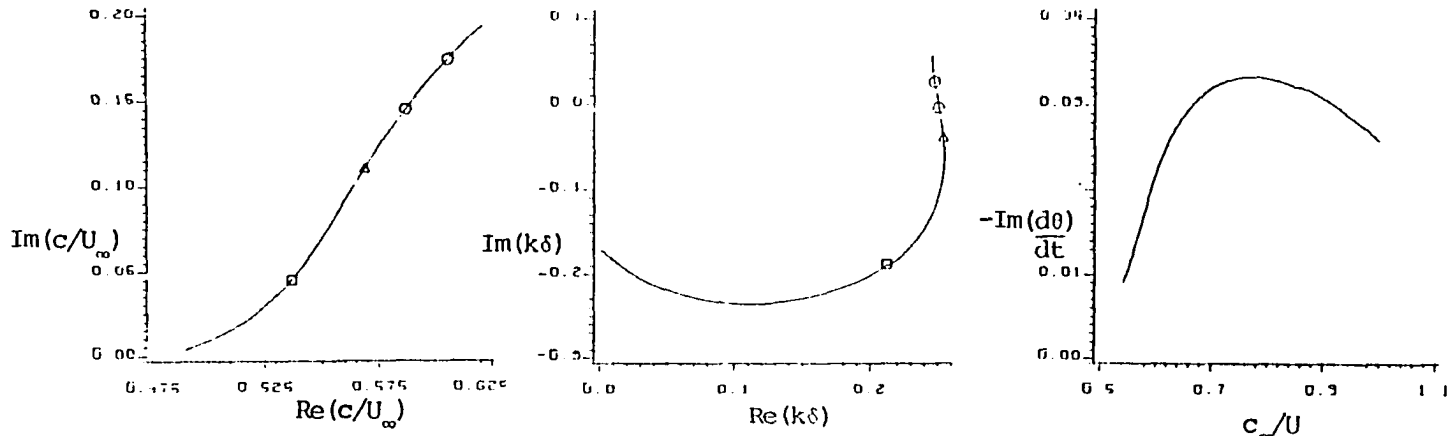

(b) Instantaneous Station D

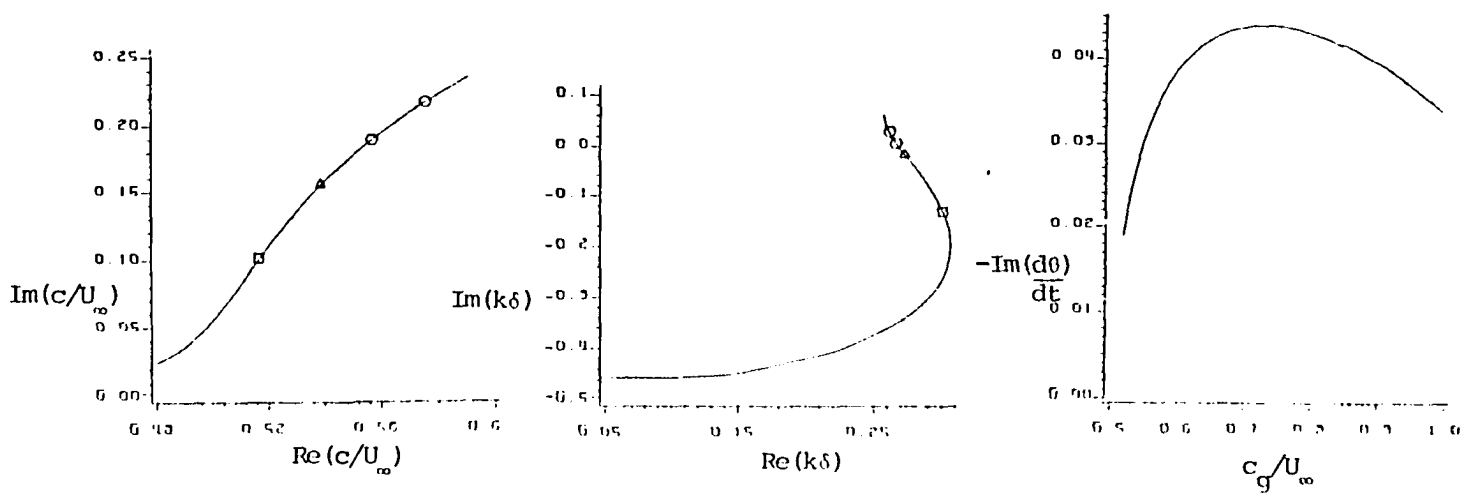

(c) Instantaneous Station C

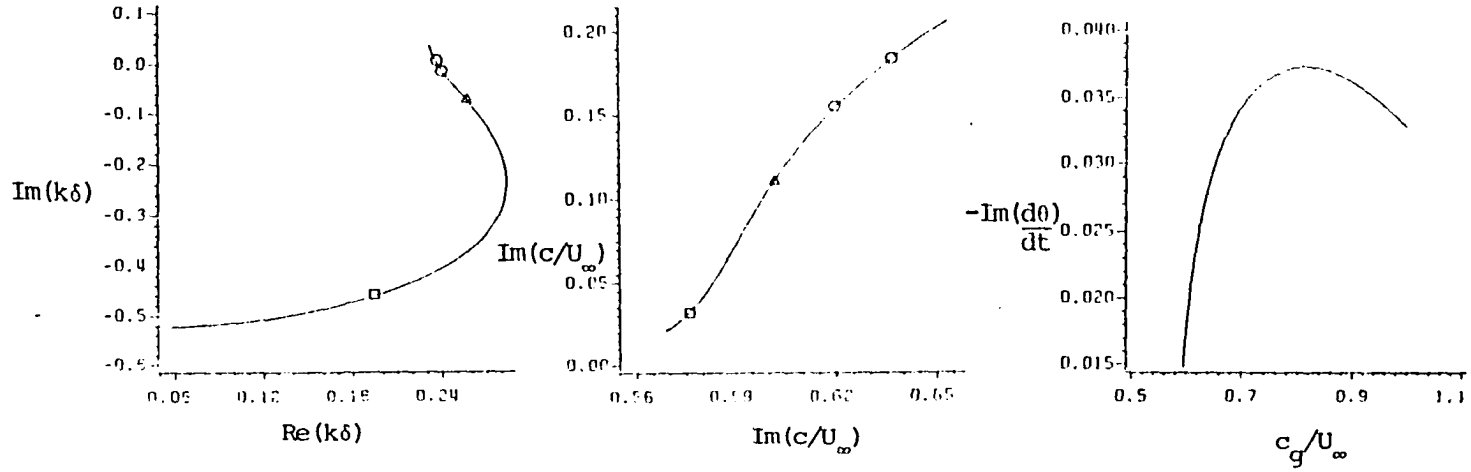

Figure 4.4: (a) Dispersion relations for the velocity profile fit to the average velocity data at station D. The group velocity is the input parameter, giving the results shown. On the graphs for Im(c) versus Re(c) and Im(kδ) versus Re(kδ) the input values for group velocity, c_g, are indicated by the following symbols: □ c_g/U_∞ = 0.6; Δ c_g/U_∞ = 0.7; ○ c_g/U_∞ = 0.8; ○ c_g/U_∞ = 0.9.

(b) Dispersion relations for the velocity profile fit to the instantaneous velocity data at station D. The group velocity is the input parameter, giving the results shown. The same symbols were used to indicate increments in c_g.

(c) Dispersion relations for the velocity profile fit to the instantaneous velocity data at station C. The group velocity is the input parameter, giving the results shown. The same symbols were used to indicate increments in c_g.

approximation used to define the dispersion relation. On the other hand, perhaps for doubly-inflectional velocity profiles with $(d^2U/dy^2)_{wall} < 0$, there is a small group velocity cutoff point for the "mixed" stability problem analogous to the longwave cutoff value for real phase velocity in the temporal stability problem.

At station D for the instantaneous velocity profile, the minimum group velocity for physically realistic wavenumber was $c_g/U_\infty \approx 0.52$. At station C the minimum group velocity for physically realistic wavenumber was $c_g/U_\infty \approx 0.48$. Thus at station D focussing is possible because $c_g/U_\infty = c_o/U_\infty = 0.575$ has meaningful values for complex k and c. However at station C for the instantaneous profile, focussing is not possible since the phase velocity of the primary wave $c_o/U_\infty = 0.45$ is not within the range of acceptable solutions. It must be emphasized that this may be fortuitous. A better understanding of doubly-inflectional profiles and the "mixed" stability problem must be obtained before any definite claim about focussing at station C can be stated.

The previous results give dispersion relations for fixed locations in space and time. By letting

$$n = 0.3 - 0.15 \cos(\epsilon \xi) \tag{4.40}$$

$$y_o = 1 - 0.2 \cos(\epsilon \xi) \tag{4.41}$$

where

$$\epsilon = 0.1 \tag{4.42}$$

$$\xi = x - c_o t$$

we model a slowly varying background flow. Such a flow might be produced by a primary wave with phase velocity c_o. ξ is the position as seen by an observer moving with the primary wave and ε is a small parameter which determines how slowly varying the background flow will be. Figure 4.5 shows the background profiles for various values of ξ. $\xi = 0$ corresponds to the primary wave crest which we assume is the instantaneous profile at station D while $\xi = \pi/2$ corresponds to the average profile at station D. We used a cosine dependence for the parameters n and y_o, so that Ω_ξ in (4.15) will be zero at the crest, $\xi = 0$.

The first results of ray tracing are shown in figure 4.6 for the neighborhood of the crest. The primary wave moves at fixed velocity $c_o/U_\infty = 0.575$ and $\xi = 0$ respresents the crest. Trajectory D represents a secondary wave packet which always moves slower than the primary wave -- the packet speeds up slightly as it approaches the primary wave crest, but then it is passed by the primary wave. In a similar fashion, trajectory B represents a secondary wave packet that always moves faster than the primary wave -- the packet slows down slightly as it approaches the crest but then moves out in front of the crest. Trajectories A and C are of considerable interest. Trajectory C represents a packet that slows down and approaches the crest, but then moves out again in front of the crest. Trajectory A represents a packet that speeds up and approaches the crest but then

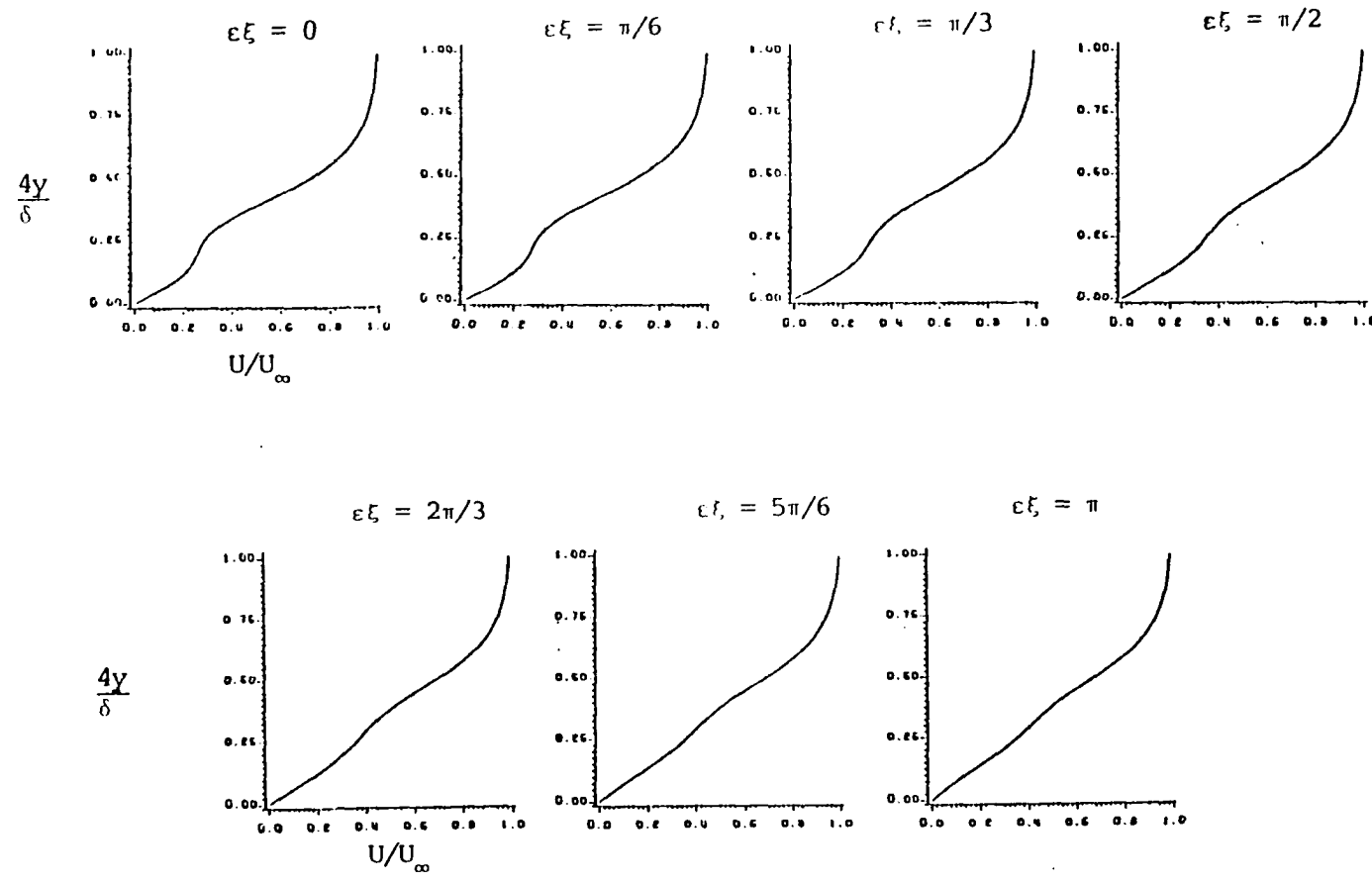

Figure 4.5: Velocity profiles of the cubic-tanh family of profiles that model the slowly varying background flow "felt" by the secondary wave packet.
$y_o = 1 - 0.2\cos(\varepsilon\xi)$; $n = 0.5 - 0.15\cos(\varepsilon\xi)$

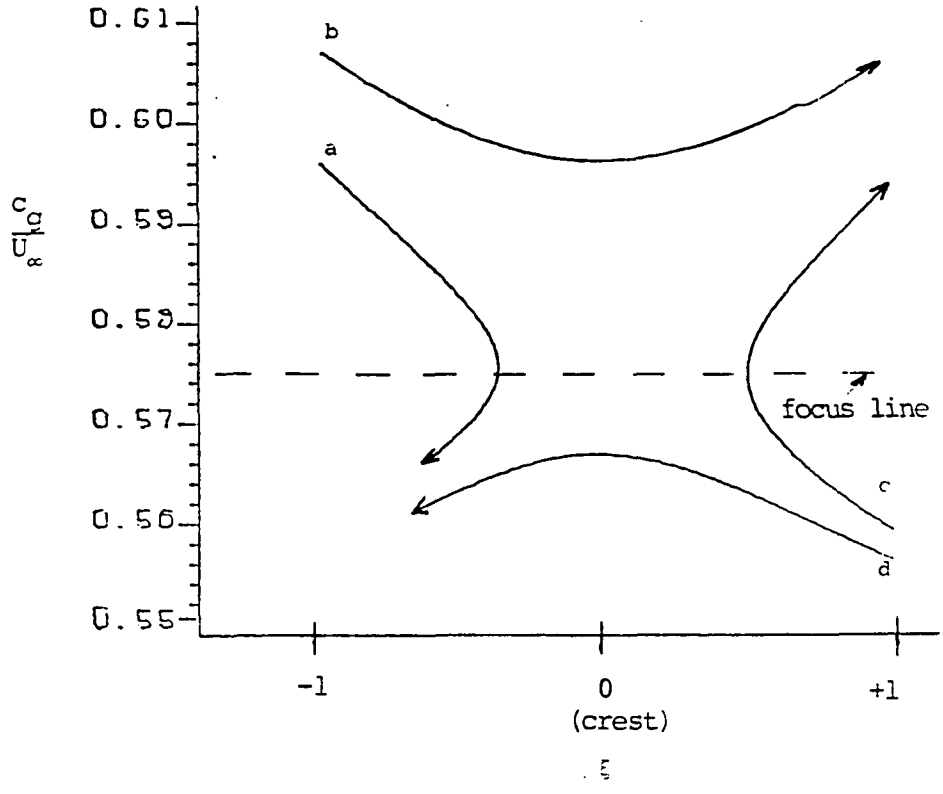

Figure 4.6: Secondary wave packet trajectories in the vicinity of the primary wave crest. $\xi = 0$ corresponds to the primary wave crest where $\xi = x - c_o t$. $c_o/U_\infty = 0.575$, the phase velocity of the primary wave. Focussing occurs when $c_g/U_\infty = c_o/U_\infty = 0.575$.

slows down and receeds from the crest. These results are in agreement with Landahl's approximate analysis of trajectories near the crest. They also agree with the results of Viney and Russell (1983) for the mixed stability problem with a less physically realistic background flow.

It must be emphasized that packets on trajectories A and C experience space-time focussing and the amplitude at the focus becomes infinite, representing a tremendous buildup of energy near focus. The flow responds to this situation by breaking down into a new configuration of higher frequency oscillations. Hence the behavior of the trajectories B and D near and beyond the line $c_g = c_o$ is not predicted by this theory and probably should not be drawn in the sketch except to emphasize the hyperbolic behavior of the trajectories.

Figure shows a family of trajectories for different initial group velocities and wavenumbers all originating at $\xi = -1.0$. Table 4.1 summarizes the initial data and also the number of time steps required to reach the focus $c_g = c_o$. The dashed line shows a possible asymptote which divides focussing and non-focussing trajectories. In Landahl's 1972 article he demonstrated infinite number of time steps would be required to travel along the asymptote to the focus point. This result seems to be born out in the calculations here -- trajectory 6 requires almost

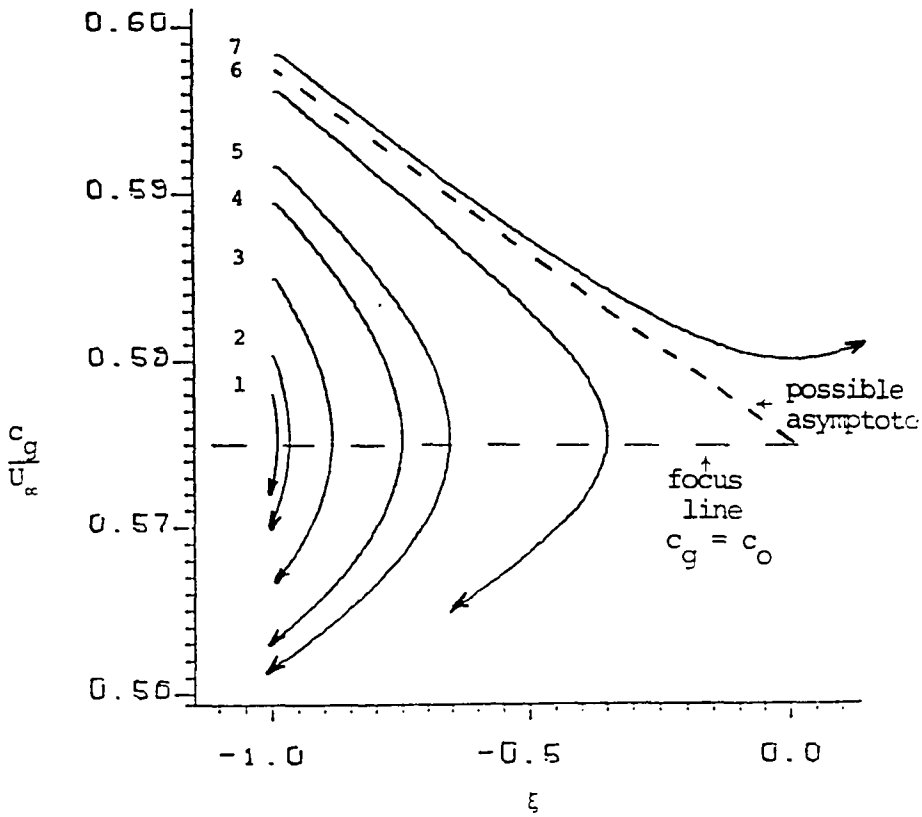

Figure 4.7: A family of trajectories with initial position, $\xi = -1.0$. The phase velocity of the primary wave is $c_o/U_\infty = 0.575$.

twice as many time steps as its neighboring trajectory 5 to reach the focus point.

In 1981, Itoh wrote a paper on the secondary instability problem. He applauded the pioneering work of Landahl in presenting the theory of breakdown in terms of secondary wavepackets traveling through a weakly non-uniform background flow. His main disagreement with Landahl was on the breakdown mechanism. Itoh argued space-time focussing was not the main mechanism, but rather "wave trapping". Disturbances travelling on the asymptotes are "trapped" and take an infinite time to reach the crest. A packet caught on the asymptote becomes "the most dangerous disturbance", in Itoh's words, as it dwells in a zone of exponential growth for a long time.

Table 4.1

	Initial values t=0	=-1	Focus values required	
Traj.	c_0/U_∞	$k\delta$	time steps	location
1	0.5781	0.3027-0.1479i	5	-0.9334
2	0.5804	0.3110-0.1423i	8	-0.9656
3	0.5850	0.3005-0.1231i	15	-0.8844
4	0.5895	0.2939-0.1228i	24	-0.7492
5	0.5917	0.2981-0.1185i	30	-0.6542
6	0.5962	0.2966-0.1105i	51	-0.3476
7	0.5984	0.2958-0.1067i	does not focus	

The above results shown in Figures 4.6 and 4.7 where found by applying the filtering scheme, $Im(c_g) = 0$, after each iteration in the Runge-Kutta scheme. This scheme was applied to preserve the nature of the solution given by the partial differential equation (4.5) and shall be referred to as the "manipulated" case. It is possible however to solve (4.23) and (4.24) with complex values for k, ξ, and c_g which we shall call the "unmanipulated" case. Consider trajectories 6 and 4 from figure 4.7 in both the "manipulated" and "unmanipulated" solution. Figure 4.8 shows these results. In the case of trajectory 4, the unmanipulated one focuses at $\xi = -0.7124$, while the manipulated trajectory focuses at $\xi = -0.7492$, roughly a 5% difference. Trajectory 6 is closer to the asymptote and hence takes twice as many time steps to reach its focus. The increase in time to focus is also reflected in the difference in focus locations. $\xi_{manipulated} = -0.3476$ and $\xi_{unmanipulated} = -0.2199$, which is a 41% difference in location. ($\xi_{manipulated}$ is taken to be the "true" location.)

Applying the filtering scheme of $Imag(c_g) = 0$ results in a different focus position than in the unmanipulated case. The closer to the asymptote the greater the difference in the focus location becomes. It must be emphasized however that although the focus point

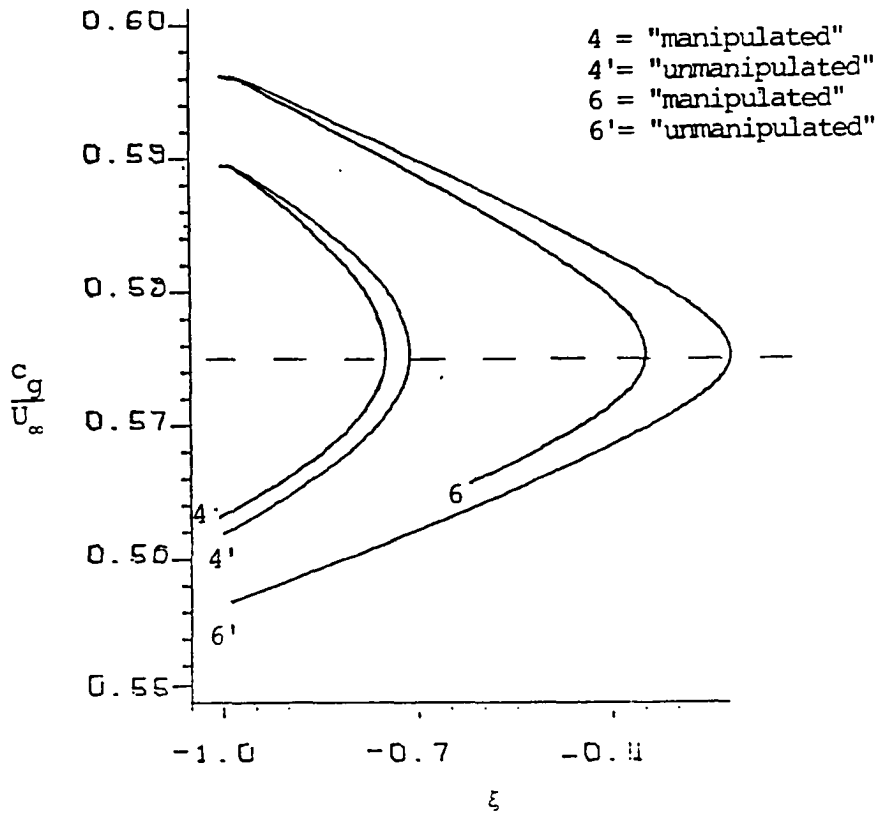

Figure 4.8: Two sets of trajectories plotted in order to compare the "manipulated" solution ($Im(c_g) = 0$) with the "unmanipulated" solution ($Im(c_g) \neq 0$, $\xi = x + it$) All have the same initial position, $\xi_o = -1.0$. The phase velocity of the primary wave is $c_o/U_\infty = 0.575$.

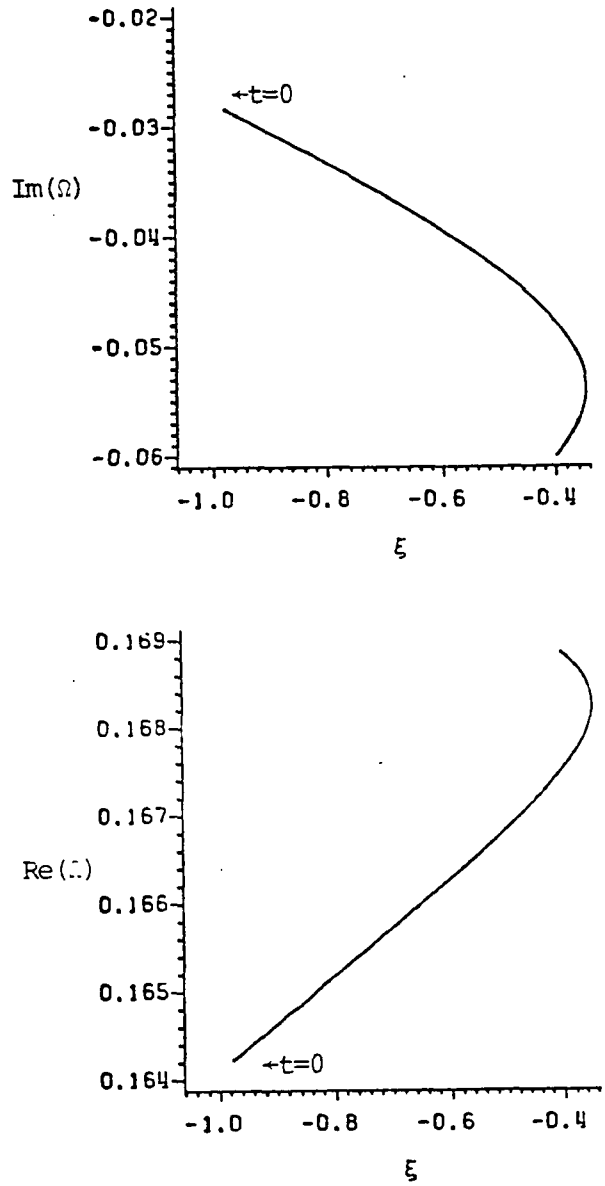

Figure 4.9: (a) The value of $Im(\Omega)$ as a function of distance, ξ is shown in the top graph. The value of $Re(\Omega)$ as a function of distance, ξ, along a trajectory is shown in the bottom graph. Note that $|\Omega_i| << |\Omega_r|$.

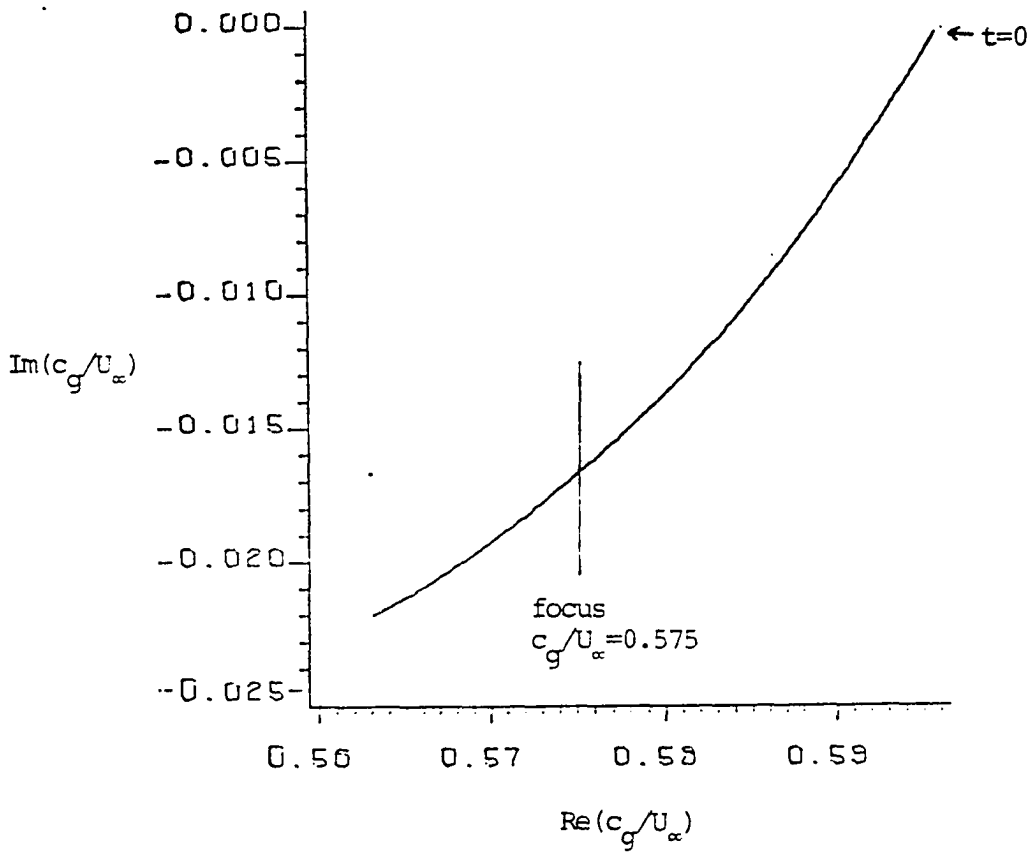

Figure 4.5 (b) The value of $Im(c_g)$ along a trajectory is plotted versus the value of $Re(c_g)$. The focus point is indicated in the figure, along with the initial value of c_g. Note that $Im(c_g) << Re(c_g)$.

may vary, the character of the solution is the same in both the manipulated and unmanipulated case --both do indeed focus. The filtering scheme was applied with the assumption that $\left|\frac{\Omega_i}{\Omega_r}\right| \ll 1$. Figure 4.9(a) shows the change in Im(Ω) and Re(Ω) along trajectory 6. It is pleasing to see that Im(Ω) is an order of magnitude smaller than Re(Ω). We can also consider growth in Im(c_g) along a slowly focussing trajectory, such as 6. In the unmanipulated case, at the focus point, Im(c_g) equals -0.017, which is small compared to the real value of group velocity at the focus. These results are shown in figure 4.9(b), and validate equation (4.18). We can also Compare the wavenumber propagation along trajectory 6. Initially, both wavenumbers are the same, $k\delta_{\text{manipulated}} = k\delta_{\text{unmanipulated}} = 0.2666-0.1105i$. At the focus $k\delta_{\text{manipulated}} = 0.3039 - 0.1553i$ while $k\delta_{\text{unmanipulated}} = 0.3488-0.1413i$, roughly a 13% difference in Re($k\delta$) with only a 10% difference in Im($k\delta$). Overall it appears that applying the filtering scheme Im(c_g) = 0 does not alter the solution greatly. More importantly, the nature of the original wavenumber equation 4.5 is preserved when the scheme is applied.

The next step of the analysis is to consider trajectories farther from the wave crest $\xi = 0$. Consider as the initial position, $\xi = -5.235988$ which corresponds to $\epsilon\xi = \pi/6$ in (4.40) and (4.41). Figure 4.10 shows the trajectories found for various initial group velocities. Trajectories 2 and 3 both focus while trajectory 4 is moving at too high an initial wavenumber and consequently sweeps

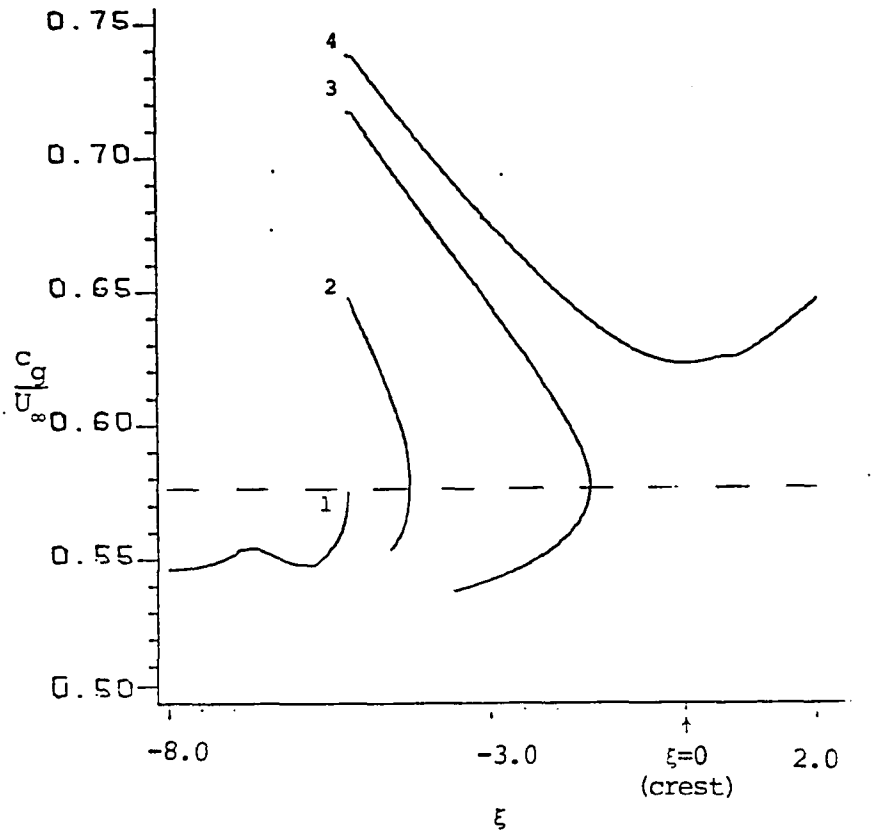

Figure 4.10: Trajectories for a secondary wave packet whose initial position is farther from the primary wave crest, $\varepsilon\xi = -\pi/6$. The phase velocity of the primary wave, $c_o/U_\infty = 0.575$.

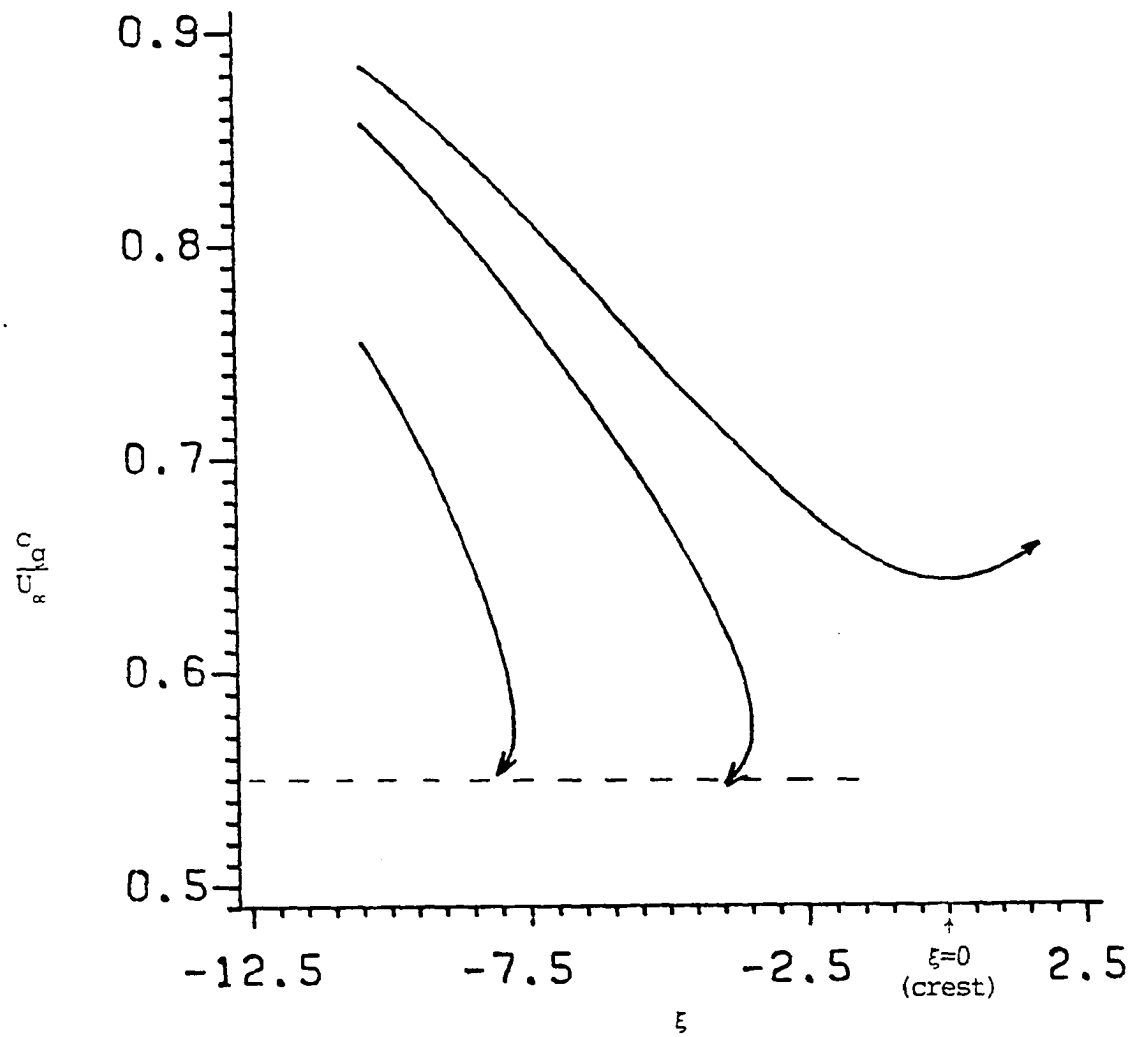

Figure 4.11: Trajectories of a secondary wave packet whose initial position is $\varepsilon\xi = -\pi/3$. The bottom two trajectories focus at $c_g/U_\infty = 0.575$.

past the wave crest. The range of initial group velocities which focus is much larger than for the near-crest analysis shown in Figure 4.7. For initial position $\xi = -1.0$, the range of focussing initial group velocities is roughly $0.575 \leq c_{go}/U_\infty \leq 0.597$, while at $\xi = -5.235988$, the range is $0.575 \leq c_{go}/U_\infty \leq 0.72$. This widening band is to be expected since the dividing asymptote takes in a larger range of group velocities for decreasing ξ values. It seems that wave packets moving with velocity faster than the phase velocity of the primary wave will focus if they originate sufficiently far from the primary wave crest, provided $\epsilon\xi \geq -\pi/2$.

Trajectory 1 is interesting. For $\xi = -5.235988$ and $c_{go}/U_\infty = 0.575$ the wave packet is initially moving at the phase velocity of the primary wave. The wave packet slows down and recedes from the crest for a time, but then speeds up slightly to a local maximum value.

Even farther from the wave crest, we see results similar to the previous ones. For $\xi = -10.471976$ ($\epsilon\xi = -\pi/3$), the trajectories are shown in Figure 4.11. Focussing occurs for the range of wavenumbers $0.575 \leq c_g/U_\infty < 0.87$. The secondary wave packets could focus at ξ values in the range $-10.471976 \leq \xi < 0$. The fastest moving wave packets, i.e., the highest energy packets, collect in the neighborhood of the crest. Slower moving wave packets head toward the crest but focus before the wave crest.

The asymptote dividing focussing and non-focussing trajectories is not simply a straight line. Looking at the results in Figure 4.7, we see that the asymptote makes an angle of around 35° with the line $c_g = c_o$. However in Figure 4.10, the asymptote appears to make an angle of around 50° with the line $c_g = c_o$. The dividing asymptote in Figure 4.11 is also roughly 50°. The equation for the dividing asymptote can be roughly inferred from the results shown in these figures. Selecting three different points on the asymptote shown in Figures 4.7, 4.10, and 4.11 and fitting a parabola through these points gives a crude estimate for the equation of the asymptote. The equation is approximated as

$$\xi = -15.35723\ (c_g/U_\infty)^2 - 11.47049\ (c_g/U_\infty) + 11.321338 \qquad (4.34)$$

and is valid in the range $-15.707963 \leq \xi \leq 0$.

The equation for the asymptote indicates focussing occurs for any secondary wave packet moving with a group velocity greater than the phase velocity of the primary wave, <u>provided</u> the packet's initial position is sufficiently far from the wave crest. Those wave packets that focus near the wave crest for an arbitrary initial position are the most dangerous. They closely follow the asymptote that divides focussing and non-focussing waves and consequently take a large number of time steps to focus. While these wave packets follow the long-time trajectory to the focus, the value of

-Imag($d\theta/dt$) is greater than zero -- the wave packets are experiencing exponential amplification as they approach the focus point. Following Landahl and Itoh, we will refer to this amplification on a long-time trajectory as "wave trapping". For breakdown to occur it appears from these results that secondary wave packets must experience "wave trapping" in addition to focussing.

In the above equation , (4.43), for $\xi \geq -15.506382$, the asymptote value of c_g/U_∞ is greater than or equal to one. We rule out wavepackets moving faster than the freestream velocity as physically unrealistic. Thus wave trapping on long-time trajectories originating beyond $\xi = -15.506382$ is not possible.

4.3 Comparison With the Experimental Results of Williams et al.

Landahl proposed his theory based on the experimental results of Klebanoff et al. A more recent investigation of the boundary-layer transition process has been conducted by Williams, Fasel, and Hama (1985). Their studies concerned mapping the instantaneous velocity and vorticity fields of the vortex loop observed in the vicinity of breakdown. In particular, their report provides instantaneous profiles plotted as a function of the phase angle of the reference signal. The profiles were measured at x=60cm, in the region of rapid growth in u'-fluctuations, as shown in Figure 1.1. These instantaneous velocity profiles provide the slightly

inhomogeneous background flow through which secondary wave packets travel. If Landahl's theory is correct focussing should occur.

Figure 4.12 (a) shows the instantaneous profiles measured by Williams et al. Figure 4.12(b) shows the cubic-tanh profile of equation 4.26 fitted at phase angles 0° and 120°. At 0°, n=0.1 and y_o = 1.2 while at 120°, n=0.65 and y_o = 1.4. Based on these two curve fits, we assume the profiles vary slowly in the form

$$y_o = -0.133333 \cos(\epsilon \xi) + 0.133333$$

$$n = -0.366667 \cos(\epsilon \xi) + 0.466667$$

where ϵ = 0.1 in order to produce a slowly varying background flow. Figure 12 shows the family of velocity profiles generated by the above expression for various values of ξ.

The phase velocity of the primary wave, c_o, can be approximated based on the work of William's et al. Figure 4.14 is reproduced from Figure 10 of their work. Using the phase of the fundamental at the height of amplitude maximum of the fundamental, find wavelength $\lambda = -\partial\chi/\partial\phi$ and then compute $c_o = f\lambda$, where f is the frequency of the wire oscillation, f = 0.263 Hz. If χ is the length between 55 and 65 cm, then $c_o/U_\infty \approx 0.5$. If χ is the length between 55 and 60 cm, then $c_o/U_\infty = 0.78$. We will use the average value $c_o/U_\infty \approx 0.64$. Williams et al. calculated the average phase velocity across the length $0 \leq \chi \leq 70$ to be $c_o/U_\infty \approx 0.45$; this is so locally close to the point of breakdown that the primary wave is accelerating. This was also the case in the Klebanoff et al. work.

(a)

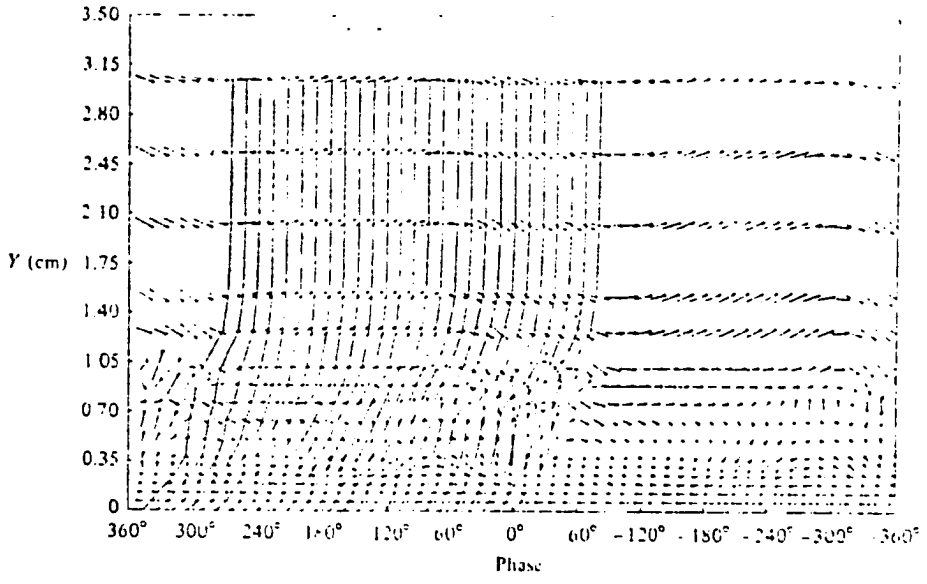

(b)

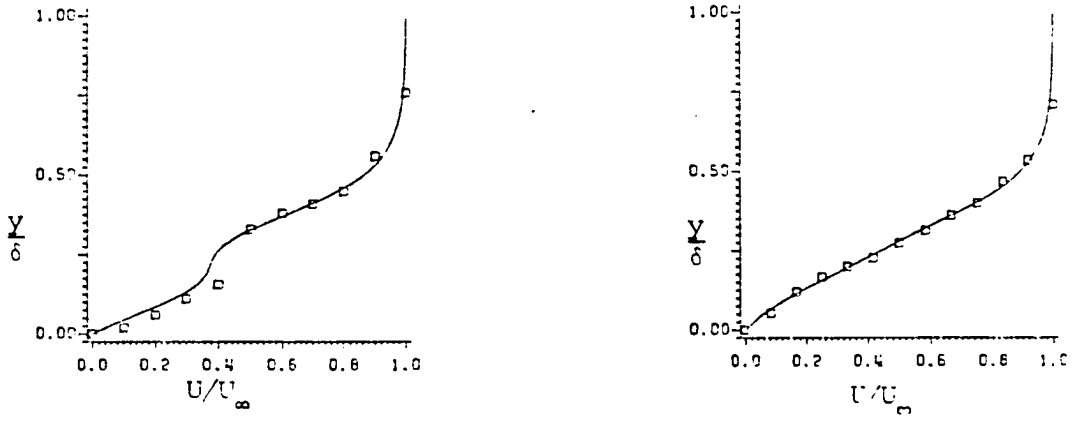

Figure 4.12: (a) The top figure is reproduced from Williams et al. (1984) for the instantaneous velocity profiles in the (Y,T)-plane superposed with the instantaneous projections of the velocity vectors at X=60 cm. The circle shows the approximate location of the tip of the vortex loop observed by Williams et al.

(b) Members of the cubic-tanh family of velocity profiles fitted to the Williams data at phase = 0°, and 120°. For phase equal to 0°, y_o = 1.2 and n=0.1. For phase equal to 120°, y_o=1.4, n=0.65. The squares represent data points taken from Williams et al. data.

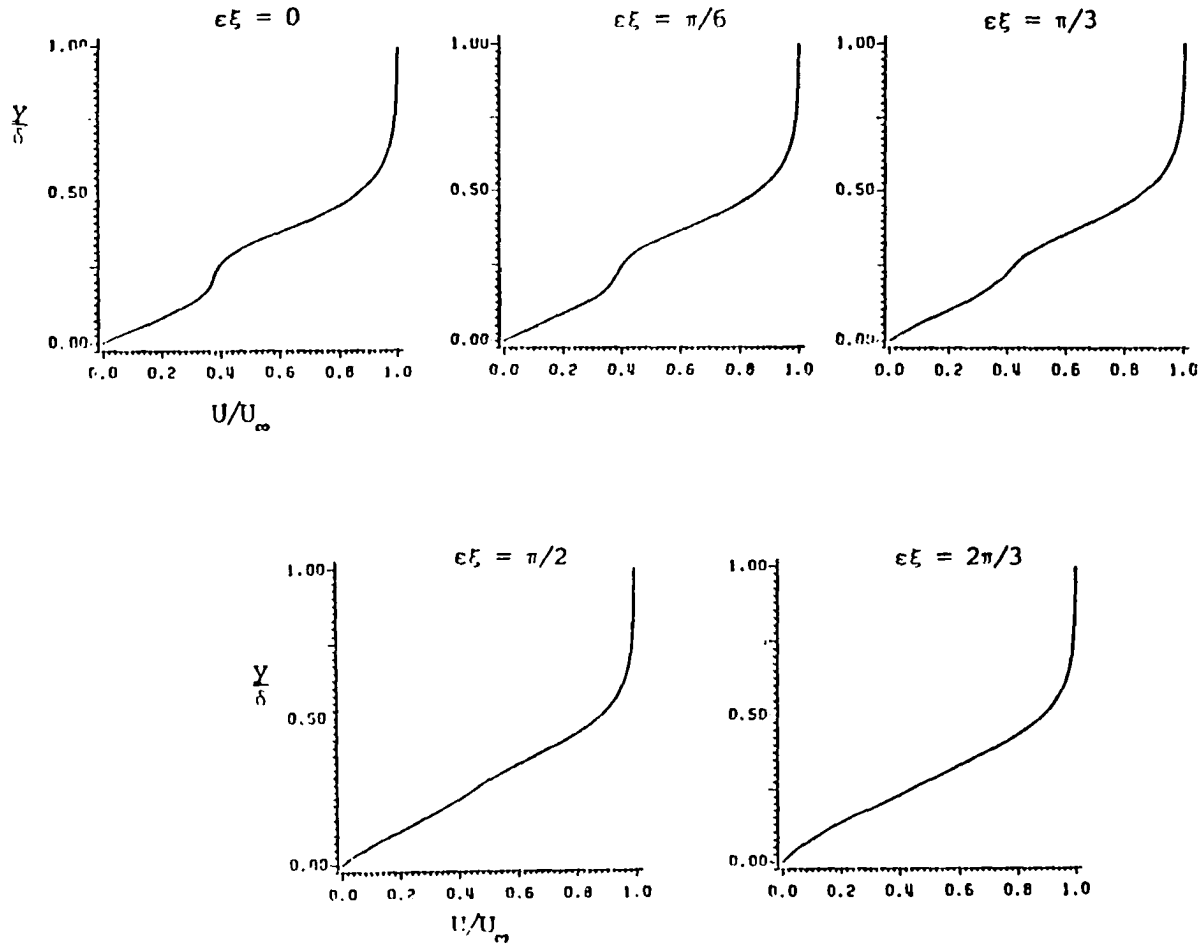

Figure 4.13: Velocity profiles of the cubic-tanh family of profiles that model that slowly varying background flow "felt" by the secondary wave packet for the Williams et al. data.
$y_o = -0.133333 \cos(\varepsilon\xi) + 1.333333$
$n = -0.3666667 \cos(\varepsilon\xi) + 0.466667$

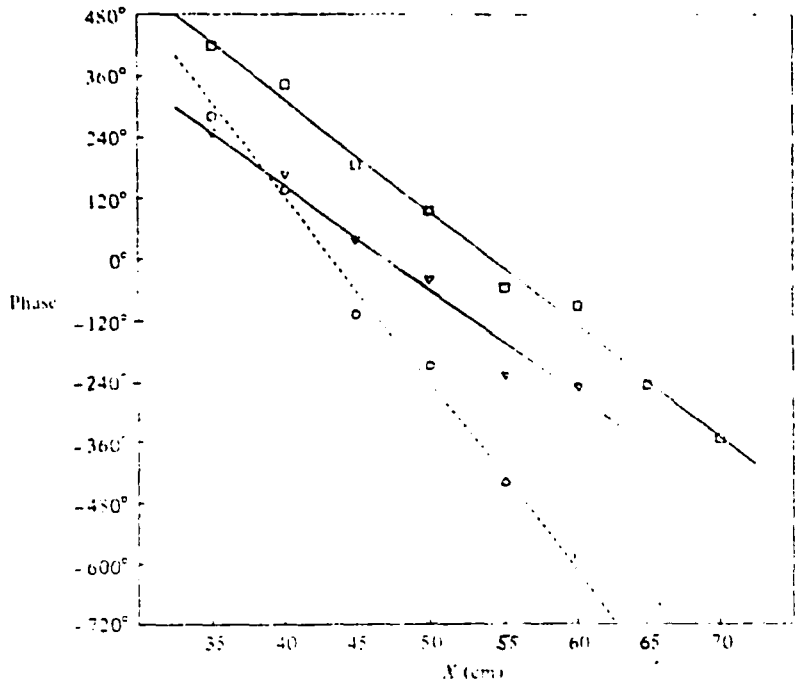

FIGURE 10. Streamwise phase variation of the u' velocity; ▽, phase of the fundamental at $Y = 2.54$ cm; □, phase of the fundamental at the height of amplitude maximum of the fundamental; ○, phase of the second harmonic at the height of amplitude maximum of the second harmonic.

Figure 4.14: Copy of a figure from Williams et al. (1984). The results presented in this figure were used to calculate the phase velocity of the primary wave, c_o.

Figure 4.15 shows the dispersion relations for the profiles at $\xi = 0^o$ and 120° for the case of temporal and spatial instability. The results for $\xi = 0^o$ show the "small group velocity cutoff point" which was discussed earlier. In the case of $\xi = 120^o$, the results are different. The measured velocity profile appears to be monotonic, with $(d^2U/dy^2)_{wall} > 0$. The so-called "small group velocity cutoff" is no longer present, the results are well-behaved for $0.1 \leq c_g/U_\infty \leq 1$. For $c_g/U_\infty \leq 0.1$, $-Im(\frac{d\theta}{dt}) \approx 0$ and $Im(c_i) \approx 0$. These results are similar to the Falkner-Skan like family discussed in Chapter 3.

The results of ray tracing near the crest, $\xi = 0$, are shown in Figure 4.16. They agree well with those calculated for the Klenbanoff et al. results shown in Figure 4.6.

It was pleasing to note that the velocity profiles of Williams et al. resulted in focussing of the secondary wave packet. The next question to be answered is whether focussing occurs only in the region of the wave crest or if wave trapping is important in the breakdown process for the Williams et al. data as well.

Figure 4.16 shows a family of trajectories in the neighborhood of the crest. Trajectory 1 is close to the asymptote dividing focussing and non-focussing trajectories. Figure 4.17 shows a family of trajectories each beginning at the initial position

(a) Results for 0°

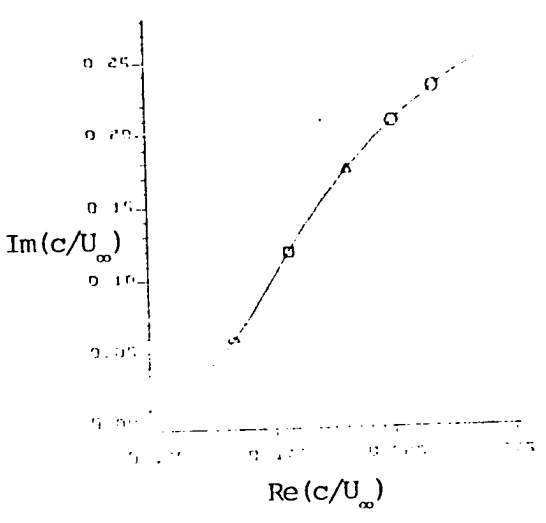

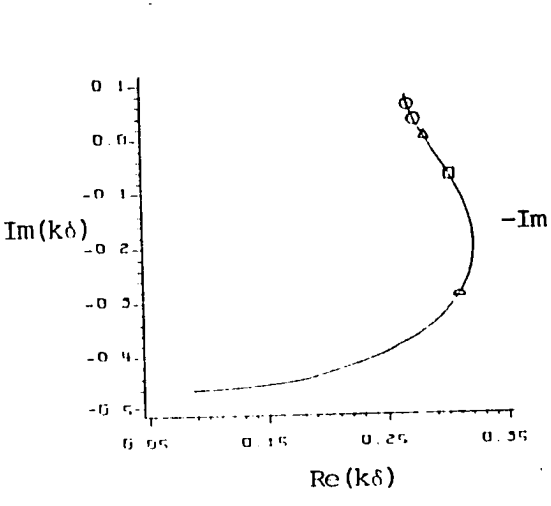

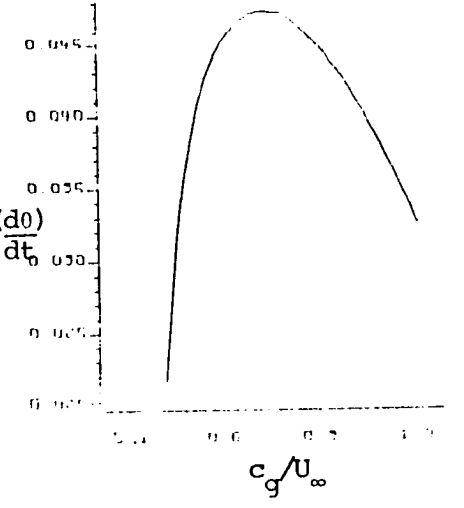

(b) Results for 120°

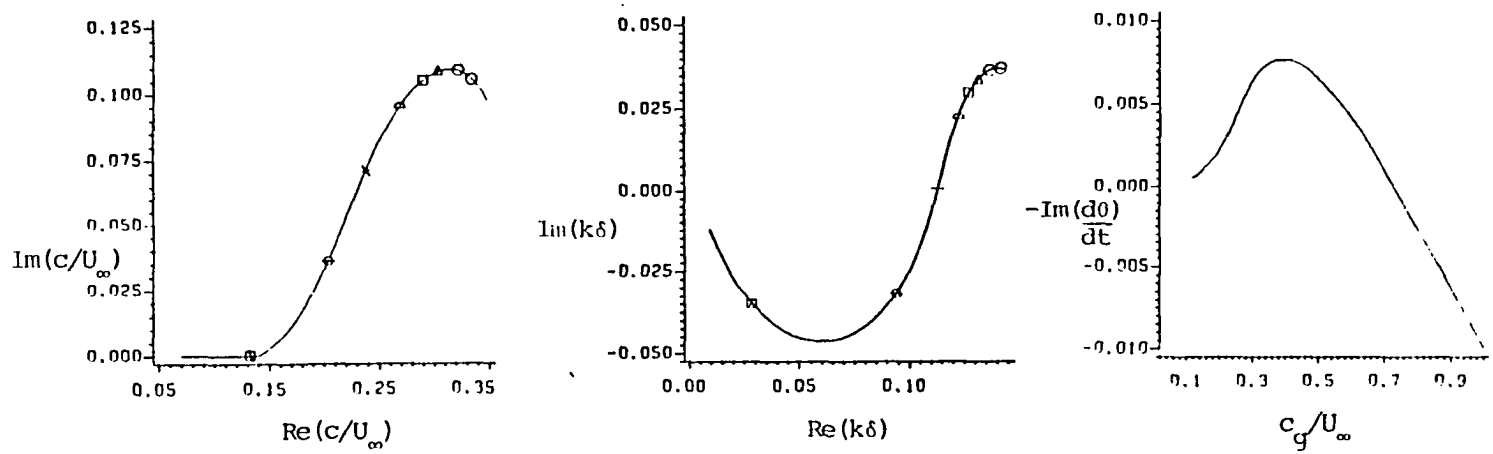

Figure 4.15: (a) Dispersion relations for the velocity profile fit to the data of Williams, et al. at 0°. The group velocity is the input parameter, giving the results shown. On the graphs for Im(c) versus Re(c) and Im(kδ) versus Re(kδ) the input values for group velocity, c_g, are indicated by the following symbols: ⌓ $c_g/U_\infty = 0.5$; □ $c_g/U_\infty = 0.6$; △ $c_g/U_\infty = 0.7$; ○ $c_g/U_\infty = 0.8$; ○ $c_g/U_\infty = 0.9$.

(b) Dispersion relations for the velocity profile fit to the data of Williams, et al. at 120°. The group velocity is the input parameter, giving the results shown. On the graphs for Im(c) versus Re(c) and Im(kδ) versus Re(kδ) the input values for group velocity, c_g, are indicated by the following symbols: ⍁ $c_g/U_\infty = 0.2$; ⊖ $c_g/U_\infty = 0.3$; + $c_g/U_\infty = 0.4$; ⌓ $c_g/U_\infty = 0.5$; □ $c_g/U_\infty = 0.6$; △ $c_g/U_\infty = 0.7$; ○ $c_g/U_\infty = 0.8$; ○ $c_g/U_\infty = 0.9$.

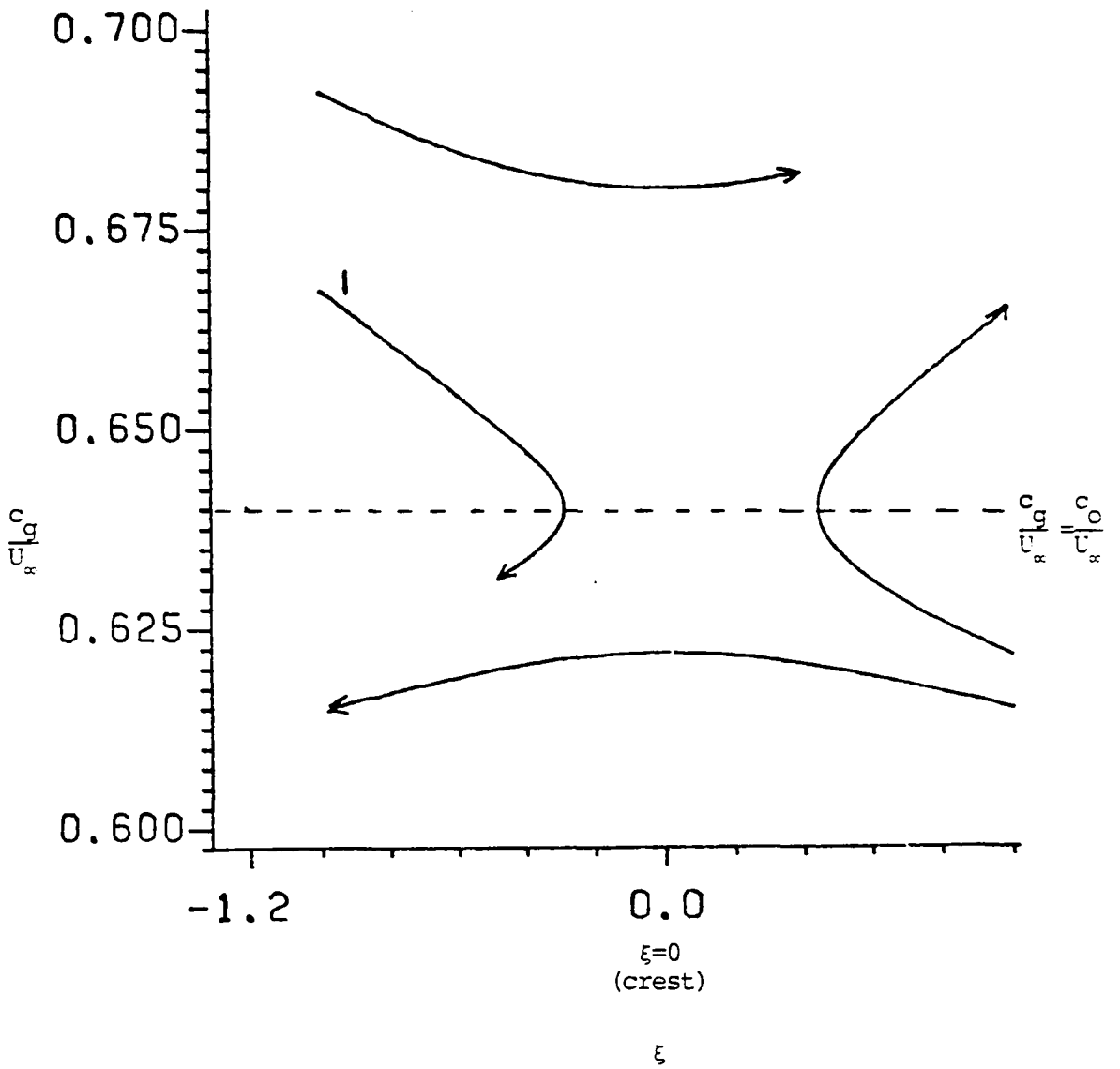

Figure 4.16: Secondary wave packet trajectories in the vicinity of the primary wave crest. $c_o/U_\infty = 0.64$, the phase velocity of the primary wave. $\xi = 0$ is the primary wave crest. Trajectory 1 will be referred to in the text.

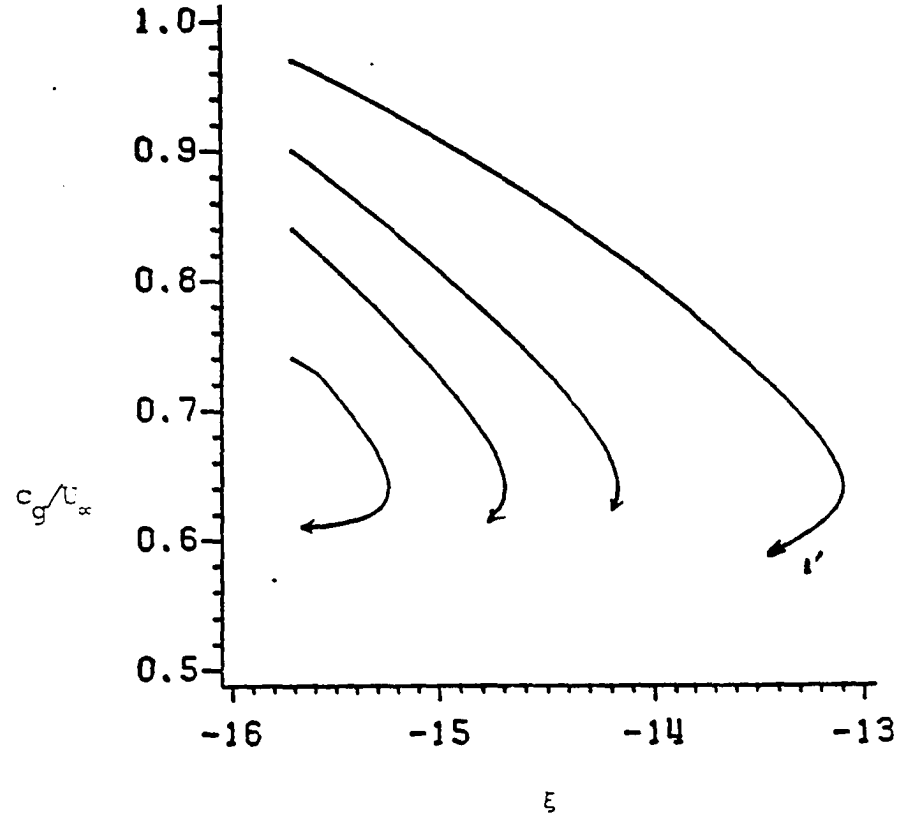

Figure 4.17: Secondary wave packet trajectories far from the primary wave crest. $c_o/U_\infty = 0.64$, the phase velocity of the primary wave. These trajectories have the same initial position, $\xi_o = \pi/2$. Trajectory 1' will be referred to in the text.

$(\epsilon\xi) = -\pi/2$ which focus. The long-time trajectories which approach the wave crest all have $c_g/U_\infty > 1$. This case is ruled out as physically unreasonable; so in the region of $\xi = -15.707963$ there are no long-time trajectories. Trajectory 1' has initial group velocity, $c_{go}/U = 0.97$. Comparing trajectory 1 and 1', we see the importance of wave trapping in addition to focussing for breakdown:

Trajectory 1	time to focus: 41.5
initial position: $\xi = -1.0$	ξ at focus : -0.2867
	$-\mathrm{Im}(d\theta/dt)$ at focus: -0.02823
Trajectory 1'	time to focus: 7.7
initial position: $\xi = -10\pi/2$	ξ at focus: -13.08
	$-\mathrm{Im}(d\theta/dt)$ at focus: -0.0167

The long-time trajectory 1 covers a distance of $\Delta\xi \approx 0.71$ in 41.5 time steps. The value of $-\mathrm{Im}(d\theta/dt)$ is greater than zero for all time. The trajectory 1' far from the crest covers a distance $\Delta\xi \approx 2.6$ in 7.7 time steps. Although focussing occurs in both cases, the wavepackets on trajectory 1' do not "feel" exponential amplification for a very long time period.

Comparing the breakdown theory of Landahl with two independent experiments on boundary-layer transition gave favorable results. By fitting velocity profiles to the experimental results,

we model a slowly varying background flow produced by a primary wave. We assume the secondary wave packets are higher frequency, smaller wavelength than the primary wave. The secondary wavepackets "ride" the primary wave. The most dangerous secondary wave packets travel on long-time trajectories and experience spatial and temporal amplification as they approach the wave crest. In the vicinity of the wave crest, space-time focussing of these highly amplified secondary wave packets occurs. The flow field responds to this high energy situation by breaking down into higher frequency oscillations. Both Klebanoff et al. and Williams et al. observed this order-of-magnitude increase in frequency where Landahl's theory predicted it would occur (see Figures 1.4 and 1.3).

It is unfortunate, however, that instantaneous velocity profiles upstream of the region of breakdown, observed by Williams et al. were not available. Although we use Landahl's focussing condition to verify the location of breakdown based on the findings of Williams et al., we cannot make any statement about conditions upstream. In particular, we cannot claim focussing does not occur upstream of X=60 cm without additional data.

One final note is in order on the need for both focussing and exponential amplification as the mechanism producing breakdown. Recall equation (4.20) for the observed square-amplitude, A^2,

$$A^2 = \mathcal{A}_\omega \exp[-2\,\mathrm{Im}(\theta)]$$

Wave trapping results in infinite growth in the exponential term $[-2\ \mathrm{Im}(\Theta)]$ while focussing results in an infinite value for the wave action density term, $\mathcal{A}_\omega$. In general, shear flow instability waves need contributions from both terms in order to describe their dispersive, non-conservative nature. It is not surprising then that both terms seem to contribute in making the observed square-amplitude become infinitely large, resulting in breakdown.

CHAPTER FIVE

SUMMARY AND CONCLUSIONS

5.1 Summary

This dissertation has been concerned with tracing the trajectories of secondary wave packets traveling through a weakly nonuniform background flow. The slowly varying background flow is the result of a primary wave moving through the flow of much longer wavelength and lower frequency than the secondary wave packet. The instantaneous velocity profiles measured in the experimental results of Klebanoff et al. (1962) were fitted with members of the cubic-tanh family of velocity profiles in order to model the background flow. The local dispersion relation was found as a solution of a small wavenumber approximation to the Rayleigh equation for a particular member of the cubic-tanh profiles. The secondary wave packets exhibited focussing when their group velocity equaled the phase velocity of the primary wave.

Landahl's theory was formulated after the experimental results of Klebanoff et al. In order to test his theory against data that were not available when it was formulated, the trajectories of secondary wave packets were found for a background flow modelled after the recent results of Williams et al. Again focussing was found for secondary wave packets whose group velocity equaled the phase velocity of the primary wave at the focus point, thus achieving an independent verification of Landahl's theory.

Our results seem to indicate the importance of wave trapping as well as focussing. When the initial group velocity, c_{go}, was greater than the fixed phase velocity, c_o, of the primary wave , focussing occurred provided the packet's initial position, ξ_o , was sufficiently far from the wave crest. Only trajectories traveling close to the asymptote dividing focussing and non-focussing trajectories, however, would focus in the neighborhood of the wave crest. These near-asymptote trajectories took a large number of time steps to reach the focus point, and for each time step, $-\mathrm{Im}(d\theta/dt) > 0$. Wave packets traveling along these long-time trajectories would receive exponential amplification along each step of their journey to the near crest focus point. This is in contrast with the trajectories that would focus far from the wave crest. Packets on the latter trajectories travelled too rapidly to the focus point to receive much amplification.

The local dispersion relation is given by a small wavenumber approximation to the Rayleigh equation. The dispersion relation involves complex wavenumber and complex phase velocity so that both spatial and temporal amplification is possible -- the so-called "mixed" stability problem. The group velocity is fixed as real in this analysis. The use of the Rayleigh equation to provide the dispersion relation is novel, and, since focussing occurs, it suggests the viscous effects are unimportant in the process leading to focussing. The use of a mixed stability relation for the dispersion relation for doubly inflectional boundary layer velocity profiles is also novel.

Chapter Three explores the mixed stability problem. First Russell's solution of a small wavenumber asymptotic approximation to the Rayleigh equation is studied in the case of temporal instability for a Falkner-Skan-like family of velocity profiles. The temporal stability results are compared with the classic results of Tollmien for vanishingly small wavenumber and agree well. Having gained confidence in the validity of Russell's solution, we were able to perform a mixed stability calculation for the Falkner-Skan-like family of profiles. Using real group velocity as the input eigenvalue gives complex phase velocity and complex wavenumber as output. The mixed dispersion relations are presented. A generalization of Tollmien's vanishingly small wavenumber approximation is derived for the mixed stability

problem. For $|c| \to 0^+$ and $|k| \to 0^+$, the total rate of amplification was found to behave as

$$Im\left(\frac{d\theta}{dt}\right) \sim \left(\frac{c_g}{z}\right)^3$$

which is a novel contribution to hydrodynamic stability theory.

5.2 Conclusions

In the introduction, there were three questions posed which this work proposed to answer. The first question was concerned with the generality of Landahl's theory of breakdown. Did Landahl's space-time focussing hold only in the Klebanoff et al. results, or could space-time focussing be found in other experimental results? The answer to question one has become clear during the course of this investigation -- Landahl's theory seems to fit the recently published results of Williams et al. One would anticipate space-time focussing with wave trapping as the mechanism of breakdown in boundary-layer transition. It appears that Landahl has provided a theory for one small part of the "blank" region shown in the transition diagram in Figure 1.1.

The breakdown process results from highly amplified near crest packets that focus in the neighborhood of the crest. Focussing results in a build-up of secondary vorticity in the neighborhood of the crest, which corresponds to the high shear layer seen in the instantaneous velocity profiles at 0° of the Williams et al. data shown in Figure 4.12a. Williams et al. report that the magnitude of

the vorticity in the high shear layer is about 3 times larger than in the primary vortex loop. One result of this concentration of vorticity at the crest is a buckling of the shear layer. The high shear layer smears out, and the instantaneous profiles resemble those at 180° of the Williams et al. data in Figure 4.12 a.

Another effect of the secondary vorticity in the neighborhood of the crest was proposed by Landahl. Since a condition for focussing is $c_g = c_o$, some secondary vorticity is convected downstream with the wave crest. Continuity of vorticity requires the secondary disturbance vortex line continue to some spanwise position in the quasi-steady primary flow. The collection of secondary vorticity on the crest of the primary wave may be the "head" of the hairpin vorticies observed after breakdown. The "leg" is the vortex line extending to a spanwise asymptote. As the head is convected downstream, the legs tilt over more and become stretched, which creates an upward velocity component that tends to lift the head further away from the surface.

The next logical step in tracing wave packet trajectories is the three dimensional problem. To date, no one has traced the trajectories of secondary wave packets travelling through slowly varying flow of the form $u = (U(y),0,W(y))$ -- the three dimensional problem relative to some appropriately chosen reference frame. Perhaps the span-wise irregularities observed prior to breakdown can

be explained in terms of converging and diverging secondary wave packets. From the dissertation research results of Russell (1978,1984) for an evolving flat eddy, three-dimensional unsteady instantaneous background velocity profiles are available. In the streamwise direction these profiles resemble the inflectional profiles observed in the boundary-layer transition experiments prior to breakdown. Tracing the secondary wave packet trajectories may lead to focussing. The location of focussing would be of interest since the results of Landahl indicate focussing occurs at a "crest", or point of symmetry. The final section of this work sets up the secondary instability problem for a three-dimensional background flow.

The second major question posed in Chapter One concerned the applicability of kinematic wave theory to non-conservative systems. The filtering scheme, $Im(c_g) = 0$, preserves the character of the original wavenumber propagation equation. Applying the filtering scheme indicates space-time focussing where the experimentalists have observed breakdown.

The final question posed in Chapter One was concerned with the nature of the mixed spatial-temporal instability problem. It was very exciting to note that classic hydrodynamic stability results for

temporal instability could be generalized to the mixed instability case. With effort, perhaps, one could derive most known results of stability theory for the mixed temporal-spatial instability case and then show the existing temporal results are a special case.

Future work in this area will go in two different directions. The first focus would be in exploring the mixed stability problem in greater detail. The total rate of amplification of a packet in a reference frame following the packet, $-\mathrm{Im}(d\theta/dt)$, behaves differently for singly and doubly inflectional profiles. In Chapter 4, the doubly inflectional velocity profiles with d^2U/dy^2 less than zero at the wall have $-\mathrm{Im}(d\theta/dt) > 0$ for a range of group velocities. There appeared to be a "small group velocity cutoff point" where $\mathrm{Re}(k\delta) = 0$. Whether this result is an anomaly of the small wavenumber approximation for the dispersion equation or is valid must be explored.

In Chapter 3, the Falkner-Skan-like family of flows which were singly inflectional, $d^2U/dy^2 > 0$ at the wall, had a band of unstable values of $-\mathrm{Im}(d\theta/dt)$ for a range of group velocities. The dispersion relations exhibited the behavior $-\mathrm{Im}(d\theta/dt) \sim c_g^3$ in the vicinity of vanishingly small wavenumbers. This behavior was not observed for the doubly inflectional profiles with $d^2U/dy^2 < 0$ at the wall. Furthermore, for the Blasius-like profile which had no inflection point in the

range $0 < y \leq \delta$, there was no band of unstable values of $-\mathrm{Im}(d\theta/dt)$. Thus there seems to be a generalization of the Rayleigh inflection point theory for the mixed stability problem. It seems that this idea can be studied more carefully by first formulating an expression comparable to the Rayleigh equation in terms of group velocity.

APPENDIX

Equations Governing the Motion of Secondary Instability Waves in a Three Dimensional Shear Flow

The dispersion relation found as solution of the small wavenumber approximation to the Rayleigh equation was derived in Chapter 2. This dispersion relation held for a reference flow of the form u = U(y). This section will generalize the results of Chapter 2 to hold for a skewed boundary-layer profile. Consider a reference flow of the form

$$\vec{U} = (U(y),0,W(y))$$

subjected to small disturbances of the form

$$(\vec{u},p) = (u,v,w,p)$$

Ignoring products of the disturbance quantities, and subtracting out the reference flow equations gives the small disturbance equations

$$\partial u/\partial t + \vec{U} \cdot \nabla \vec{u} + v \left(\frac{dU}{dy}\right) = -\nabla(P/\rho) \quad (5.1a,b,c)$$

$$\nabla \cdot \vec{u} = 0 \quad (5.2)$$

Following the standard procedure used for deriving the Rayleigh equation, introduce the horizontal gradient operator

$$\nabla_H (\ ) = \hat{\imath}_1 \frac{\partial (\ )}{\partial x} + \hat{\imath}_3 \frac{\partial (\ )}{\partial z}$$

Taking the horizontal divergence of (5.1) and using continuity to eliminate $\frac{\partial u}{\partial x} + \frac{\partial w}{\partial z}$ wherever possible gives

$$\left(\frac{\partial}{\partial t} + \vec{U}\cdot\nabla_H\right)\left(-\frac{\partial v}{\partial y}\right) + \nabla_H v \cdot \left(\frac{d\vec{U}}{dy}\right) = -\nabla_H^2\left(\frac{p}{\rho}\right) \qquad (5.3a)$$

$$\left(\frac{\partial}{\partial t} + \vec{U}\cdot\nabla_H\right) v = -\left(\frac{\partial p/\rho}{\partial y}\right) \qquad (5.3b)$$

Assume the solution to (3) take the form of travelling waves given as

$$v = Re\left[\tilde{v}\ \exp\left[i(\alpha x + \beta z - \omega t)\right]\right] \qquad (5.4)$$

$$p = Re\left[\tilde{p}\ \exp\left[i(\alpha x + \beta z - \omega t)\right]\right] \qquad (5.5)$$

Here ω is the frequency, $\alpha\hat{i}_1 + \beta\hat{i}_3 \equiv \vec{k}$ is the wavenumber vector, and $\tilde{v}$ and $\tilde{p}$ are mode-shape functions independent of (x,z,t). Substituting (5.4) and (5.5) into (5.3) gives

$$-i(\vec{k}\cdot\vec{U} - \omega)\left(\frac{d\tilde{v}}{dy}\right) + i\tilde{v}\,\vec{k}\cdot\left(\frac{d\vec{U}}{dy}\right) = \vec{k}\cdot\vec{k}\left(\frac{\tilde{p}}{\rho}\right) \qquad (5.6)$$

$$i(\vec{k}\cdot\vec{U} - \omega)\tilde{v} = \frac{-1}{\rho}\frac{d\tilde{p}}{dy} \qquad (5.7)$$

Introduce the polar coordinate components of the wavenumber vector

$$\alpha = k\cos\gamma \qquad \beta = k\sin\gamma$$

and the velocity field

$$Q(y,\gamma) = \cos(\gamma)\,U(y) + \sin(\gamma)\,W(y) \qquad (5.8)$$

Here γ is the obliqueness angle or "wave heading" angle. Equations (5.6) and (5.7) become

$$(Q-c)\left(\frac{d\tilde{v}}{dy}\right) - \tilde{v}\frac{dQ}{dy} = -\left(\frac{k}{i}\right)\frac{\tilde{p}}{\rho} \qquad (5.9)$$

$$(Q-c)\tilde{v} = -(ik)^{-1}\frac{1}{\rho}\frac{d\tilde{p}}{dy} \qquad (5.10)$$

where the phase velocity $c \equiv \omega/k$. Cross differentiating to eliminate $\tilde{p}$ from (5.9) and (5.10) gives the familiar Rayleigh equation

$$(Q-c)\left[\frac{d^2\tilde{v}}{dy^2} - k^2\tilde{v}\right] - \left(\frac{d^2Q}{dy^2}\right)\tilde{v} = 0 \qquad (5.11)$$

which holds for skewed boundary-layer profiles.

From the boundary conditions

$$\frac{d\tilde{p}}{dy} + k\tilde{p} = 0 \quad , \quad \frac{d\tilde{v}}{dy} + k\tilde{v} = 0 \qquad \text{for } y \geq y_{o.e.}$$

and

$$\frac{d\tilde{p}}{dy} = 0 \quad , \quad \tilde{v} = 0 \qquad \text{for } y = 0$$

one may show from (5.9), (5.10), (cf. Russell (1985b)) that

$$\frac{\int_0^\infty \tilde{v}\, e^{-ky}\, dy}{\int_0^\infty \tilde{v}\, dy} + k\delta (Q_\infty - c)^2 \int_0^\infty \frac{\tilde{p}}{\tilde{p}_w} \left[\frac{1}{(Q-c)^2} - \frac{1}{(Q_\infty - c)^2} \right] dy$$

Under the small wavenumber approximation $(ky_{o.e.}) \to 0$, the first term tends to 1 while

$$\frac{\tilde{p}}{\tilde{p}_w} = 1 + \mathcal{O}(|k y_{o.e.}|)$$

It then follows we can write the small wavenumber approximation to (5.11) as

$$1 + k\delta\, (Q_\infty - c)^2 \int_0^\infty \left[\frac{1}{(Q-c)^2} - \frac{1}{(Q_\infty - c)^2} \right] dy = \mathcal{O}[k y_{oe}] \tag{5.12}$$

where y_{oe} is the height above the wall where $Q = Q_\infty$. Equation (5.12) holds for the case of long waves

$$|k y_{oe}| << 1 \tag{5.13}$$

Russell's solution of equation (5.12) can be generalized for a family of skewed boundary layer profiles of the form (cf. Russell (1985b))

$$U = U_o[\tanh^3(\eta) + B_2\tanh^2(\eta) + B_1\tanh(\eta) + B_0] \tag{5.14}$$

$$W = W_o[\tanh^3(\eta) + C_2\tanh^2(\eta) + C_1\tanh(\eta) + C_0] \tag{5.15}$$

where

$$\eta = \frac{(y - y_o)}{\delta}$$

$$U_o = Q_o \cos\beta \tag{5.16}$$

$$W_o = Q_o \cos\beta \tag{5.17}$$

Let Q_o be a reference velocity and δ be a reference length for the particular problem. Define γ as the polar angle the reference velocity Q_o makes relative to the x-axis. Free parameters $B_2, B_1, B_0, C_2, C_1, C_0, y_o/\delta$ determine the shape of the profiles. Substituting (5.16) into (5.14) and (5.17) into (5.15) and the result into (5.8) gives

$$Q = Q_1[\tanh^3(\eta) + A_2\tanh^2(\eta) + A_1\tanh(\eta) + A_0] \tag{5.18}$$

where

$$Q_1 = Q_o(\cos\gamma\cos\theta + \sin\gamma\sin\theta) \tag{5.19}$$

$$A_n = \frac{(\cos\gamma\cos\theta)B_n + (\sin\gamma\sin\theta)C_n}{\cos\gamma\cos\theta + \sin\gamma\sin\theta} \tag{5.20}$$

Equation (5.18) is a two-dimensional generalization of the one-dimensional cubic-tanh profile presented in Chapter 3. Substituting (5.18) into (5.12) gives an integral expression which can be evaluted exactly by the method of partial fractions.

The dispersion relation c = c(k) is given as

$$c = Q_s + Q_1[r_{c_1}(r_{c_1}^2 - 3r_e^2)] \tag{5.21}$$

where r_{c1} is found from the transcendental equation

$$1 = -K\delta(Q_\infty - c)^2 \sum_{m=1}^{3} \frac{1}{[3Q_1(r_{cm}^2 - r_e^2)^2[1-(r_{cm}-r_\infty+1)^2]}$$
$$\left[\left(\frac{1}{(r_w - r_{cm})} - \frac{1}{(r_\infty - r_{cm})}\right) - 2\left\{\frac{r_{cm}}{r_{cm}^2 - r_e^2} - \frac{r_{cm}-r_\infty+1}{1-(r_{cm}-r_\infty+1)^2}\right\}\right.$$
$$\left.\ln\left[\frac{r_\infty - r_w}{r_w - r_{cm}}\ \frac{2+r_w-r_\infty}{2}\right]\right] \tag{5.22}$$

Using the definitions given in Chapter 3, we have

$$Q_s \equiv Q_1 \left[(2/27) A_2^3 - A_1 A_2 /3 + A_0 \right] \tag{5.23a}$$

$$r_e \equiv \left[(A_2/3)^2 - (A_1/3) \right]^{1/2} \tag{5.23b}$$

$$r_w \equiv - \tanh (y_0/\delta) + A_2/3 \tag{5.23c}$$

$$r_\infty \equiv 1 + A_2/3 \tag{5.23d}$$

$$Q_\infty \equiv Q_1 \left[1 + A_2 + A_1 + A_0 \right] \tag{5.23e}$$

$$r_{c2} \equiv -\frac{r_{c1}}{2} + \sqrt{(2r_e)^2 - r_{c1}^2}\ \frac{\sqrt{3}}{2} \tag{5.23f}$$

$$r_{c3} \equiv -\frac{r_{c1}}{2} - \sqrt{(2r_e)^2 - r_{c1}^2}\ \frac{\sqrt{3}}{2} \tag{5.23g}$$

Once the dispersion relation for skewed boundary layer geometry is given, it is possible to trace the trajectories of secondary wave packets in the x-z plane. The equations for the trajectories are

$$\frac{dx}{dt} = \Omega_\alpha \tag{5.24}$$

$$\frac{dz}{dt} = \Omega_\beta \tag{5.25}$$

with wavenumber propagation

$$\frac{d\alpha}{dt} = -\Omega_x \tag{5.26}$$

$$\frac{d\beta}{dt} = -\Omega_z \tag{5.27}$$

where the dispersion relation is a slowly varying function of x,z, and t of the form

$$\omega = \Omega(\alpha, \beta, x, z, t) \tag{5.28}$$

The equation for square-amplitude propagation is given as

$$\begin{aligned} \frac{dA^2}{dt} = -A^2 \Big[& \Omega_{\alpha x} + \Omega_{\alpha\alpha} \frac{\partial \alpha}{\partial x} + \Omega_{\alpha\beta} \frac{\partial \beta}{\partial x} \\ & + \Omega_{\beta z} + \Omega_{\alpha\beta} \frac{\partial \alpha}{\partial z} + \Omega_{\beta\beta} \frac{\partial \beta}{\partial z} \Big] \\ & + 2A^2 \left[Im(\Omega) - \Omega_\alpha Im(\alpha) - \Omega_\beta Im(\beta) \right] \end{aligned} \tag{5.29}$$

where the wavenumber gradient terms, $\frac{\partial \alpha}{\partial x}$, $\frac{\partial \alpha}{\partial z}$, $\frac{\partial \beta}{\partial x}$, and $\frac{\partial \beta}{\partial z}$ are given along a trajectory as

$$\frac{d[B]}{dt} = -[B][C][B] - [D]^T[B] - [B][D] - [E] \qquad (5.30)$$

where

$$[B] = \begin{bmatrix} \frac{\partial \alpha}{\partial x} & \frac{\partial \alpha}{\partial z} \\ \frac{\partial \beta}{\partial x} & \frac{\partial \beta}{\partial z} \end{bmatrix} \qquad [C] = \begin{bmatrix} \Omega_{\alpha\alpha} & \Omega_{\alpha\beta} \\ \Omega_{\beta\alpha} & \Omega_{\beta\beta} \end{bmatrix}$$

$$[D] = \begin{bmatrix} \Omega_{\alpha x} & \Omega_{\alpha z} \\ \Omega_{\beta x} & \Omega_{\beta z} \end{bmatrix} \qquad [E] = \begin{bmatrix} \Omega_{xx} & \Omega_{xz} \\ \Omega_{zx} & \Omega_{zz} \end{bmatrix}$$

Since [B] is symmetric, equations (30) represents 3 independent equations for its 3 independent elements. Equation (5.30) is the "derived ray equation" of Hayes (1970).

Solving equations (5.24,25,26,27, and 30) with the known relation equation (5.38) involves employing a Runge-Kutta technique for 7 equations with 7 unknowns. Seven initial conditions must be given at t = 0:

$$\begin{array}{ll} \alpha_o & \left(\frac{\partial \alpha}{\partial x}\right)_o \\ \beta_o & \left(\frac{\partial \beta}{\partial z}\right)_o \\ x_o & \\ z_o & \left(\frac{\partial \alpha}{\partial z}\right)_o \end{array} \qquad (5.31)$$

Once these values are known for one time iteration, equation (5.29) can be solved. We will apply the filter scheme $\mathrm{Imag}(c_g) = 0$ after each time iteration.

Elaborating on the calculation of the group velocities Ω_α and Ω_β, we can write the transcendental equation (5.22) in the form

$$\frac{1}{K} = H(\gamma, c) \tag{5.32}$$

Starting with $\omega = ck$, we get

$$d\omega = k\,dc + c\,dk \tag{5.33}$$

From (5.32), we obtain

$$-\frac{dk}{K^2} = H_\gamma\, d\gamma + H_c\, dc$$

or

$$dc = \frac{-dk}{H_c K^2} - \frac{H_\gamma}{H_c}\, d\gamma \tag{5.34}$$

Substituting (5.34) into (5.33) yields

$$\begin{aligned} d\omega &= K\left[\frac{-dk}{H_c K^2} - \frac{H_\gamma d\gamma}{H_c}\right] + c\,dk \\ &= \left[c - \frac{1}{H_c K}\right] dk - K\frac{H_\gamma}{H_c}\, d\gamma \end{aligned} \tag{5.35}$$

We have the following relationship between k and γ:

$$\alpha = K\cos\gamma \qquad \beta = K\sin\gamma$$

Consequently, we have

$$\begin{pmatrix} d\alpha \\ d\beta \end{pmatrix} = \begin{bmatrix} \cos\gamma & -K\sin\gamma \\ \sin\gamma & -K\cos\gamma \end{bmatrix} \begin{pmatrix} dk \\ d\gamma \end{pmatrix}$$

Inverting gives

$$\begin{pmatrix} dk \\ K\,d\gamma \end{pmatrix} = \begin{bmatrix} \cos\gamma & \sin\gamma \\ -\sin\gamma & \cos\gamma \end{bmatrix} \begin{pmatrix} d\alpha \\ d\beta \end{pmatrix}$$

Substituting this result into (5.35) gives

$$d\omega = \left(c - \frac{1}{k H_c}\right)(\cos\gamma\, d\alpha + \sin\gamma\, d\beta)$$
$$+ \left(\frac{-H_\gamma}{H_c}\right)(-\sin\gamma\, d\alpha + \cos\gamma\, d\beta)$$

Since $d\omega$ can also be written

$$d\omega = \Omega_\alpha\, d\alpha + \Omega_\beta\, d\beta$$

we have after equating coefficients of $d\alpha$ and $d\beta$

$$\Omega_\alpha = \left(c - \frac{H}{H_c}\right)\cos\gamma + \left(\frac{H_\gamma}{H_c}\right)\sin\gamma \qquad (5.36)$$

$$\Omega_\beta = \left(c - \frac{H}{H_c}\right)\sin\gamma + \left(\frac{H_\gamma}{H_c}\right)\cos\gamma \qquad (5.37)$$

We see that for the case $\gamma = 0$, $\beta = 0$, and from (5.32)

$$\Omega_\alpha = c - \frac{H}{H_c}$$

And since $H = 1/k$, we can write

$$\frac{1}{H_c} = \frac{1}{\frac{dH}{dr_{c_1}}\frac{dr_{c_1}}{dc}} = \frac{dc}{dr_{c_1}}\left(\frac{-1}{k^2}\right)^{-1}\frac{1}{\frac{dk}{dr_{c_1}}}$$

Then the expression for group velocity is given as

$$\Omega_\alpha = c + k\frac{dc}{dr_{c_1}}\frac{dr_{c_1}}{dk}$$

which is the result used for one-dimensional waves given earlier.

Terms Ω_x and Ω_z in (5.26) and (5.27) can be found in an analogous fashion. Writing the transcendental equation (5.22) in the form

$$c = F(\gamma, k)$$
$$= F\left(\gamma(z,x,t),\, k,\, r_{c_1}(z,x,t)\right)$$

we can find

$$\Omega_x = k\frac{dc}{dx}$$
$$= k\left[F_x + F_\gamma\frac{d\gamma}{dx}\right]$$
$$= k\left[\frac{dF}{dr_{c_1}}\frac{dr_{c_1}}{dx} + F_\gamma\frac{d\gamma}{dx}\right]$$

Likewise, we have

$$\Omega_z = K\left[\frac{dF}{dr_0}\frac{dr_0}{dz} + F_\gamma \frac{d\gamma}{dz}\right]$$

Terms like $\Omega_{\alpha\alpha}$ and $\Omega_{\alpha\gamma}$ in equations (5.29) and (5.30) would be cumbersome to evaluate exactly. Once Ω_α, Ω_β, Ω_γ, Ω_z are known for an iteration, one could use a finite difference scheme to find the second derivative terms.

In summary, the problem of tracing secondary wave packets through a weakly non-uniform background flow which is unsteady and three dimensional is well posed. The bulk of the research effort at this point would be to fit velocity profiles, and then develop some clever x,z,t dependent function in order to model the slowly changing non-uniform background flow. The physical interpretation of the results would require original insight and this would take some time on the part of the researcher.

REFERENCES

Benjamin, T.B. (1959) "Shearing flow over a wavy boundary." J. Fluid Mech. vol. 6, pp 161-205.

Chin, W.C. (1980) "Effect of dissipation and dispersion on slowly varying wavetrains." AIAA Journal, vol. 18, pp. 149-158.

Criminale, W.O.,Jr. and Kovasznay, L.S.G. (1962) "The growth of localized disturbances in a laminar boundary layer." J. Fluid Mech. vol. 14, pp 59-80.

Drazin, P.G. and Howard, L.N. (1962) "The instability to long waves of unbounded parallel inviscid flow." J. Fluid Mech. vol 14, pp. 257-283

Drazin, P.G. and Howard, L.N. (1966) "Hydrodynamic stability of parallel flow of inviscid flow." Advances in Applied Mechanics, vol. 9, pp.1-89, New York: Academic Press.

Drazin, P.G. and Reid, W.H. (1981) Hydrodynamic Stability, Cambridge: Cambridge University Press.

Emmons, H.W. (1951) "The laminar-turbulent transition in a boundary layer." J. Aero. Sci., vol. 18, p. 490.

Fox, R. and McDonald, A. (1978) Introduction to Fluid Mechanics, Second Edition. John Wiley and Sons, New York.

Gaster, M. (1962) "A note on the relation between temporally-increasing and spatially-increasing disturbances in hydrodynamic stability." J. Fluid Mech., vol. 14, pp. 350-352..

Gaster, M. (1965) "On the generation of spatially growing waves in a boundary layer." J. Fluid Mech., vol. 22, pp. 433-441.

Hama, F.R., Long, J.D., and Hegarty, J.C. (1957) "On transition from laminar to turbulent flow." J. Appl. Phys., vol. 28, p 388.

Hama, F.R., and Nutant, J. (1963) "Detailed flow field observations in the transition process in a thick boundary layer." Proceedings of the Heat Transfer and Fluid Mechanics Institute, Stanford University Press, pp. 77-93.

Hayes, W.D. (1970) "Conservation of action and modal wave action." Proc. R. Soc. Lond A 32, pp. 187-208.

Heisenberg, Werner (1924) "Ueber Stabilitaet und Turbulenz von Flussigkeitstroemungen." Annalen der Physik, vierte Folge, Band 74, s. 579-627.

Herbert, T. (1983) "On perturbation methods in nonlinear stability theory." J. Fluid Mech., vol. 126, pp. 167-186.

Itoh, N. (1980) in Proceedings, IUTAM Symposium on Laminar-Turbulent Transition, edited by R. Eppler and H. Fasel (Springer, Berlin, 1980) pp. 86-95.

Itoh, N. (1981) "Secondary instability of laminar flows." Proc. R. Soc. Lond. A 375, pp. 565-578.

Jimemez, J. and Whitham, G.B. (1976) "An averaged lagrangian method for dissipative wavetrains," Proc. R. Soc. Lond. A 349, pp. 277-287

Klebanoff, P.S., Tidstrom, K.D., and Sargent, L.M. (1962) "The three dimensional nature of boundary layer instability." J. Fluid Mech. vol 12, pp. 1-34.

Kovasznay, L.S.G., Komoda, H., and Vasudeva, B.R. (1962) "Detailed flow field in transition." Proceedings of the Heat Transfer and Fluid Mechanics Institute, Stanford University Press, pp. 1-26.

Landahl, M.T. (1969) Phys. Fluids, vol. 12 (suppl. II), p. 146.

Landahl, M.T. (1972) "Wave mechanics of breakdown." J. Fluid Mech. vol 56, pp. 775-802.

Landahl, M.T. (1982) "The application of kinematic wave theory to wave trains and packets with small dissipation." Phys. Fluids, vol. 25, pp. 1512-1516.

Lighthill, M.J. (1957) "The fundamental solution for a small steady three dimensional disturbance to a two dimensional parallel shear flow." J. Fluid Mech. vol. 3, pp. 113-144.

Lighthill, M.J. (1978) Waves in fluids . Cambridge University Press.

Lin, C.C. (1955) The theory of hydrodynamic stability, Cambridge: Cambridge University Press.

Nayfeh, A.H. (1980) in Proceedings, IUTAM Symposium on Laminar-Turbulent Transition, edited by R. Epper and H. Fasel (Springer, Berlin) pp. 201-217.

Obremski, H.J. and Fejer, A.A. (1967) J. Fluid Mech., vol 29, page 93

Obremski, H.J., Morkovan, M.V., Landahl, M.T., Wazzan, A.R., Okamura, T.T., and Smith, A.M.O. (1969) "A portfolio of the stability characteristics of incompressible boundary layers." NATO AGARDograph 134.

Pierrehumbert, R.T. (1974) "Local and global baroclinic instability of zonally varying flow." J. Atm. Sciences, vol. 41, pp. 2141-2162

Rayleigh, J.W.S. (1913) "On the stability of the laminar motion of an inviscid fluid." Phil. Mag. vol. 26, pp 1001-1010. (also Papers vol. VI, pp 197-204).

Rayleigh, J.W.S. (1894) The theory of sound, 2nd edn. London: Macmillan (new edition published by Dover Publications, New York, 1945.)

Reynolds, O. (1883) "On the experimental investigation of the circumstances which determine whether the motion of water shall be direct or sinuous, and the law of resistnace in parallel channel." Phil. Trans. Roy. Soc. A, vol. 186, pp. 123-164.

Russell, J.M. (1981) "The evolution of a flat eddy near a wall in an inviscid shear flow." Ph.D. Dissertation, M.I.T.

Russell, J.M. (1983) "Inflectional instability of a two parameter family of boundary layer profiles." Bull. Am. Phys. Soc., vol. 28, p.1372.

Russell, J.M. (1985) "Amplitude propagation in slowly varying trains of shear flow instability waves." Submitted to J. Fluid Mech. pp. 1-51.

Russell, J.M. (1985b) "Long wave inviscid of skewed boundary layer flows." Submitted to J. Fluid Mech. pp. 1-41.

Schubauer, G.B. and Klebanoff, P.S. (1956) "Contributions on the mechanics of boundary layer transition." NACA Report No. 1289.

Schubauer, G.B. and Skramstad, H.K. (1948) "Laminar boundary layer oscillations on a flat plate." NACA Report No. 909.

Stewartson, K. (1974) "Some aspects of nonlinear stability theory," Fluid Dynamics Transactions, Polish Academy of Sciences, Warsaw, vol. 7, pp. 101-128.

Stewartson, K. and Stuart, J.T. (1971) "A nonlinear instability theory for a wave system in plane poiseuille flow," Journal of Fluid Mechanics, vol. 48, pp 529-545.

Stuart, J.T. (1960) "On the non-linear mechanics of wave disturbances in stable and unstable parallel flows. Part 1. The basic behaviour in plane Poiseuille flow." J. Fluid Mech., vol. 9, pp 353-370.

Tani, I. (1967) "Review of some experimental results on boundary layer transition." Phys. of Fluids Suppl., vol. 10, pp. 11-16.

Tani, I. (1962) "Some aspects of boundary layer transition at subsonic speeds." Advances in Aeronautical Sciences, Pergamon Press, New York and London.

Tollmien, W. (1935) "Ein allgemeines kriterium der instabilitaet laminarer geschwindigkeitsverteilungen." Gesellschaft der Wissenschaft (Goettingen). Nachrichten. Mathematische und Physische Klasse. Fachgruppe I Neue Folge, Band 1, s. 79-114. (translated as "General instability criterion of laminar velocity distributions." NACA TM 792, 1936.)

Viney, C.E.M., and Russell, J.M. (1983) "Tracing of Rayleigh instability waves through weakly nonuniform background flow." Bull. Am. Phys. Soc., vol. 28, pp. 1372-1373.

Watson, J. (1960) On the nonlinear mechanics of wave disturbances in stable and unstable parallel flows. Part 2. The development of a solution for plane Poiseuille flow and for plane Couette flow." J. Fluid Mech., vol. 9, pp. 371-389.

Watson, J. (1962) "On spatially-growing finite disturbances in plane Poiseuille flow." J. Fluid Mech., vol. 14, pp. 211-221.

Whitham, G.B., (1965) "A general approach to linear and nonlinear dispersive waves using a lagrangian," Journal of Fluid Mechanics, vol. 22, pp 273-283.

Whitham, G.B., (1970) "Two-timing, variational principles and waves," Journal of Fluid Mechanics, vol. 44, pp 373-395.

Whitham, G.B. (1974), Linear and Nonlinear Waves (Wiley, Interscience, New York).

Williams, D.R., Fasel, H., and Hama, F.R. (1984) "Experimental determination of the three-dimensional vorticity field in the boundary-layer transition process." J. Fluid Mech., vol 149, pp 179-203